Modeling and Simulation of a Moving Rigid Body in a Rarefied Gas

Dem Fachbereich Mathematik
der Technischen Universität Kaiserslautern
zur Verleihung des akademischen Grades
Doktor der Naturwissenschaften
(Doctor rerum naturalium, Dr. rer. nat.)
vorgelegte

Dissertation

von

Samir Shrestha

December 16, 2014

Abstract

We present a numerical scheme to simulate a moving rigid body with arbitrary shape suspended in a rarefied gas micro flows, in view of applications to complex computations of moving structures in micro or vacuum systems. The rarefied gas is simulated by solving the Boltzmann equation using a DSMC particle method. The motion of the rigid body is governed by the Newton-Euler equations, where the force and the torque on the rigid body is computed from the momentum transfer of the gas molecules colliding with the body. The resulting motion of the rigid body affects in turn again the gas flow in the surroundings. This means that a two-way coupling has been modeled. We validate the scheme by performing various numerical experiments in 1-, 2- and 3-dimensional computational domains. We have presented 1-dimensional actuator problem, 2-dimensional cavity driven flow problem, Brownian diffusion of a spherical particle both with translational and rotational motions, and finally thermophoresis on a spherical particles. We compare the numerical results obtained from the numerical simulations with the existing theories in each test examples.

Zusammenfassung

Wir stellen eine numerisches Schema vor, welches zur Simulation eines bewegten Teilchens von beliebiger Form in einem Mikro-Fluss eines verdünnten Gases genutzt werden kann, was in komplexen Berechnung von bewegten Strukturen in Mikro- oder Vakuumsystemen Anwendung findet. Das verdünnte Gas wird durch die Lösung der Boltzmann Gleichung mittels einer DSMC Partikelmethode simuliert. Die Bewegung des starren Teilchens ist durch die Newton-Euler-Gleichungen dominiert, wobei Kraft und Drehmoment auf dem starren Körper durch den Impulstransfer der auf den Körper kollidierenden Gas-Teilchen berechnet werden. Die resultierende Bewegung des starren Körpers beeinflusst andererseits den Gasfluss in seinem Umfeld. Das bedeutet, dass eine beiderseitige Kopllung modelliert wurde. Das Schema wurde durch zahlreiche numerische Experiment in ein-, zwei und drei-dimensionalen Gebieten validiert. Wir stellen das 1-dimensionale Aktuator Problem, das 2-dimensionale Hohlraumströmungsproblem, Brownsche Diffusion von kugelförmigen Partikeln mit translativen und Rotationsbewegungen soie die Thermophorese auf sphärischen Partikeln vor. Wir vergleichen dabei numerische Ergebnisse von Simulationen mit den existierenden Theorien für jedes Fallbeispiel.

Contents

List of Figures

Chapter 1
Introduction

1.1 Motivation

Past few decades science and engineering are increasingly operating at micro- and nano-scales, application to microelectromechanical systems (MEMS), Lab-on-a-Chip (LOC), micro system technologies (MST) etc [13, 73, 78]. Many important physical and chemical processes occur across this range of time and length scales, for example: nucleation and phase separation; combustion and ignition; fluid instabilities; and surface science, such as catalytic processes [13]. A wide varieties of microscale devices like sensors, actuators and valves are now extensively used in our everyday life. Some MEMS devices have also been designed in the field of fluid application such as micropumps, microvalves, and microturbines [73]. All devices that operate at molecular scales, from MEMS to natural biomolecules, function in chaotic conditions due to the thermal fluctuations. It is well-known that the hydrodynamic fluctuations play an important role in the Brownian motion of suspended microscopic objects but other examples include: the breakup of droplets in jets; Brownian molecular motors; Rayleigh-Bernard convection; Rayleigh-Taylor mixing; and combustion and explosive detonation. Fluctuations also alter pattern formations in reaction-diffusion systems [13]. On the other hand, nanoparticles play a vital role in many industrial processes and natural phenomenon in wide fields including chemical engineering, chemistry, physics, public health and biology. Nanoparticle technology is expected to have major impacts in medicine, catalysis, electronics and life science. Furthermore, science and engineering of nanoparticles is central to the environment (e.g. air pollution, climate change, and green house effect), energy utilization (e.g. fossil fuel combustion, and fly ash formation), and food engineering (e.g. flavor retention). Nanoparticles are suspended in fluids during production, handling, processing, and by unintentional and/or undesired release to the environment. In many cases the suspending fluid is a gas, as in the case of large scale commercial production (million tons of nanoparticles per year for fillers in rubber, opacifiers in paints etc.), air pollution (e.g. diesel emission and coal combustion), clean room applications (semiconductor industry) and many more. A key concept

of the nanoparticle technologies with gases as the suspending fluids is the transport of nanoparticles and their deposition [59].

These all sets of industrial and scientific research problems for the particles suspended in the fluid can be categorized as the fluid particle interaction or moving boundary in the fluid or two phase flow of the solid and the fluid. A number of research has been done in past years theoretically and numerically to understand the flow behavior and the particles motion in the fluid, see for example [10, 26, 41, 50, 69]. Basically two kinds of fluids, either in the continuum or in the free molecular (rarefied) regime, are in the consideration for the motion of the solid particles. The Knudsen number, the ratio between the mean free path and the typical length, is a parameter that represents the degree of rarefaction fluid. Gas flows in the micro-scale devices or in the vacuum equipments are typical examples of the free molecular gas flows. In both cases, the Knudsen number is not negligible, because the typical length is small in the former case and the mean free path is large in the latter case, otherwise the fluid is said to be in the continuum regime. The fluid in the continuum regime is modeled by the Navier-Stokes equations which solves the fluid flow for the macroscopic field variables like density, velocity, pressure, and temperature, and the fluid in the rarefied regime is modeled by the Boltzmann equation which describes the behavior of the velocity distribution function of the gas molecules. The velocity distribution function contains the mesoscopic (a scale between micro and macro) information of the gas. The macroscopic quantities such as density, flow velocity, pressure and temperature can be expressed by the suitable moments of the distribution function. The solid particle that interacts with the surrounding fluid is described by usual equations of motion given by the Newton-Euler equations.

Numerical simulation of fluid-solid two-phase flow system can be classified into different categories. In the continuum fluid assumption there are number of numerical schemes for the flow of fluid with suspended solid particles. The fluid and the solid particles can be modeled as multiphase continuum flow or continuum approach for the fluid phase and a Lagrangian approach for the solid particles [69]. The most usual approach is to use the continuum-continuum theory that views the solid and the fluid as inter-penetrating mixture, each being governed by conservation laws, either postulated or derived by averaging. This Eulerian continuum approach results in the field equations for the flow properties for all phases in the system. It also leads to unknown terms representing the interaction between the phases. Once the interaction is modeled to close the system description, the Eulerian continuum approach is most efficient and has been widely used in multiphase flow simulations [42, 99].

Lagrangian numerical simulation (LNS) is another approach in multiphase flow where fluid satisfies the continuum equations that are solved on fixed field in the usual Eulerian way and the particle is described by the Newton's equation of motion with the knowledge of empirical forms of surrounding hydrodynamic forces. When the particle concentration is low, model with one way coupling is often used where

the particle motion does not influence the fluid flow. In the models with two-way coupling, a momentum exchange term could be introduced into the fluid equations to take the effect of the particle motion on the fluid flow into account [42].

The third type of approach which simulates the motion of both the fluid and the solid particles is termed as direct numerical simulation (DNS), where hydrodynamic force acting on the particle is directly computed from the fluid flow, and the motion of the fluid flow and the solid particles are fully coupled. It is possible to simplify the flow description considerably by ignoring the viscosity completely (inviscid potential flow) or by ignoring the fluid inertia completely (Stokes flow), see [42] for more references.

The flow simulation for the fluid-solid system at finite Reynolds numbers, a number of methods have been developed in the last decades. The arbitrary Lagrangian-Eulerian (ALE) particle method that uses a technique based on a combined formulation of the fluid and the solid particle momentum equations, together with an arbitrary Lagrangian-Euler (ALE) moving, unstructured, finite-element mesh technique to deal with the movement of particles [41, 42, 43]. This method has been used to solve particle motions in both Newtonian and viscoelastic fluids under two and three dimensional flow geometries. It also handles the particles of different sizes, shapes and materials.

Second method for solving problems with moving boundaries and interfaces uses space-time finite element methods. In this approach, along with the spatial coordinates, the temporal coordinate is also discretized by using finite-element methods. The deformation of the spatial domain with time is reflected simply in the deformation of the mesh in the temporal coordinate [40, 45, 46, 90]. Using this technique parallel 3D simulations have been performed for sedimentation of large number of spherical particles in a Newtonian fluid by the authors [46, 47].

The distributed Lagrange multiplier (DLM) particle method is another type of numerical technique to simulate the fluid-solid systems to extend a problem on a time-dependent geometrically complex domain to a stationary larger, but simpler domain (fictitious domain). On this fictitious domain, the constraints of the rigid-body motion of the particles are enforced using a distributed Lagrange multiplier, which represents the additional body force needed to maintain the rigid-body motion inside the particle, much like the pressure in incompressible fluid flows is used to maintain the constraint of incompressibility [32, 33, 42, 81]

All the methods mentioned above are based on the finite-element or finite difference methods. An approach, called the lattice Boltzmann method (LBM), has been developed into an alternative and promising numerical scheme for simulating the fluid flows. Unlike the conventional numerical schemes based on discretizations of macroscopic continuum equations, LBM is based on the microscopic models and the mesoscopic kinetic equations. The fundamental idea of the LBM is to construct

simplified kinetic models that incorporate the essential physics of the microscopic or mesoscopic processes so that the macroscopic-averaged properties obey the desired macroscopic equations; see the review by [22]. The LBM has been adapted to simulate the motion of solid particles in a Newtonian fluid. Most of the work in this area can be found in the articles by [2, 3, 8, 51, 52, 72]. Their schemes are based on a fully explicit scheme, where the hydrodynamic forces and moments acting on solid particles are first calculated from lattice Boltzmann simulation, and the motion of the solid particles is then determined from these forces and moments using Newton's second law. The LBM simulations can be easily performed on parallel computers. The computational cost for simulating particle motion scales linearly with the number of particles.

All the methods mentioned above are to simulate the fluid-solid system where fluid is always modeled as a continuum regime. Gas flow in micro/nano scale geometries, for example, MEMS (Micro Electro Mechanical Systems), where device size is small enough that flow of the gas can not be modeled correctly as a continuum regime. In such systems, the flow of the gas requires the kinetic treatment even at the normal pressure and the temperature conditions, and such a regime of gas is known as the rarefied gas. The rarefied gas flow is generally modeled by the Boltzmann equation. There are a number of deterministic and stochastic numerical techniques to solve the rarefied gas flow problems.

Deterministic methods based on the model Boltzmann equations are usually employed with the help of known techniques in computational fluid dynamics (CFD), such as the moving mesh technique and the immersed boundary method [26, 76, 86]. An immersed boundary method is a standard Eulerian approach to simulate the incompressible viscous flows with moving boundaries. This approach has been extended by Dechristé et al [26] to a deterministic simulation of rarefied flows based on the Bhatnagar-Gross-Krook (BGK) model of the Boltzmann equation. The immersed boundary approach consists in keeping the same mesh all along the calculation: every cell of the mesh remains fixed for all time steps while domain occupied by gas changes. This technique avoids to use moving mesh and re-meshing approaches, and should be easily implemented to the problems with complex geometries. This method has been tested with both specular and diffuse boundary conditions, and it has been implemented to validate on 1D problems (moving piston, actuator, etc.) [26]. Russo et al. [75, 76] have presented a semilagrangian numerical method of BGK model of the Boltzmann equation in a rarefied gas domain with moving boundary. The method is based on the discretization of the equation on a fixed grid in the space and the velocity. The equation is discretized in the characteristic form, and the distribution function is reconstructed at the foot of the characteristics by a third order piecewise Hermit interpolation. Recently, Tsuji et al. [86] have investigated, numerically on the basis of BGK model of the Boltzmann equation, unsteady flows of a rarefied gas in a full space caused by the oscillation of an infinitely wide plate in its normal direction. They have developed a numerical method on the basis of method of characteristics which is capable of describing

singularities caused by the oscillating plate. They have applied the method to two problems on oscillating plates with forced and free motion.

This increasing interest in the micro/nano fluidics has demanded the development of numerical schemes for hydrodynamic calculations at molecular level. Direct simulation Monte Carlo (DSMC) of Bird [9] was developed to model the gas flows in which Knudsen number is large, and the original applications were rarefied gas flows in which transport properties are not well-approximated by the Navier-Stokes equations. Since the early 90's DSMC has also been used in modeling molecular-scale devices with system length of microns down to nanometers. DSMC is also an ideal particle based scheme for the study of hydrodynamic fluctuations. Interestingly, it also turns out that hydrodynamic transport models are often still accurate at the microscopic scales for which thermodynamic fluctuations are significant. Specifically, the fluctuating Navier-Stokes equations, introduced by Landau and Lifshitz, have been validated by laboratory experiments and molecular simulations [13]. Generally DSMC simulations have been performed for fixed geometry, however Ohwada et al. [65] have analyzed numerically, a non-linear wave driven by a plane wall oscillating in its normal direction, on the basis of the Boltzmann equation for hard-sphere and Maxwellian type boundary conditions by using DSMC method. Recently Radar et al. [77] have investigated the moving-boundary algorithm for DSMC method for a microbeam that moves towards and away from a parallel substrate, and one-dimensional situation of a piston between to parallel walls using two moving-boundary algorithms has been studied.

Gallis et al. [36] have presented an approach for computing the force on and heat transfer to a spherical particle from a rarefied flow of a monoatomic gas that is computed using direct simulation Monte Carlo (DSMC) method. They have also found analytically the Green's function for the force and the heat transfer and are verified by showing that they yield certain well-known results, and are implemented numerically within DSMC code. They have performed the simulation for the gas confined between plates at different temperatures for broad range of pressures and particle velocities.

To simulate moving the rigid bodies in a rarefied gas, not only the influence of the moving boundary on the gas has to be included in the simulation, but also the forces exerted by the gas accelerating the rigid body. See, for example [86, 89] for one-dimensional situations with such a two-way coupling. We remark that, on the one hand, using DSMC based approaches for the above time-dependent problems with slow fluid flows requires some control over the large fluctuations inherent in these methods. On the other hand, the deterministic approaches are complicated to extend and computationally costly for higher dimensions. Finally, we note that DSMC methods are especially suited to couple moving rigid objects due to the Lagrangian nature of the gas molecules.

In this thesis we present a simulation scheme for the moving rigid bodies of arbitrary shape suspended in a rarefied gas suited for 1-, 2- and 3-dimensional problems. The rarefied gas flow is simulated by solving the Boltzmann equation in a time dependent domain of computation using a DSMC method. The rigid body motion is given by the Newton-Euler equations, where the forces and the torque on the rigid body are calculated from the momentum transfer due to gas molecules impinging on the surface of the rigid body. The resulting motion of the rigid body affects in turn again the gas flow in the surroundings. This means that a two-way coupling has been modeled. To validate our numerical scheme, we investigate various test examples performed in 1-, 2-, and 3-dimensional geometries where a rigid body is suspended in a gas, and we compare the numerical results with the existing theories.

The thesis is organized as follows: In chapter 2, a short description of the Boltzmann equation complemented with different models of the boundary conditions are presented. The important properties of the Boltzmann equation are also presented, and using some of these properties the local conservations equations are derived. From these local conservation laws, two macroscopic balance equations are presented. In chapter 3, the numerical schemes to solve the Boltzmann equation and the compressible Navier-Stokes equations are explained. The direct simulation Monte Carlo (DSMC) method is used to solve the Boltzmann equation and the finite pointset method (FPM) is used to solve the Navier-Stokes equations. Both the schemes are based on particle methods. In chapter 4, the fluid dynamic force and the torque exerted on the rigid body in a gas are explained. The usual way of computing the force and the torque on the rigid body is by integrating the stress tensor on its surface. The expression of the stress tensor is based on the type of model that is used to describe the fluid flow. For example, when the fluid is modeled by the Navier-Stokes equations, the stress tensor is expressed in terms of the macroscopic quantities like pressure and the derivatives of the fluid velocity. On the other hand when the fluid is modeled by the Boltzmann equation, the stress tensor is given by the suitable moment of the velocity distribution function. A simple naive approach is proposed to compute the force and the torque on the rigid body when the fluid is modeled by the Boltzmann equation and solved numerically by DSMC method. This is a microscopic approach where the rigid body collides massively with the gas molecules, and the force and the torque are computed by calculating the momentum transfered due to the impinging and the re-emitting gas molecules on the surface of the rigid body. In chapter 5, four different numerical experiments are presented to validate the proposed scheme to compute the force and the torque on the rigid body in the rarefied gas flow. In section 5.1, the first numerical experiment is performed to simulate a 1-dimensional actuator problem where the movement of the piston is induced by the temperature difference in both sides of the piston, and it reaches to its equilibrium position after the system recovers its the equilibrium state. In section 5.2, a 2-dimensional driven cavity gas flow problem is presented where a rigid circular body is suspended inside a square domain. The flow of the gas is driven by moving one of the wall of the domain. The flow of the gas is solved by using the Navier-Stokes equations and the Boltzmann equation separately. The numeri-

cal results, obtained from these two models for the motion of the rigid body in the gas domain, are compared for small and large values of Knudsen numbers. In section 5.3, the third numerical experiment is performed for the translational and the rotational Brownian motion of a spherical particle suspended in a rarefied gas in 3-dimensional domain, and the translational Brownian motion of the circular particle suspended in a rarefied gas in 2-dimensional domain. A detailed derivation of the translation and the rotational diffusion coefficients of the spherical particle in the rarefied gas in thermally equilibrium state is also presented. The numerical results are presented for the diffusion of the Brownian spherical particle in the rarefied gas by solving the Boltzmann equation using DSMC method, and finally compared the results with the theoretical values. In section 5.4, the last numerical experiment is performed for the thermophoresis on the rigid body in the rarefied gas. We have numerically computed the thermophoretic force on a rigid spherical body for different values of Knudsen numbers ranging from larger to smaller by using DSMC method, and compared the results with the existing theoretical values. The thermophoretic velocity of a spherical rigid body in the transition regime is proposed, and compared with the numerical results obtained from DSMC simulations. The motions of the circular and the spherical Janus particle caused by the thermophoresis are also studied numerically by using DSMC method. The distributions of the orientation of the Janus particles in the rotational motion are also presented.

Chapter 2
Mathematical Model for Gas Flow

The flow of the gas can be modeled at either the macroscopic or the microscopic level. The macroscopic model regards the gas as a continuum medium and description is in terms of the spatial and temporal variation of the flow properties such as density, velocity, pressure, and temperature. The Navier-Stokes equations provide the conventional mathematical model of a gas as a continuum. The macroscopic properties are the dependent variables in spatial coordinates and time. The alternative to the continuum model is the microscopic or molecular model which recognize the gas as a swarm of discrete molecules and ideally provides the information on the position, velocity, and the state of every molecule at all time. The mathematical model at this level is the Boltzmann equation whose solution is the only dependent variable that gives the fraction of molecules in a given location and state, but the independent variables are increased by the number of physical variables in which the state depends. The macroscopic properties can be identified with the average values of the appropriate molecular quantities at any location in a flow. These quantities can be defined as long as there are a sufficient number of molecules within the smallest significant volume of flow. This condition is almost always satisfied and the results from the molecular model can therefore be expressed in terms of the familiar continuum flow properties. Moreover, the equations that express the conservation of mass, momentum, and energy in a flow are common to, and can be derived from, either model. While this might suggest that neither of the approaches can provide information that is not also accessible to the other, it must be remembered that the conservation equations are not closed unless the stress tensor and heat flux can be expressed in terms of the lower-order macroscopic quantities. It is the failure to meet this condition, rather than the breakdown of the continuum description, which imposes a limit on the range of validity of the continuum equations. More specifically, the transport terms in the Navier-Stokes equations of continuum gas dynamics fail when the gradient of macroscopic variables become so steep that their scale is of the same order of the mean free path [9].

Flow of the gas is described by variety of dimensionless quantities. The most useful for our purpose is the Knudsen number Kn. The Knudsen number is a mea-

sure of the degree of rarefaction of gases encountered in the flow in the domain. It is defined as the ratio of the gas mean free path λ and the characteristic length scale L of the physical system [9], that is,

$$Kn = \frac{\lambda}{L},$$

where mean free path λ is the average distance traveled by gas molecules between successive collision. In kinetic theory of gases, the mean free path is given by [31]

$$\lambda = \frac{k_{\text{B}}}{\sqrt{2}\pi\rho R d^2}, \tag{2.1}$$

where k_{B} is the Boltzmann constant in J/K, ρ is the density of the gas in kg/m^3 and R is the specific gas constant in J/(kgK).

The traditional requirement for the Navier-Stokes equations to be valid is that the Knudsen number should be less than 0.1. The error in the Navier-Stokes result is significant in the regions of the flow where the appropriately defined local Knudsen number exceeds 0.1, and the upper limit on the Knudsen number at which the continuum model fails to describe the fluid flow may be taken to be 0.2 [9]. The transport terms vanish in the limit of zero Knudsen number and the Navier-Stokes equations then reduce to the inviscid Euler equations. The flow is then isentropic from the continuum viewpoint, while the equivalent molecular viewpoint is that the velocity distribution function is everywhere of the local equilibrium or Maxwellian form. The opposite limit of infinite Knudsen number is the collisionless or free-molecular flow regime. A large Knudsen number may result either from a large mean free path or a small scale length of the flow. The former is a consequence of the very low gas density. Figure 2.1 describes different regimes of fluid flow depending on the Knudsen numbers [9]. As Knudsen number increases, the rarefaction effects become more dominant and eventually the continuum assumption break down.
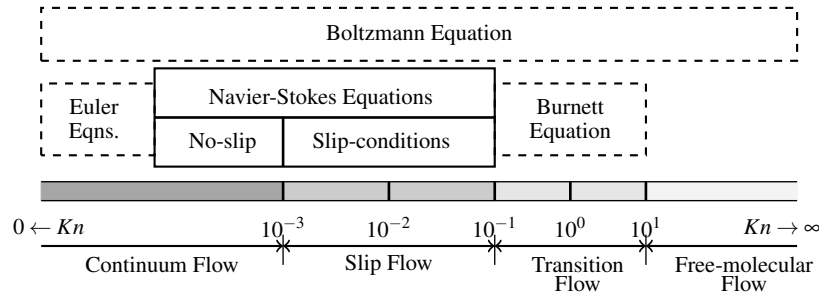
Fig. 2.1: The Knudsen number limits on fluid models [9].

2.1 The Boltzmann Equation

2.1.1 Physical model

We consider a simple rarefied monoatomic gas, which has only translational degree of freedom. The time evolution of the one particle distribution function $f(t,\mathbf{x},\mathbf{v})$ for a gas with velocity $\mathbf{v} \in \mathbb{R}^3$ and position $\mathbf{x} \in \mathbb{R}^3$ at time $t > 0$ is described by the Boltzmann equation [9, 24, 89]

$$\frac{\partial f}{\partial t} + \mathbf{v} \cdot \nabla_{\mathbf{x}} f = J(f,f) \tag{2.2}$$

with initial condition

$$f(t = 0, \mathbf{x}, \mathbf{v}) = f_0(\mathbf{x}, \mathbf{v}). \tag{2.3}$$

The left hand side of (2.2) is the transport term, which describes the free transport flow of the gas molecules and the right hand side is the collision term or collision operator, which describes the binary collision between the gas molecules. The collision operator $J(f,f)$ is described by the integral

$$J(f,f) = \int_{\mathbb{R}^3} \int_{S^2_+} k(||\mathbf{v} - \mathbf{v}_*||, \boldsymbol{\eta})[f'f'_* - ff_*] d\omega(\boldsymbol{\eta}) d\mathbf{v}_*, \tag{2.4}$$

where $S^2_+ = \{\boldsymbol{\eta} \in \mathbb{R}^3 : ||\boldsymbol{\eta}|| = 1 \text{ and } (\mathbf{v} - \mathbf{v}_*) \cdot \boldsymbol{\eta} > 0\}$, $d\omega(\boldsymbol{\eta})$ is the surface element on S^2_+ described by $\boldsymbol{\eta}$, $f' = f(t,\mathbf{x},\mathbf{v}')$, $f = f(t,\mathbf{x},\mathbf{v})$ and so on. The post-collision velocity pair $(\mathbf{v}', \mathbf{v}_*{}')$ is associated to the pre-collision velocity pair $(\mathbf{v}, \mathbf{v}_*)$ and the parameter $\boldsymbol{\eta}$ by the relation [9, 71], (derivation is presented in Appendix A)

$$\mathbf{v}' = \mathbf{v}_c + \frac{1}{2}||\mathbf{v}_r||\boldsymbol{\eta}, \quad \mathbf{v}_*{}' = \mathbf{v}_c - \frac{1}{2}||\mathbf{v}_r||\boldsymbol{\eta}, \tag{2.5}$$

where $\mathbf{v}_c = \frac{\mathbf{v} + \mathbf{v}_*}{2}$ and $\mathbf{v}_r = \mathbf{v} - \mathbf{v}_*$ are the velocity of the center of mass and the relative velocity between the pair of colliding molecules, respectively. The collision kernel $k(||\mathbf{v} - \mathbf{v}_*||, \boldsymbol{\eta})$ is a non-negative function which characterizes the details of the binary interaction between the gas molecules. For the general class of interaction, the kernel can be written as

$$k(||\mathbf{v} - \mathbf{v}_*||, \boldsymbol{\eta}) = \beta(\theta)||\mathbf{v} - \mathbf{v}_*||^{\frac{\sigma-4}{\sigma}}, \tag{2.6}$$

where θ is the scattering angle between $\mathbf{v}_r$ and $||\mathbf{v}_r||\boldsymbol{\eta}$. σ is the collision parameter such that $\sigma > 4$ corresponds to the "hard" collision, $\sigma = 4$ corresponds to the so-called "Maxwell molecules", and $2 < \sigma < 4$ corresponds to the "soft" interaction. In particular, the hard sphere model corresponds to the case of σ tending to infinity. We have considered the hard sphere model in our study.

Remark 2.1. The collision operator can also be written as a bilinear operator given by

$$J(f,g) = \frac{1}{2} \int_{\mathbb{R}^3} \int_{S_+^2} k(||\mathbf{v} - \mathbf{v}_*||, \boldsymbol{\eta})[f'g'_* - fg_* + f'_*g' - f_*g]d\omega(\boldsymbol{\eta})d\mathbf{v}_*. \quad (2.7)$$

It is clear that when $g = f$ equation (2.7) reduces to equation (2.4), and $J(f,g) = J(g,f)$.

2.1.2 Boundary conditions

Equations (2.2) and (2.3) are usually complemented with the boundary conditions for $\mathbf{v} \cdot \mathbf{n} \geq 0$ and $\mathbf{x} \in \partial\Omega$, where $\mathbf{n}$ is the unit vector normal to the surface $\partial\Omega$ at $\mathbf{x}$ and directed from the wall into the gas, given by (see [19] in detail)

$$| \mathbf{v} \cdot \mathbf{n} | f(t, \mathbf{x}, \mathbf{v}) = \int_{\mathbf{v}' \cdot \mathbf{n} < 0} | \mathbf{v}' \cdot \mathbf{n} | \mathscr{R}(\mathbf{v}' \to \mathbf{v}; t, \mathbf{x}) f(t, \mathbf{x}, \mathbf{v}')d\mathbf{v}', \quad (2.8)$$

for all $t \in \mathbb{R}_+$, $\mathbf{x} \in \partial\Omega$. The boundary condition (2.8) is the so-called reflective condition on $\partial\Omega$. The ingoing flux is defined in terms of the outgoing flux modified by the boundary kernel $\mathscr{R}$ according to the integral in (2.8). This kernel is called the scattering kernel and satisfies the positivity and mass conservation at the boundaries:

$$\mathscr{R}(\mathbf{v}' \to \mathbf{v}; t, \mathbf{x}) \geq 0, \quad \int_{\mathbf{v} \cdot \mathbf{n} \geq 0} \mathscr{R}(\mathbf{v}' \to \mathbf{v}; t, \mathbf{x})d\mathbf{v} = 1 \quad (2.9)$$

One can use different models for $\mathscr{R}$. For example classical models for $\mathscr{R}$ are specular, diffuse and mixed reflections.

Model 2.1. *(Specular reflection)*
The simplest possible model of the gas-surface interaction is to assume that the gas molecules are specularly reflected at the solid boundary, that means, the re-emitted molecules have same flow mass, temperature and tangential momentum of the incoming molecules. From physical point of view this model is not realistic. The scattering kernel of the specular reflection is given by

$$\mathscr{R}(\mathbf{v}' \to \mathbf{v}; t, x) = \delta(\mathbf{v}' - \mathbf{v} + 2(\mathbf{v} \cdot \mathbf{n})\mathbf{n}).$$

Then from (2.8), we have

$$f(t, \mathbf{x}, \mathbf{v}) = f(t, \mathbf{x}, \mathbf{v} - 2(\mathbf{v} \cdot \mathbf{n})\mathbf{n}).$$

Model 2.2. *(Diffuse reflection)*
On the other hand, diffuse reflection model is quite realistic with respect to the physical point of view. In this model the re-emitted molecules completely loose the memory of incoming molecules, except the conservation of the number of molecules, and re-emit with the velocity corresponding to those in a still gas at the temperature and moving frame of reference of the solid wall. The scattering kernel of the diffuse reflection is given by

$$\mathscr{R}(\mathbf{v}' \to \mathbf{v}; t, x) = | (\mathbf{v} - \mathbf{V}_{\mathrm{w}}) \cdot \mathbf{n} | f^0(\mathbf{x}, \mathbf{v}),$$

where

$$f^0(\mathbf{x}, \mathbf{v}) := \frac{1}{2\pi (RT_{\mathrm{w}})^2} exp\left(- \frac{||\mathbf{v} - \mathbf{V}_{\mathrm{w}}||^2}{2RT_{\mathrm{w}}} \right),$$

T_{w} is the temperature and $\mathbf{V}_{\mathrm{w}}$ is the velocity of the solid wall, and R the specific gas constant. Then from (2.8), we have

$$f(t, \mathbf{x}, \mathbf{v}) = f^0(\mathbf{x}, \mathbf{v}) \int_{\mathbf{v}' \cdot \mathbf{n} \leq 0} | \mathbf{v}' \cdot \mathbf{n} | f(t, \mathbf{x}, \mathbf{v}') d\mathbf{v}'.$$

Model 2.3. *(Mixed reflection)*
One can construct a more complicated intermediate model which is devoted to be more physically realistic. This model is the intermediate between the specular and diffuse reflection models. In this model there is a fraction α of molecules which accommodates to the temperature of the solid wall, while remaining portion $1 - \alpha$ is perfectly reflected by the solid wall. In this case the scattering kernel is given by

$$\mathscr{R}(\mathbf{v}' \to \mathbf{v}; t, x) = (1 - \alpha)\delta(\mathbf{v}' - \mathbf{v} + 2(\mathbf{v} \cdot \mathbf{n})\mathbf{n}) + \alpha | \mathbf{v} \cdot \mathbf{n} | f^0(\mathbf{x}, \mathbf{v}).$$

Then from (2.8), we have

$$f(t, \mathbf{x}, \mathbf{v}) = (1 - \alpha)f(t, \mathbf{x}, \mathbf{v} - 2(\mathbf{v} \cdot \mathbf{n})\mathbf{n}) + \alpha f^0(\mathbf{x}, \mathbf{v}) \int_{\mathbf{v}' \cdot \mathbf{n} \leq 0} | \mathbf{v}' \cdot \mathbf{n} | f(t, \mathbf{x}, \mathbf{v}') d\mathbf{v}'.$$

Here, the coefficient α, with $0 \leq \alpha \leq 1$, is called the accommodation coefficient. It represents the tendency of gas to accommodate to the wall. It means that a fraction $(1 - \alpha)$ of molecules satisfies specular boundary condition whereas a fraction α satisfies half-range Maxwell diffuse boundary condition. The main drawback of this model is that it gives the same accommodation coefficient for energy and momentum though it is known that energy and the momentum accommodate differently in the physical molecule-wall interaction [20]. However, this model has been widely used, both for theoretical studies and numerical simulations for practical applications.

Remark 2.2. The above mentioned models are the boundary conditions for the solid walls. We may have other kinds of boundary conditions, for example, inflow/outflow as well as the periodic boundary conditions.

2.2 Properties of the Boltzmann Equation

In this section we state few important properties of the Boltzmann equation without proof. For other properties and detailed proofs we refer [9, 19, 24].

Lemma 2.1. (Collision invariants) *The collision invariants are the functions $\psi(\mathbf{v})$ satisfying*

$$\int_{\mathbb{R}^3} \psi(\mathbf{v}) J(f,g) d\mathbf{v} = 0, \ \forall f,g \geq 0$$

if and only if $\psi(\mathbf{v}) = a + \mathbf{b} \cdot \mathbf{v} + c \, ||\mathbf{v}||^2$, *where the constants a, c are the scalars and the vector* $\mathbf{b} \in \mathbb{R}^3$.

The elementary collision invariants are ψ_α $(0 \leq \alpha \leq 4)$ where $\psi_0 = 1$, $\psi_i = v_i$, $(1 \leq i \leq 3)$ and $\psi_4 = \frac{1}{2} ||\mathbf{v}||^2$. For $f = g \geq 0$, we have

$$\int_{\mathbb{R}^3} \psi_\alpha J(f,f) d\mathbf{v} = 0, \ \ (0 \leq \alpha \leq 0). \tag{2.10}$$

Equation (2.10) physically tells that during the evolution process the collision operator $J(f,f)$ preserves mass, momentum and energy.

Lemma 2.2. *For every distribution function* $f \geq 0$ *satisfying the Boltzmann equation, the following inequality holds*

$$\int_{\mathbb{R}^3} J(f,f) \ln f d\mathbf{v} \leq 0.$$

"Equality" holds if and only if $\ln f$ *is collision invariant or equivalently*

$$f = e^{a + \mathbf{b} \cdot \mathbf{v} + c||\mathbf{v}||^2}.$$

Theorem 2.1. *The equilibrium distribution function satisfying* $J(f,f) = 0$ *is given by Maxwellian distribution, or Maxwellian*

$$f_M(\mathbf{v}) = A e^{-\beta ||\mathbf{v} - \mathbf{w}||^2}, \tag{2.11}$$

where A, β *and* $\mathbf{w} \in \mathbb{R}^3$ *are the parameters.*

Theorem 2.2. (H-theorem) *In the spatially homogeneous case, the tendency of a gas relax to a thermodynamic equilibrium is expressed by the Boltzmann's H-theorem*

$$\frac{d}{dt} H \leq 0, \ \ H = \int_{\mathbb{R}^3} f \ln f d\mathbf{v}. \tag{2.12}$$

"Equality" holds if and only if f *is Maxwellian.*

Remark 2.3. There are two interpretation of the Boltzmann H-theorem [19]. First one is at the microscopic level which describes it as the likelihood of a microscopic state that in an isolated system the evolution is towards the most probable states. That means H, as a measure of unlikelihood, is also a measure of the information which f contains about the microscopic state, and this information decrease with time, because the Boltzmann equation describes an evolution towards more likely one. The second interpretation of H is at macroscopic level where negative H is related to the thermodynamic entropy of the gas and it is non-decreasing quantity in the system.

2.3 The Macroscopic Balance Equations

The microscopic description or the solution $f(t,\mathbf{x},\mathbf{v})$ of the Boltzmann equation (2.2) itself is often not the quantity of interest. The basic quantities of the interest are the macroscopic observable ones, like the density $\rho(t,\mathbf{x})$, bulk (or mean) velocity $\mathbf{u} = \mathbf{u}(t,\mathbf{x})$ and the specific total energy $E = E(t,\mathbf{x})$ of the gas, which are the different moments of $f(t,\mathbf{x},\mathbf{v})$ and defined by [19, 24, 89]

$$\rho = \int_{\mathbb{R}^3} f(t,\mathbf{x},\mathbf{v})d\mathbf{v}, \tag{2.13}$$

$$\rho\mathbf{u} = \int_{\mathbb{R}^3} \mathbf{v}f(t,\mathbf{x},\mathbf{v})d\mathbf{v}, \tag{2.14}$$

$$\rho E = \int_{\mathbb{R}^3} \frac{1}{2}||\mathbf{v}||^2 f(t,\mathbf{x},\mathbf{v})d\mathbf{v}. \tag{2.15}$$

The quantity $\rho\mathbf{u}$ that appears in the equation (2.14) is the mass flux or the momentum density of the gas. The quantity of similar nature are the momentum flux, specific internal energy and the energy flux of the gas.

We can express the momentum flux by

$$m_{ij} = \int_{\mathbb{R}^3} v_i v_j f(t,\mathbf{x},\mathbf{v})d\mathbf{v} = \rho u_i u_j + \varphi_{ij} \ \ (1 \leq i \leq 3), \tag{2.16}$$

where $\mathbf{v} = (v_1, v_2, v_3)$, $\mathbf{u} = (u_1, u_2, u_3)$ denote the components of velocities and $\varphi = (\varphi_{ij})$, $1 \leq i, j \leq 3$, is the stress tensor defined by

$$\varphi_{ij} = \int_{\mathbb{R}^3} (v_i - u_i)(v_j - u_j) f(t,\mathbf{x},\mathbf{v})d\mathbf{v} \ \ (1 \leq i \leq 3). \tag{2.17}$$

Equation (2.16) shows that the momentum flux is described by the components of a symmetric tensor of second order, because we need to describe the flow in the ith direction of the momentum in the jth direction. It can also be seen in a macroscopic description that only a part of this tensor will be identified as a bulk momentum flow, because in general, m_{ij} will be different from zero even in the absence of a macroscopic motion ($\mathbf{u} = \mathbf{0}$). The microscopic momentum flow is associated with the stress tensor φ and it is equivalent to the force distributed on the boundary of any region of gas, according to the macroscopic description. We can also rewrite the specific total energy (2.15) into the form

$$\rho E = \int_{\mathbb{R}^3} \frac{1}{2}||\mathbf{v}||^2 f(t,\mathbf{x},\mathbf{v})d\mathbf{v} = \frac{1}{2}\rho||\mathbf{u}||^2 + \rho e, \tag{2.18}$$

where e is the internal energy, defined by

$$\rho e = \int_{\mathbb{R}^3} \frac{1}{2}||\mathbf{v} - \mathbf{u}||^2 f(t,\mathbf{x},\mathbf{v})d\mathbf{v}. \tag{2.19}$$

Finally, we define the energy flux of the gas by

$$r_i = \int_{\mathbb{R}^3} \frac{1}{2} ||\mathbf{v}||^2 v_i f(t, \mathbf{x}, \mathbf{v}) d\mathbf{v}$$

$$= \rho u_i \left(\frac{1}{2} ||\mathbf{u}||^2 + e \right) + \sum_{j=1}^{3} u_j \varphi_{ij} + q_i \quad (1 \leq i \leq 3), \qquad (2.20)$$

where $\mathbf{q} = (q_1, q_2, q_3)$ is the heat flux vector, defined by

$$q_i = \int_{\mathbb{R}^3} (v_i - u_i) \frac{1}{2} ||\mathbf{v} - \mathbf{u}||^2 f(t, \mathbf{x}, \mathbf{v}) d\mathbf{v}. \qquad (2.21)$$

The decomposition of energy flux (2.20) show that the microscopic energy flow is a sum of a macroscopic flow of energy (both kinetic and internal), of the work (per unit area and unit time) done by stresses, and of the heat flow. We also have

$$\sum_{i=1}^{3} \varphi_{ij} = \int_{\mathbb{R}^3} ||\mathbf{v} - \mathbf{u}||^2 f(t, \mathbf{x}, \mathbf{v}) d\mathbf{v} = 2\rho e \qquad (2.22)$$

and, therefore, it is convenient to define the gas pressure as 1/3 of the trace (i.e. sum of the three diagonal terms) of φ and thus given by

$$p = \frac{1}{3} \sum_{i=1}^{3} \varphi_{ij} = \frac{2\rho e}{3} = \frac{1}{3} \int_{\mathbb{R}^3} ||\mathbf{v} - \mathbf{u}||^2 f(t, \mathbf{x}, \mathbf{v}) d\mathbf{v}. \qquad (2.23)$$

For the monoatomic perfect gas, equation of state

$$p = \rho RT \qquad (2.24)$$

holds, where R is the specific gas constant and T is the temperature of the gas. Using the equation of state (2.24) in (2.23), we have

$$T = \frac{2e}{3R} \quad \text{or} \quad e = \frac{3}{2} RT \qquad (2.25)$$

Now, to get the macroscopic description supplied by the continuum gas dynamics from the microscopic description supplied by the kinetic theory, we multiply the Boltzmann equation (2.2) by its five collision invariants $1, v_i, \frac{1}{2} ||\mathbf{v}||^2 \ (1 \leq i \leq 3)$, and integrate with respect to the velocity space $\mathbf{v} \in \mathbb{R}^3$, and by changing the order of integration and differentiation, we get the local conservation laws

$$\left. \begin{aligned} \frac{\partial}{\partial t} \int_{\mathbb{R}^3} f(t, \mathbf{x}, \mathbf{v}) d\mathbf{v} + \nabla_{\mathbf{x}} \cdot \int_{\mathbb{R}^3} \mathbf{v} f(t, \mathbf{x}, \mathbf{v}) d\mathbf{v} = 0, \\ \frac{\partial}{\partial t} \int_{\mathbb{R}^3} v_i f(t, \mathbf{x}, \mathbf{v}) d\mathbf{v} + \nabla_{\mathbf{x}} \cdot \int_{\mathbb{R}^3} v_i \mathbf{v} f(t, \mathbf{x}, \mathbf{v}) d\mathbf{v} = 0, \\ \frac{\partial}{\partial t} \int_{\mathbb{R}^3} \frac{1}{2} ||\mathbf{v}||^2 f(t, \mathbf{x}, \mathbf{v}) d\mathbf{v} + \nabla_{\mathbf{x}} \cdot \int_{\mathbb{R}^3} \frac{1}{2} ||\mathbf{v}||^2 \mathbf{v} f(t, \mathbf{x}, \mathbf{v}) d\mathbf{v} = 0, \end{aligned} \right\} \qquad (2.26)$$

for $(1 \leq i \leq 3)$, which correspond to the mass, momentum and energy conservation, respectively. Now using the definitions introduced in (2.13 - 2.21) to the system of equations (2.26), we have the following lemma:

Lemma 2.3. (Conservation laws) *Assume that f is the solution of the Boltzmann equation (2.2). Then the above moments of f satisfies the following system of conservation equations*

$$\left.\begin{aligned}
\frac{\partial \rho}{\partial t} + \nabla \cdot (\rho \mathbf{u}) &= 0 \\
\frac{\rho \mathbf{u}}{\partial t} + \nabla \cdot (\rho \mathbf{u} \otimes \mathbf{u} + \varphi) &= \mathbf{0} \\
\frac{\partial}{\partial t}\left(\rho\left(\frac{1}{2}\|\mathbf{u}\|^2 + e\right)\right) + \nabla \cdot \left(\rho \mathbf{u}\left(\frac{1}{2}\|\mathbf{u}\|^2 + e\right) + \varphi \cdot \mathbf{u} + \mathbf{q}\right) &= 0
\end{aligned}\right\} \qquad (2.27)$$

The system of equations (2.27) is the basic equations of continuum mechanics, in particular of macroscopic gas dynamics, however, this system of equation is not closed, since there are five equations for the 13 unknowns $\rho, \mathbf{u}, T, \varphi, \mathbf{q}$ if the equation (2.25) is taken into account. In order to have a closed system, one must have some expression for stress tensor φ and heat flux $\mathbf{q}$ in terms of $\rho, \mathbf{u}, e$. Otherwise, one has to go back to Boltzmann equation (2.2) and solve it; and once this has been done, everything is done, and system of equation (2.27) is useless ! One way to close this system is by assuming the distribution function f to be Maxwellian. In this case, we get the well-known model for the fluid so-called the Euler equations [24, 83].

We note that if we apply the equations (2.13), (2.14) and (2.19) to the Maxwellian given by (2.11), we find that the constant $\mathbf{w}$ appearing in the latter equation is actually the mean flow velocity $\mathbf{u}$, while

$$A = \left(\frac{\rho}{2\pi RT}\right)^{3/2}, \quad \beta = \frac{3}{4e} = \frac{1}{2RT} \qquad (2.28)$$

Thus the Maxwellian f_M in the equation (2.11) has the following form

$$f_{\mathrm{M}}(\mathbf{v}) = \frac{\rho}{(2\pi RT)^{3/2}} exp\left(-\frac{\|\mathbf{v} - \mathbf{u}\|^2}{2RT}\right). \qquad (2.29)$$

Here, the parameters ρ, $\mathbf{u}$ and T depend on the position $\mathbf{x}$ and time t. Therefore we call f_{M} a local Maxwellian. If the distribution function f is the local Maxwellian (2.29), applying it in the equations (2.17) and (2.21) yield

$$\varphi = p\mathbb{I} = (\rho RT)\mathbb{I} \quad \text{and} \quad \mathbf{q} = \mathbf{0}, \qquad (2.30)$$

where $\mathbb{I}$ is the identity matrix. Therefore we have the following corollary:

Corollary 2.1. (Euler equations) *If f is the local Maxwellian f_M, then the macroscopic quantities ρ, $\mathbf{u}$ and T of f_M satisfy the following compressible Euler equa-*

tions:

$$\left.\begin{array}{r} \dfrac{\partial \rho}{\partial t} + \nabla \cdot (\rho \mathbf{u}) = 0, \\[2mm] \dfrac{\partial}{\partial t}(\rho \mathbf{u}) + \nabla \cdot (\rho \mathbf{u} \otimes \mathbf{u}) + \nabla p = \mathbf{0}, \\[2mm] \dfrac{\partial}{\partial t}\left(\rho\left(\dfrac{1}{2}\|\mathbf{u}\|^2 + e\right)\right) + \nabla \cdot \left(\rho \mathbf{u}\left(\dfrac{1}{2}\|\mathbf{u}\|^2 + e + p\right)\right) = 0, \end{array}\right\} \qquad (2.31)$$

where the pressure p and the specific internal energy e are given by the equations (2.24) and (2.25), respectively. This system consists of five equations and six unknowns, and it is a closed system together with the equation of state (2.24). One has to solve the compressible Euler equations with appropriate initial and boundary conditions. There exist other ways to obtain the Euler equations from the Boltzmann equation [24].

The fact that the distribution function f is a Maxwellian (or close enough to it) can be justified by scale analysis. The limit obtained from scale analysis is called the hydrodynamic limit [24].

We consider the parameter ε, arbitrary small. We introduce the new space and time variables

$$\mathbf{r} = \varepsilon \mathbf{x}, \ \ \tilde{t} = \varepsilon t.$$

The velocity is kept fixed in this scaling. Then the scaled Boltzmann equation can be expressed in the form

$$\frac{\partial f}{\partial \tilde{t}} + \mathbf{v} \cdot \nabla_{\mathbf{r}} f = \frac{1}{\varepsilon} J(f, f). \qquad (2.32)$$

Usually, one considers ε to be the order of the Knudsen number Kn [24]. As ε tends to zero, we expect that the collision operator $J(f,f)$ tends to zero and by theorem 2.1, f tends to f_{M}, where the macroscopic quantities ρ, $\mathbf{u}$ and T obtained as the moments of the solution of the Boltzmann equation satisfying the compressible Euler equations (2.31).

The classical asymptotic methods for solving the Boltzmann equation are methods of Hilbert's expansion [24], Chapman-Enskog's expansion [23] and Grad's 13 moments expansion [30]. In these expansions, the hydrodynamic limits of the Boltzmann equation are derived in terms of macroscopic variables. The resulting equations are either the Euler or the Naviver-Stokes equations. For example, the Chapman-Enskog method provides a solution of the Boltzmann equation for a restricted set of problems in which the distribution function f is perturbed by a small amount from the equilibrium Maxwellian distribution. It is assumed that the distribution function may be expressed in the form of the power series [9]

$$f = f_0 + \varepsilon f_1 + \varepsilon^2 f_2 + \cdots, \qquad (2.33)$$

where ε is a parameter which may be regarded as a measure of either the mean collision time or the Knudsen number. The zeroth order approximation f_0 is the Maxwellian f_M in the equation (2.29) whose parameters are the solution of the compressible Euler equations (2.31). The first order approximation gives the Chapman-Enskog distribution [9, 89]

$$f_{CE}(t,\mathbf{x},\mathbf{v}) = f_M(t,\mathbf{x},\mathbf{v})\left[1 + \frac{2}{5}\frac{\mathbf{q}\cdot\mathbf{c}}{\rho(RT)^2}\left(\frac{||\mathbf{c}||^2}{2RT} - \frac{5}{2}\right) + \frac{1}{2}\frac{\tau : \mathbf{c}\otimes\mathbf{c}}{\rho(RT)^2}\right], \qquad (2.34)$$

where $\mathbf{c} = \mathbf{v} - \mathbf{u}$, and the stress tensor φ and heat flux vector $\mathbf{q}$ for the monoatomic gas are given by

$$\varphi = p\mathbb{I} - \tau, \quad \tau = \mu\left[(\nabla\mathbf{u} + \nabla\mathbf{u}^T) - \frac{2}{3}(\nabla\cdot\mathbf{u})\mathbb{I}\right], \qquad (2.35)$$

$$\mathbf{q} = -\kappa\nabla T, \qquad (2.36)$$

where $\mu = \mu(t,\mathbf{x})$ and $\kappa = \kappa(t,\mathbf{x})$ are the dynamic viscosity and thermal conductivity of the gas, respectively. They are of order ε. For example, first approximation for the viscosity and thermal conductivity of a monoatomic gas is given by [9, 89]

$$\mu = \frac{5}{16d^2}\sqrt{\frac{m_g k_B T}{\pi}}, \quad \kappa = \frac{15k_B}{4m_g}\mu, \qquad (2.37)$$

where k_B is the Boltzmann constant, and d and m_g are the mass and the diameter of a gas molecule, respectively. Therefore we have the following corollary:

Corollary 2.2. (Navier-Stokes equations) *If f is the Chapman-Enskog distribution f_{CE}, then the macroscopic quantities $\rho, \mathbf{u}$ and T of f_{CE} satisfy the following compressible Navier-Stokes equations:*

$$\left.\begin{aligned} \frac{\partial\rho}{\partial t} + \nabla\cdot(\rho\mathbf{u}) &= 0, \\ \frac{\partial}{\partial t}(\rho\mathbf{u}) + \nabla\cdot(\rho\mathbf{u}\otimes\mathbf{u}) &= -\nabla p + \nabla\cdot\tau, \\ \frac{\partial}{\partial t}(\rho E) + \nabla\cdot(\rho E\mathbf{u}) &= \nabla\cdot\left((-p\mathbb{I} + \tau)\mathbf{u}\right) + \nabla\cdot(\kappa\nabla T), \end{aligned}\right\} \qquad (2.38)$$

where $E = \frac{1}{2}||\mathbf{u}||^2 + e$ is the specific total energy. The pressure p and the specific internal energy e are given by the equations (2.24) and (2.25), respectively. This system consists of five equations and thirteen unknowns, and it is a closed system together with the equations (2.35), (2.36) and the equation of state (2.24).

Since we solve the Navier-Stokes equations (2.38) with a mesh free Lagrangian particle method, we express them in Lagrangian form with respect to the primitive variables as

$$\left.\begin{aligned}
\frac{D\mathbf{x}}{Dt} &= \mathbf{u}, \\
\frac{D\rho}{Dt} &= -\rho\nabla\cdot\mathbf{u}, \\
\frac{D\mathbf{u}}{Dt} &= \frac{1}{\rho}\left(-\nabla p+\nabla\cdot\tau\right), \\
\frac{DT}{Dt} &= \frac{1}{c_v\rho}\left(-p\nabla\cdot\mathbf{u}+(\tau\cdot\nabla)\cdot\mathbf{u}+\nabla\cdot(\kappa\nabla T)\right),
\end{aligned}\right\} \tag{2.39}$$

where $\frac{D}{Dt}$ is the material derivative, c_v is the specific heat at the constant volume, given by $\frac{3}{2}R$ for a monoatomic gas. We have expressed the internal energy of the gas as $e = c_v T$.

The system of equations (2.39) has to be solved with appropriate initial and boundary conditions which are specified in the section where numerical experiments are performed. We take the values of the viscosity μ and thermal conductivity κ be fixed given by (2.37).

Chapter 3
Numerical Methods

We have already mentioned that the flow of the gas, in general, can be modeled by the Boltzmann equation. But it has been observed that for the small values of Knudsen numbers $Kn \ll 1$, the flow of the gas can also be modeled by the Navier-Stokes equations [9]. The analytical solution of the gas flow in a given domain is almost difficult to obtain and therefore we have to rely on an appropriate numerical scheme to solve the flow problems. In our work we mostly talk about the moving rigid body whose motion is caused by the surrounding gas in a given domain. Because of the movement of the rigid body, the domain occupied by the fluid changes continuously in time. The best numerical scheme to tackle this kind of problem is particle methods which can be simply implemented for wide varieties of flow problems with complex domain and rapidly changing geometry. In our work we have used direct simulation Monte Carlo method (DSMC) to solve the Boltzmann equation and the finite pointset method (FPM) to solve the Navier-Stokes equations. Both the numerical schemes are based on the particle methods and the brief review of these schemes are explained in the next sections.

3.1 Particle Method for the Boltzmann Equation

The flow of a dilute gas can not be described by the continuum models given by the Navier-Stokes and the Euler equations which describe the Newtonian fluids such as gases and simple liquids, over wide ranges of conditions. Although very useful, the continuum description of a fluid has its limit. The flow of a rarefied gas requires a kinetic theory description. In such cases, the continuum description based on partial differential equations is inadequate, and a particle-based approach is needed. As a result, various specialized methods for simulating such flow have been developed [1]. For the physicists, the best known particle-based algorithm is the molecular dynamics where each particle represents a gas molecule. In molecular dynamics, the trajectory of every molecule in the fluid is computed from the Newton's equations, given an empirically determined inter-molecule potential. Although molecular

dynamics is a useful technique in statistical mechanics, its application is limited to simple hydrodynamic flows due to its enormous computational effort. Molecular dynamic simulations of a dilute gas are extremely time-consuming even when run on most powerful computers. Fortunately there is an efficient alternative particle-based method to simulate a dilute gas known as direct simulation Monte Carlo (DSMC), originally developed by Bird [9] in the 1960. This method was derived on the basis of physical intuition. DSMC originated by Bird is practicable in terms of computational effort and has given satisfying results in many applications. Wagner [93] has proved that the Bird's simulation is convergent to the solution of the Boltzmann equation in the limit of infinite number of molecules. More sophisticated and involved simulation methods were also presented by various authors [18]; the consistency and convergence of some of these methods look more promising. Later Nanbu [60] suggested a different simulation procedure, which he derived directly from the Boltzmann equation. The collision was done in a totally different way from the Bird's method, and propagation of chaos seems to be assured from at least a formal viewpoint. Babovsky [5] later gave the rigorous mathematical interpretation of Nanbu's scheme; his analysis shows that one major step in the procedure amounts to a suitable linearization of the Boltzmann equation over short time intervals. This idea leads in a natural way to a linearized time-discretized version of the Boltzmann equation, and the effect of the collision operator in this equation is efficiently modeled by a certain Markov process.

DSMC method can be viewed as a Monte Carlo method for solving the time dependent non-linear Boltzmann equation which describes the evaluation of a dilute gas at the level of the single-molecular distribution function. Rather than exactly calculating the collisions as in the molecular dynamics, the DSMC method generates collision stochastically with the scattering rates and post collision velocity distribution determined from the kinetic theory of a dilute gas. The method has been thoroughly tested in high Knudsen number flows over past more than 30 years and found to be in excellent agreement with both experimental data and molecular dynamic computations. The DSMC method has been used successfully for several decades in the study of rarefied gas flows and its exciting application can also be found in chemistry and physics [1]. We present a brief description of DSMC method for flow of the rarefied gas in a micro-scale domain. Detailed explanation of DSMC method can be found in [9].

In the micro geometry flow problems, the system consists of a spatial bounded domain with thermal boundary wall at temperature T_{w}. The domain contains simple monoatomic gas, for example Argon gas in our study, which has only three translational degrees of freedom. The physical domain is divided into $\mathscr{N}$ number of regular DSMC cells, each of which has linear dimension less than a mean free path λ [9]. A rigid body that is suspended in the gas domain overlaps the DSMC cells. The overlapped cells, we call inactive DSMC cells. We store all the information, if needed, only in the non-overlapping cells, we call them active DSMC cells. Initially n_0 molecules are randomly distributed in each active DSMC cell with uniform den-

sity throughout the system with position of each molecule being $\mathbf{x}$, such that there are at least minimum number of simulated molecules in each cell. Each simulated molecule represents a large number of real physical molecules in the system. In this sense DSMC method solves the Boltzmann equation using a representative random sample drawn from the actual velocity distribution. This representation allows us to model many systems of interest using only $(10^4 - 10^5)$ simulated molecules (although simulations using over 10^8 simulated molecules are not uncommon) [1]. In addition to its location $\mathbf{x}$, each molecule is initialized with a velocity $\mathbf{v}$ chosen from initial velocity distribution (2.3). Thus in DSMC algorithm the state of the system is given by the position and the velocity of the DSMC molecules $\{\mathbf{x}, \mathbf{v}\}$. The molecule evolution is integrated in time step Δt and the method is based on the time splitting of the Boltzmann equation for free transport and the collision. This splitting of the evaluation between the advection and collision is accurate only when the time step Δt is a fraction of the mean collision time [9].

Introducing the fractional steps, one first solves the free transport equation (the collisionless Boltzmann equation). In this step, the molecules are moved as if they did not interact, that is, their positions are updated to $\mathbf{x} + \mathbf{v}\Delta t$. Molecules that reach a boundary are processed according to appropriate boundary condition as described below. If a molecule strikes a wall, the time for the collision is determined by tracing the straight line trajectory from the initial location $\mathbf{x}$ to the point of impact $\mathbf{x}_\mathrm{w} \in \partial\Omega$ to the wall. The time of flight from the molecule's initial position to the point of impact is $\Delta t_\mathrm{w} = (\mathbf{x}_\mathrm{w} - \mathbf{x}) \cdot \mathbf{n}/(\mathbf{v} \cdot \mathbf{n})$, where $\mathbf{n}$ is the unit normal to the surface. After striking the surface, the molecule moves off with a new velocity as prescribed by the boundary conditions and with the remaining time $\Delta t - \Delta t_\mathrm{w}$.

DSMC method employs various types of boundary conditions, for example, specular, diffuse and periodic surfaces. When a molecule strikes a specular surface, its component of velocity normal to the surface is reversed and other two tangential components remain unchanged. When molecule strikes a diffuse boundary wall which is at temperature T_w and velocity $\mathbf{V}_\mathrm{w}$, all the three components of the velocity are reset according to half-range Maxwellian distribution given by [83]

$$f_d = |\,(\mathbf{v} - \mathbf{V}_\mathrm{w}) \cdot \mathbf{n}\,|\, \frac{1}{2\pi(RT_\mathrm{w})^2} exp\Big(-\frac{||\mathbf{v} - \mathbf{V}_\mathrm{w}||^2}{2RT_\mathrm{w}}\Big),\ (\mathbf{v} - \mathbf{V}_\mathrm{w}) \cdot \mathbf{n} > 0. \qquad (3.1)$$

In other words, each molecule colliding with the diffuse boundary wall is re-emitted with the new molecular velocity $\mathbf{v}'$ sampled from distribution given by (3.1). Let $\mathbf{t}_1, \mathbf{t}_2, \mathbf{n}$ be a local orthonormal basis with $\mathbf{n}$ normal to the wall, then the three components of the re-emitted velocity $\mathbf{v}'$ relative to the wall velocity $\mathbf{V}_\mathrm{w}$ with respect to the basis $\mathbf{t}_1, \mathbf{t}_2, \mathbf{n}$ are given by (derivation is presented in the Appendix B)

$$v'_{t_1} = \sqrt{-2RT_w \log \alpha_1} \cos(2\pi\alpha_2),$$
$$v'_{t_2} = \sqrt{-2RT_w \log \alpha_1} \sin(2\pi\alpha_2),$$
$$v'_n = \sqrt{-2RT_w \log \alpha_3},$$

where $\alpha_1, \alpha_2, \alpha_3$ are the uniformly distributed random numbers between 0 and 1. Hence the re-emitted velocity from the diffuse boundary wall is given by

$$\mathbf{v}' = v'_{t_1}\mathbf{t}_1 + v'_{t_2}\mathbf{t}_2 + v'_n\mathbf{n} + \mathbf{V}_w. \tag{3.2}$$

The problem of surface effects can be overcome by implementing periodic boundary conditions. In mathematical models and computer simulations, periodic boundary conditions are a set of boundary conditions that are often used to simulate a large system by modeling a small part that is far from its edge. Periodic boundary conditions resemble the topologies of some video games; a simulation box of a geometry suitable for perfect three-dimensional tiling is defined, and when an object passes through one face of the box, it reappears on the opposite face with the same velocity [4].

After, all the molecules have been moved and boundary conditions are processed, a given number of molecules are selected randomly for the collision. The rules for this random selection process are obtained from the kinetic theory, for example, see [9] . We select those molecules that are near to each other as collision partners. In other words, molecules far from each other should not be allowed to interact. To implement this condition, we sort the molecules into spatial active DSMC cells and allow only molecules in the same cell to collide. In each cell, a set of representative collisions is processed at each time step. All pairs of molecules in a cell are considered to be candidate for collision partners, regardless of their positions within the cell. Because only the magnitude of the relative velocity between molecules is used in determining their collision probability, even the molecules that are moving away from each other may collide. This condition allows two molecules to collide by simply being located within the same cell; no other positional information is used in the evaluation of collisions. We give a brief explanation of elastic binary collision for hard sphere model to compute the post-collision velocity of the two colliding gas molecules.

The collision operator $J(f, f)$ in the Boltzmann equation (2.2) is derived under the consideration of binary collisions involving just two molecules. The collision is considered to be an elastic in which there is no interchange of translation and internal energy. Given the pre-collision velocities $\mathbf{v}$ and $\mathbf{v}_*$, and the given physical properties of the molecules and the orientation of the trajectories of the two collision partners in a typical binary collision, we can determine the post-collision velocities $\mathbf{v}'$ and $\mathbf{v}'_*$.
The linear momentum and the energy must be conserved in the elastic collision and hence the post-collision velocities are given by [9], (detailed derivation is presented in the Appendix A)

$$\left.\begin{array}{l} \mathbf{v}' = \mathbf{v}_c + \dfrac{1}{2}\mathbf{v}'_r \\[2mm] \mathbf{v}'_* = \mathbf{v}_c - \dfrac{1}{2}\mathbf{v}'_r, \end{array}\right\} \tag{3.3}$$

where $\mathbf{v}_c = \frac{1}{2}(\mathbf{v}+\mathbf{v}_*)$ is the velocity of the center of mass of the pair of colliding molecules. It can be found that the magnitude of pre-collision and post-collision relative velocities $\mathbf{v}_r = \mathbf{v} - \mathbf{v}_*$ and $\mathbf{v}'_r = \mathbf{v}' - \mathbf{v}'_*$ between the molecules is unchanged by collision, i.e. $||\mathbf{v}_r|| = ||\mathbf{v}'_r||$. Since both $\mathbf{v}_c$ and $\mathbf{v}_r$ may be calculated from the pre-collision velocities, the determination of the post-collision velocities reduces to the calculation of the change in direction θ of the relative velocity vector after collision. The calculation of direction θ depends on the choice of the collision model, see [9] for detail. The required expression of the components (u'_r, v'_r, w'_r) of the post-collision relative velocity vector $\mathbf{v}'_r$ are given by [9]

$$\left.\begin{array}{l} u'_r = u_r\cos\theta + \sqrt{v_r^2 + w_r^2}\,\sin\theta\sin\varepsilon, \\[3mm] v'_r = v_r\cos\theta + \dfrac{(||\mathbf{v}_r||\,w_r\cos\varepsilon - u_r v_r\sin\varepsilon)\sin\theta}{\sqrt{v_r^2 + w_r^2}}, \\[4mm] w'_r = w_r\cos\theta - \dfrac{(||\mathbf{v}_r||\,v_r\cos\varepsilon + u_r w_r\sin\varepsilon)\sin\theta}{\sqrt{v_r^2 + w_r^2}}, \end{array}\right\} \tag{3.4}$$

where (u_r, v_r, w_r) are the components of the pre-collision relative velocity vector $\mathbf{v}_r$, and ε is the angle between the collision plane (plane in which the trajectories of two colliding gas molecules lie in the center of mass frame of reference) and some reference plane. In our DSMC simulation we employ the hard sphere collision model, and for this model the deflection angle θ has the following expression

$$\cos\left(\frac{\theta}{2}\right) = \frac{b}{d}, \text{ and } 0 \le \frac{b}{d} \le 1, \tag{3.5}$$

where d is the diameter of the gas molecule and b is the distance of the closest approach of the undisturbed trajectories of two colliding gas molecules in the center of mass frame of reference. In hard sphere collision it can be concluded that the scattering from the hard sphere molecules is isotropic in the center of mass reference. That means, all directions are equally likely for $\mathbf{v}'_r$. Thus in our numerical simulation we compute $\sin\theta$, $\cos\theta$ from equation (3.5) by using uniformly distributed random number $\alpha_1 \in [0,1]$, and $\sin\varepsilon$ and $\cos\varepsilon$ are computed by using another uniformly distributed random number $\alpha_2 \in [0,1]$. From equation (3.5), we can write

$$\cos\theta = 2\left(\frac{b}{d}\right)^2 - 1$$

and $\left(\frac{b}{d}\right)^2$ is uniformly distributed between 0 and 1 so that selection rule can be written as [9]

$$\cos\theta = 2\alpha_1 - 1,$$
$$\sin\theta = 2\sqrt{\alpha_1(1-\alpha_1)}.$$

Since ε is uniformly distributed in $[0, 2\pi]$, so

$$\cos\varepsilon = \cos(2\pi\alpha_2),$$
$$\sin\varepsilon = \sin(2\pi\alpha_2).$$

Now substituting the expressions of $\cos\theta$, $\sin\theta$, $\cos\varepsilon$ and $\sin\varepsilon$ in the equations (3.4), we get the complete information of the post-collision velocity of two colliding gas molecules from the equation (3.3). The flow chart for a typical DSMC simulation is shown in the figure 3.1. For more detail we refer to [1, 9].
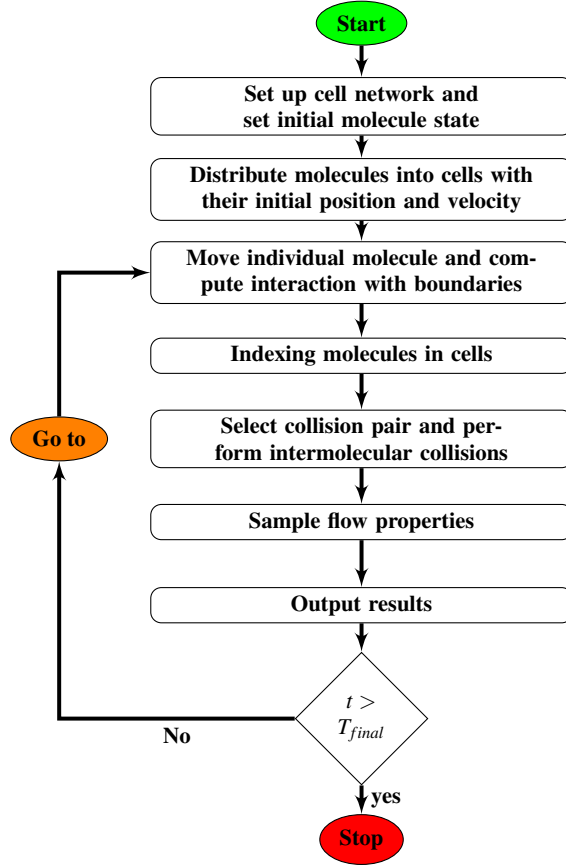
Fig. 3.1: DSMC flow chart.

Since the DSMC method is inherently stochastic in nature, the most physical quantities of interest are computed as averages. Let $n = n(t, \tilde{\mathbf{x}})$ be the number of molecules at position $\tilde{\mathbf{x}}$ at time t. Here, position $\tilde{\mathbf{x}}$ is generally taken as the DSMC cell center. Initially $n_0 = n(0, \tilde{\mathbf{x}})$ number of simulated gas molecules are distributed at each active DSMC cell at position $\tilde{\mathbf{x}}$. The values of mass density $\rho(t, \tilde{\mathbf{x}})$, velocity $\mathbf{u}(t, \tilde{\mathbf{x}})$, temperature $T(t, \tilde{\mathbf{x}})$, pressure $p(t, \tilde{\mathbf{x}})$, pressure tensor $\varphi(t, \tilde{\mathbf{x}})$ at the position $\tilde{\mathbf{x}}$ at time t are measured as

$$\rho = \frac{n}{n_0} \rho_0, \tag{3.6}$$

$$\mathbf{u} = \frac{1}{n} \sum \mathbf{v}, \tag{3.7}$$

$$T = \frac{1}{3R} \left(\frac{1}{n} \sum |\mathbf{v}|^2 - |\mathbf{u}|^2 \right), \tag{3.8}$$

$$p = \rho R T, \tag{3.9}$$

$$\varphi = \frac{\rho_0}{n_0} \sum \mathbf{v} \otimes \mathbf{v} - \rho \mathbf{u} \otimes \mathbf{u}, \tag{3.10}$$

where ρ_0 is the initial density of the gas molecules and sum is taken over the number of molecules in the cell at location $\tilde{\mathbf{x}}$.

3.2 FPM for the Compressible Navier-Stokes Equations

We solve the Navier-Stokes equations (2.39) by the finite pointset method (FPM). The FPM is a messfree and fully Lagrangian particle method. The fluid domain is represented by finite number of particles (pointset), which are so-called the numerical grid points and can be arbitrarily distributed. Particles move with fluid velocity and carry with them all the fluid information like density, velocity, pressure and so on. This method is found to be appropriate for flow problems with complicated and rapidly changing geometry, free surface flows and multiphase flows [84, 87]. In order to solve the Navier-Stokes equations (2.39) by using the FPM, one first fills the computational domain $\Omega \subset \mathbb{R}^d$, $d = 1, 2, 3$ by particles $\mathbf{x}_i \in \Omega$ and then approximates the spatial derivatives occurring on the right hand side of (2.39) at each particle position from its neighboring particles with the help of the weighed least squares method. This reduces the system of partial differential equations (2.39) into a time dependent system of ordinary differential equations (ODE). This system of equations can be solved by a simple integration scheme. The time steps for the compressible as well as the incompressible Navier-Stokes equations are restricted by CFL condition and by the value of the transport coefficient $max[\mu/\rho, \kappa/(\rho c_v)]$. The brief introduction of the least square approximation for the spatial derivatives is presented in the next subsection and detail can be found in papers [84, 88]. We note that we need to introduce a particle management scheme during the simulation. Because of the Lagrangian description of the method, particles may accumulate or thin out causing the holes in the computational domain. This gives rise to some in-

stability of the method. Therefore, we have to add or remove the particles. If the distance between a particle and its nearest neighbor is large enough, we add a new particle in the center. On the other hand, if the two particles are closer enough we remove both of them and add a new particle at the mid point. Users can specify their own measure of distance between two particle, how much far enough and much close enough is not permitted, accordingly the particles can be added and removed. The fluid dynamic quantities of newly added particle are approximated from their neighbor particles with the help of the least squares method.

3.2.1 Least square approximation of the spatial derivatives

The main advantage of the least square method is that it is very general and can be applied to very irregular moving geometries. In many practical applications the mesh plays the most important role in determining the solution, and many solvers lose their accuracy if the mesh is poorly constructed [84]. The least square method can be employed for the randomly distributed grid points to approximate the derivatives. In mesh free methods even if the initial discretization of the domain is done in regular grid points, their discretization becomes quite arbitrary once the grid points move with the fluid velocity. The general procedure for the approximation the derivatives of a function by FPM is described below.

In this method the particle positions represent the grids. To approximate the spatial derivatives at every grid points means the approximation of the derivatives at every particle position. Let $\Omega \subset \mathbb{R}^d$, $d = 1, 2, 3$ and $f : [0, T] \times \Omega \to R$ be a scalar function, d denotes the dimension of the space and $f_i(t)$ is its value at $\mathbf{x}_i$ for $i = 1, 2, \ldots, N$ at time t. Consider the problem to approximate the spatial derivatives of that particular function $f(t, \mathbf{x})$ at some particle position $\mathbf{x}$ based on the discrete function values of its neighbor points. In order to restrict the number of points we introduce a weight function $w = w(\mathbf{x}_i - \mathbf{x}; h)$ with small compact support, where h determines the size of the support. The weight function can be quite arbitrary, however it makes sense to choose a Gaussian weight function of the form [84]

$$
w(\mathbf{x}_i - \mathbf{x}; h) = \begin{cases} exp(-\alpha \frac{\|\mathbf{x}_i - \mathbf{x}\|^2}{h^2}), & \text{if } \frac{\|\mathbf{x}_i - \mathbf{x}\|}{h} \leq 1 \\ 0, & \text{else} \end{cases}
$$

where α is a positive constant and the radius h defines a set of neighboring particles around $\mathbf{x}$. We work on a user given radius h so that new particles will have to be brought into play as the particle distribution becomes too sparse or particles will have to be removed from the computation as they become too dense.

Let $P(\mathbf{x}, h) = \{\mathbf{x}_j : j = 1, 2, \ldots, m\}$ be the set of m neighbor points of $\mathbf{x} = (x, y, z)$ in a ball of radius h. We note that the central particle $\mathbf{x}$ is one element of the neighbor set $P(\mathbf{x}, h)$. The distribution of neighboring points need not to be uniform and it can

be quite arbitrary. For consistency reasons, some obvious restrictions are required, for example, in 3D there should be at least 9 particles in addition to the central point and they should neither be on the same plane nor on the same sphere, and in 2D there should be at least 5 particles other than the central point and they should not on the same line. In the following we derive the least squares method for three dimensional problems.

We determine the derivatives of a function by using the Taylor series expansion, and finally we apply the method of least squares approximation. Hence, consider m Taylor expansions of $f(t, \mathbf{x}_j)$ about $\mathbf{x}$

$$f(t,\mathbf{x}_j) = f(t,\mathbf{x}) + \sum_{\mathbf{k}} \frac{\partial^{|\mathbf{k}|} f}{\partial x^{k_1} \partial y^{k_2} \partial z^{k_3}} \frac{1}{\mathbf{k}!} (x_j - x)^{k_1} (y_j - y)^{k_2} (z_j - z)^{k_3} + e_j, \quad (3.11)$$

for $j = 1, \ldots, m$, where e_j is the error in the Taylor's expansion at the point $\mathbf{x}_j$. Here $\mathbf{k} = (k_1, k_2, k_3)^T \in \mathbb{N}_0^3$ denotes the multi-index of order $|\mathbf{k}| = k_1 + k_2 + k_3$ with $|\mathbf{k}| \neq 0$, $\mathbf{k}! = k_1! k_2! k_3!$ and $\mathbf{x}_j = (x_j, y_j, z_j)$.

Considering the Taylor's series only upto second derivatives, that means, taking $|\mathbf{k}| = 2$ and denoting the coefficients by

$$a_1 = \frac{\partial f}{\partial x}, \ a_2 = \frac{\partial f}{\partial y}, \ a_3 = \frac{\partial f}{\partial z}, \ a_4 = \frac{\partial^2 f}{\partial x^2}, \ a_5 = \frac{\partial^2 f}{\partial x \partial y},$$
$$a_6 = \frac{\partial^2 f}{\partial x \partial z}, \ a_7 = \frac{\partial^2 f}{\partial y^2}, \ a_8 = \frac{\partial^2 f}{\partial y \partial z}, \ a_9 = \frac{\partial^2 f}{\partial z^2}.$$

Let us assume that $f = f(t, \mathbf{x})$ is the known discrete function value at the particle position $\mathbf{x}$. For $m > 9$, this system is overdetermined with respect to the unknowns a_i, $i = 1, 2, \cdots, 9$ and can be rewritten as

$$\mathbf{e} = M\mathbf{a} - \mathbf{b}, \quad (3.12)$$

where

$$M = \begin{pmatrix} dx_1 & dy_1 & dz_1 & \frac{1}{2}dx_1^2 & dx_1 dy_1 & dx_1 dz_1 & \frac{1}{2}dy_1^2 & dy_1 dz_1 & \frac{1}{2}dz_1^2 \\ \vdots & \vdots & \vdots & \vdots & \vdots & \vdots & \vdots & \vdots & \vdots \\ dx_m & dy_m & dz_m & \frac{1}{2}dx_m^2 & dx_m dy_m & dx_m dz_m & \frac{1}{2}dy_m^2 & dy_m dz_m & \frac{1}{2}dz_m^2 \end{pmatrix},$$

$\mathbf{a} = (a_1, a_2, \ldots, a_9)^T$, $\mathbf{b} = (f_1 - f, \ldots, f_m - f)^T$, $\mathbf{e} = (e_1, \ldots, e_m)^T$ and $dx_j = x_j - x$, $dy_j = y_j - y$, $dz_j = z_j - z$. The unknown $\mathbf{a}$ is computed by minimizing a weighted error over the neighboring points. Thus, we have to minimize the following quadratic form

$$J = \sum_{j=1}^{m} w_j e_j^2 = (M\mathbf{a} - \mathbf{b})^T W (M\mathbf{a} - \mathbf{b}) \quad (3.13)$$

with

$$W = \begin{pmatrix} w_1 & 0 & \cdots & 0 \\ 0 & w_2 & \cdots & 0 \\ \vdots & \vdots & \ddots & \vdots \\ 0 & 0 & \cdots & w_m \end{pmatrix},$$

where $w_j = w(\mathbf{x}_j - \mathbf{x}; h)$. The minimization of J with respect to $\mathbf{a}$ formally yields (if $M^T W M$ is nonsingular)

$$\mathbf{a} = (M^T W M)^{-1} (M^T W) \mathbf{b}, \tag{3.14}$$

which gives the derivatives of the function $f(t, \mathbf{x})$ at a specific position $\mathbf{x}$ as a linear combination of the known values of the function $f(t, \mathbf{x}_j)$ at neighbor points $\mathbf{x}_j$, $j = 1, \ldots, m$ at an instant of time t.

3.2.2 Approximation of the spatial derivatives of the Navier-Stokes equations

The spatial derivatives in the right hand side of the system of equation (2.39) is approximated by using (3.14) at every point $\mathbf{x}_i \in \Omega$, $i = 1, \ldots, N$ and the system of equations (2.39) is then reduced to a system of ordinary differential equations:

$$\left. \begin{aligned} \frac{D\rho_i(t)}{Dt} &= -\rho_i(t) \Pi \nabla \cdot \mathbf{u}_i(t), \\ \frac{D\mathbf{u_i}(t)}{Dt} &= \frac{1}{\rho_i(t)} (-\Pi \nabla p_i(t) + \Pi \nabla \cdot \tau_i(t)), \\ \frac{DT_i(t)}{Dt} &= \frac{1}{\rho_i(t) c_v} \left(-p_i(t) \Pi \nabla \cdot \mathbf{u}_i(t) + \Pi (\tau_i(t) \cdot \nabla) \mathbf{u}_i(t) + \Pi \nabla \cdot (\kappa \nabla T_i) \right), \end{aligned} \right\} \tag{3.15}$$

with the equation of state $p_i(t) = \rho_i(t) R T_i(t)$ for all $i = 1, \ldots, N$ number of Lagrangian particles and $\Pi \nabla (.)$ denotes the least square approximation of $\nabla (.)$. Additionally, new position of Lagrangian particles is given by

$$\frac{d\mathbf{x}_i}{dt} = \mathbf{u_i}. \tag{3.16}$$

The system of ordinary differential equations (ODEs) (3.15) and (3.16) can be solved by a simple integration scheme. We use the explicit Euler scheme to solve these ODEs system.

Chapter 4
Moving Rigid Body in a Gas

4.1 The Force and the Torque on a Rigid Body

The rigid body suspended in a fluid moves because of the force and the torque exerted on it by the surrounding fluid. The problem of finding the force and the torque on a rigid body moving inside a fluid is central in many branches of engineering, so there is an enormous literature dedicated to the subject. In principle if the motion of the fluid is known, then the computation of the force and the torque reduces to the integration of fluid stresses on the body surface [79]. There are two kinds of forces which act on a matter in bulk. The first group are long-range forces like gravity which acts equally on all the matter within a small element of volume, and the total force is proportional to the size of the volume element. Long range forces may thus also be called volume or body forces. The second group are short range forces, which have direct molecular origin, decrease extremely rapid with increase of the distance between the interacting elements, and are appreciable only when that distance is of the order of the separation of the molecules of the fluids. They are negligible unless there is direct mechanical contact between the interacting elements because without contact none of the molecules of one of the elements is sufficiently close to a molecule of the other element. If an element of mass of fluid is acted on by short-range forces arising from the reaction with matter outside this element, these short-range force can act only on a thin layer adjacent to the boundary of the fluid element. The total of the short-range forces acting on the element is thus determined by the surface area of the element, and the volume of the element is not directly relevant.

The scaling law is helpful to analyze the physical properties of the microscale systems. A scaling law expresses the variation of physical quantities with the size L of given system, while keeping other quantities such as time, pressure, temperature, etc, constant. As an example, consider volume forces, such as gravity and inertia, and surface forces, such as surface tension and viscosity. The basic scaling law for the ratio of these two classes of forces can generally be expressed by [12]

$$\frac{\text{surface force}}{\text{volume force}} \propto \frac{L^2}{L^3} = L^{-1} \to \infty \text{ as } L \to 0$$

This scaling law implies that when scaling down to the microscale systems, the volume forces, which are very prominent in our daily life, become largely unimportant. Instead the surface forces become more dominant. In our work we are interested in a micro/nano size rigid body moving in a fluid contained in a micro/nano scale domain. Hence the effect of the volume forces, like gravity, is negligibly small compared to the surface forces, and these volume forces are not incorporated in our study. Now we explain briefly on the theory to compute the surface force exerted on the rigid body by surrounding fluid.

In a continuum flow if the motion of the fluid is known by solving the Navier-Stokes equations or in a kinetic description of the fluid flow the velocity distribution function of the Boltzmann equation is known, the force and the torque on the rigid body are computed by integrating the stress tensor on its surface. Let us consider a rigid body $B \subset \mathbb{R}^d$, $d = 1, 2, 3$, suspended in a fluid. Let $S(t) = \{\mathbf{y}(t) \in B\}$ be the configuration of the rigid body with boundary $\partial S(t)$ and center of mass $\mathbf{X}(t)$ at any moment of time t. The force $\mathscr{F}$ and the torque $\mathscr{T}$ exerted on the rigid body from the surrounding fluid are given by following theorem:

Theorem 4.1. *The force $\mathscr{F}$ and the torque $\mathscr{T}$ exerted on a rigid body by surrounding fluid are given by*

$$\mathscr{F} = \int_{\partial S} (-\varphi \cdot \mathbf{n}_s) dA, \tag{4.1}$$

$$\mathscr{T} = \int_{\partial S} (\mathbf{y} - \mathbf{X}) \times (-\varphi \cdot \mathbf{n}_s) dA, \tag{4.2}$$

where $\mathbf{n}_s$ is the outward normal to the boundary ∂S of the rigid body. The stress tensor φ is given by (2.17).

Proof. Suppose that an element dA of boundary ∂S of the rigid body B with unit normal $\mathbf{n}_s$ pointing toward the gas domain is moving with velocity $\mathbf{U}$. Let $\mathbf{C} = \mathbf{v} - \mathbf{U}$ is the velocity of a gas molecule relative to the element dA. Then the total momentum $\mathbf{p}$ of the gas molecules impinging on the element dA during the time interval dt is given by

$$\mathbf{p} = dA dt \int_{\mathbf{C} \cdot \mathbf{n_s} < 0} (-\mathbf{C} \cdot \mathbf{n}_s) \mathbf{v} f d\mathbf{v}. \tag{4.3}$$

The integration is extended only over that part of the velocity-range for which $\mathbf{C} \cdot \mathbf{n}_s$, the $\mathbf{n}_s$-component of the velocity of a molecule relative to dA, is negative (since only molecules for which $\mathbf{C} \cdot \mathbf{n_s} < 0$ can impinge on the surface). The minus sign before $\mathbf{C} \cdot \mathbf{n_s}$ is introduced because $\mathbf{C} \cdot \mathbf{n_s}$ enters into the integrand through the mass of the molecules entering dA during dt, and this number is essentially positive. Similarly the total momentum $\mathbf{p}'$ of the molecules re-emitting from dA during the time interval dt is

$$\mathbf{p}' = dAdt \int_{\mathbf{C}\cdot\mathbf{n_s}>0} (\mathbf{C}\cdot\mathbf{n}_s)\mathbf{v}f d\mathbf{v}. \tag{4.4}$$

The range of integration is taken over all values of $\mathbf{v}$ for which $\mathbf{C}\cdot\mathbf{n_s}$ is positive. Thus the total momentum communicated to dA during dt is the difference $d\mathbf{p}$ between the momentum of the impinging molecules and that of those re-emitting from the surface, which is equal to

$$d\mathbf{p} = dAdt \left[\int_{\mathbf{C}\cdot\mathbf{n_s}<\mathbf{0}} (-\mathbf{C}\cdot\mathbf{n}_s)\mathbf{v}f(\mathbf{v})d\mathbf{v} - \int_{\mathbf{C}\cdot\mathbf{n_s}>\mathbf{0}} (\mathbf{C}\cdot\mathbf{n}_s)\mathbf{v}f d\mathbf{v} \right]$$

$$d\mathbf{p} = -dAdt \int (\mathbf{C}\cdot\mathbf{n}_s)\mathbf{v}f d\mathbf{v}. \tag{4.5}$$

If the gas is neither condensing upon nor evaporating from the surface, the total mass of impinging molecules on the element dA during dt, namely,

$$dAdt \int_{\mathbf{C}\cdot\mathbf{n_s}<\mathbf{0}} (-\mathbf{C}\cdot\mathbf{n}_s)f d\mathbf{v}$$

must be equal to the mass of the re-emitting molecules, which is

$$dAdt \int_{\mathbf{C}\cdot\mathbf{n_s}>\mathbf{0}} (\mathbf{C}\cdot\mathbf{n}_s)f d\mathbf{v};$$

hence

$$\int (\mathbf{C}\cdot\mathbf{n}_s)f d\mathbf{v} = 0. \tag{4.6}$$

Now using this result, we have

$$
\begin{aligned}
\int (\mathbf{C}\cdot\mathbf{n}_s)\mathbf{v}f d\mathbf{v} &= \int (\mathbf{C}\cdot\mathbf{n}_s)(\mathbf{u}+\mathbf{c})f d\mathbf{v} \\
&= \mathbf{u}\int (\mathbf{C}\cdot\mathbf{n}_s)f d\mathbf{v} + \int (\mathbf{C}\cdot\mathbf{n}_s)\mathbf{c}f d\mathbf{v} \\
&\stackrel{(4.6)}{=} \int (\mathbf{C}\cdot\mathbf{n}_s)\mathbf{c}f d\mathbf{v} \\
&= \int ((\mathbf{c}+\mathbf{u}-\mathbf{U})\cdot\mathbf{n}_s)\mathbf{c}f d\mathbf{v} \\
&= \int (\mathbf{c}\cdot\mathbf{n}_s)\mathbf{c}f d\mathbf{v} + (\mathbf{u}-\mathbf{U})\cdot\mathbf{n}_s\int \mathbf{c}f d\mathbf{v} \\
&= \int (\mathbf{c}\cdot\mathbf{n}_s)\mathbf{c}f d\mathbf{v} \\
&= \left(\int \mathbf{c}\otimes\mathbf{c}f d\mathbf{v} \right)\cdot\mathbf{n}_s,
\end{aligned}
$$

and we have

$$\int (\mathbf{C}\cdot\mathbf{n}_s)\mathbf{v}f d\mathbf{v} = \left(\int (\mathbf{v}-\mathbf{u})\otimes(\mathbf{v}-\mathbf{u})f d\mathbf{v} \right)\cdot\mathbf{n}_s \tag{4.7}$$

Using equation (4.7) in the equation (4.5), we obtain

$$d\mathbf{p} = -dA\,dt \left(\int (\mathbf{v} - \mathbf{u}) \otimes (\mathbf{v} - \mathbf{u}) f\, d\mathbf{v} \right) \cdot \mathbf{n}_s. \tag{4.8}$$

The force $d\mathscr{F}$ on the element dA is given by $\frac{d\mathbf{p}}{dt}$, and the equation (4.8) is written as

$$d\mathscr{F} = -dA \left(\int (\mathbf{v} - \mathbf{u}) \otimes (\mathbf{v} - \mathbf{u}) f\, d\mathbf{v} \right) \cdot \mathbf{n}_s. \tag{4.9}$$

Now using equation (2.17) in (4.9), we get

$$d\mathscr{F} = -\varphi \cdot \mathbf{n}_s dA \tag{4.10}$$

and the torque on element dA during time dt is given by

$$d\mathscr{T} = (\mathbf{y} - \mathbf{X}) \times (-\varphi \cdot \mathbf{n}_s) dA, \quad \mathbf{y} \in S. \tag{4.11}$$

The total force $\mathscr{F}$ and the torque $\mathscr{T}$ on the rigid body is obtained by integrating the equation (4.10) and (4.11), respectively over the boundary ∂S of the body and given by

$$\mathscr{F} = \int_{\partial S} (-\varphi \cdot \mathbf{n}_s) dA,$$

$$\mathscr{T} = \int_{\partial S} (\mathbf{y} - \mathbf{X}) \times (-\varphi \cdot \mathbf{n}_s) dA. \ \blacksquare$$

Remark 4.1. If the flow of the fluid is solved by the Boltzmann equation (2.2), the pressure tensor φ is given by (2.17), and φ is given by (2.35) if the flow of the fluid is solved by the Navier-Stokes equations (2.38).

Using the equations (4.1) and (4.2), the translational and rotational motion of the rigid body is described by the standard Newton-Euler equations [42]

$$M\frac{d\mathbf{V}}{dt} = \mathscr{F}, \tag{4.12}$$

$$\frac{d}{dt}(I\boldsymbol{\omega}) = I\frac{d\boldsymbol{\omega}}{dt} + \boldsymbol{\omega} \times I\boldsymbol{\omega} = \mathscr{T}, \tag{4.13}$$

where M and I are the mass and the moment of inertia of the rigid body, $\mathbf{V}$ and $\boldsymbol{\omega}$ are, respectively, the translational and rotational velocities of the body. The equations (4.12) and (4.13) can be solved for $\mathbf{V}$ and $\boldsymbol{\omega}$, and the total velocity $\mathbf{U}$ that combines both translational and rotational motion of the rigid body is given by $\mathbf{U} = \mathbf{V} + (\mathbf{y} - \mathbf{X}) \times \boldsymbol{\omega}$, $\mathbf{y} \in S$. Now the motion of the rigid body is given by

$$\frac{d\mathbf{y}}{dt} = \mathbf{U}, \quad \mathbf{y} \in S. \tag{4.14}$$

Remark 4.2. In 2-dimensional geometry the moment of inertia of the rigid body is proportional to the identity matrix, and in 3-dimensional geometry if the rigid body is axially symmetric like spherical object, the moment of inertia is also proportional to the identity matrix. In both the cases $\boldsymbol{\omega} \times I\boldsymbol{\omega} = \mathbf{0}$, and the Euler equation (4.13) for rotational motion reduces to

$$I\frac{d\boldsymbol{\omega}}{dt} = \mathscr{T}.$$
(4.15)

4.1.1 Numerical approximation of the force and the torque in DSMC method

To compute the force $\mathscr{F}$ and the torque $\mathscr{T}$ on the rigid body exerted by the surrounding fluid there are basically three approaches. These approaches are based on the models that have been used to solve the fluid flow problem. The flow of fluid can be solved either in the continuum model given by the Navier-Stokes equations or in the kinetic model based on the Boltzmann equation.

4.1.1.1 In the continuum model

In the continuum model the fluid flow is solved by the Navier-Stokes equations(2.38). As we have already explained in the chapter 2 that the Lagrangian form of the Navier-Stokes equations (2.39) is solved numerically by a meshfree scheme named as finite pointset method (FPM). The stress tensor (2.35) on the rigid body is approximated by computing the velocity field on its boundary, and finally plugging in this stress tensor in the equations (4.1) and (4.2) to approximate the force and the torque on the rigid body.

4.1.1.2 In the kinetic model

In the kinetic model the fluid flow is described by the Boltzmann equation. The Boltzmann equation is solved by the DSMC method. In the DSMC framework there could be two approaches to approximate the force and the torque on the rigid body.

First approach: *Moment method*
In this approach first of all we approximate the velocity distribution of the gas molecules in the domain by using the DSMC method to approximate the stress tensor (2.17) on the rigid body by using (3.10) which is a moment of the velocity distribution function in a discrete sense, and finally employing this stress tensor in the equations (4.1) and (4.2) to compute the force and the torque on the rigid body.

For moving boundary problems the correct numerical approximation of the stress tensor (3.10) by the moment method in the DSMC cell which is partially covered by the rigid body could not be accurately calculated, because of the fewer number of simulated molecules in that cell. Thus we need an efficient method to overcome this problem. Hence we have proposed a method that can be implement in the DSMC framework to compute the force and the torque on the rigid body which is based on the direct interaction of the simulated gas molecules with the rigid body.

Second approach: *Momentum method*
We have introduced a new approach to compute the force and the torque by the direct interaction of the fluid molecules with the rigid body. This is a microscopic approach where the force and the torque are computed by the collision of the rigid body by the simulated molecules. When the gas molecules collide with the rigid body, they transfer the momentum and energy. Each gas molecule transfers the momentum to the rigid body. So the total force and the torque exerted on the rigid body are computed by accumulating, respectively, the increments of the linear and angular momentum imparted by all the colliding molecules to the rigid body. This leads to the following procedure to approximate the force and the torque exerted on the rigid body in the DSMC simulation. The construction of the scheme is based on the theorem 4.1.
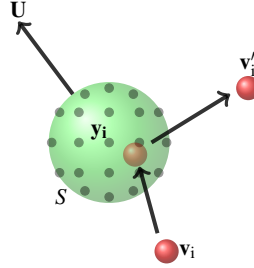
Fig. 4.1: Momentum transfer during the interaction of gas molecules with rigid body.

Let us discretize the boundary ∂S of the rigid body by finitely many mutually disjoint surface elements ∂S_i, $1, \cdots, m$ such that $\partial S = \cup \partial S_i$. Let $\mathbf{y}_i \in \partial S_i$ be the center of the surface element ∂S_i, $i = 1, \cdots, m$. Consider a gas molecule hits the rigid body at a point $\mathbf{y} \in \partial S$ with momentum $\mathbf{p}$, and reflected by the momentum $\mathbf{p}'$. The gas molecule is reflected diffusively from the boundary of the rigid body, so the reflected momentum is sampled from the half-range Maxwellian distribution given by (3.1). Then we find the element ∂S_i that contains y, and we store the pre- and post- collision momenta at the center $\mathbf{y}_i$ of the element ∂S_i due to that colliding molecule. During the time interval Δt, there could be the large number of gas molecules that hit the same surface element ∂S_i of rigid body. The total pre- and

post- collision momenta on the surface element ∂S_i are calculated by taking the sum of pre-collisional momenta $\mathbf{p}$ and post-collisional momenta $\mathbf{p}'$ respectively of those molecules that hit the surface element ∂S_i during the time interval Δt. Let $\mathbf{p}_i$ and $\mathbf{p}'_i$ be the total pre- and post- collisional momenta on the surface element ∂S_i. Then the force $\mathscr{F}_i$ and the torque $\mathscr{T}_i$ exerted on surface element ∂S_i of the rigid body in the time interval Δt are given by

$$\mathscr{F}_i = \frac{\mathbf{p}_i - \mathbf{p}'_i}{\Delta t}, \tag{4.16}$$

$$\mathscr{T}_i = (\mathbf{y}_i - \mathbf{X}) \times \mathscr{F}_i, \quad i = 1, \cdots, m, \tag{4.17}$$

where $\mathbf{X}$ is the center of mass of the rigid body.
Hence the total force $\mathscr{F}$ and the total torque $\mathscr{T}$ on the rigid body are given by

$$\mathscr{F} = \sum_i \mathscr{F}_i = \sum_i \frac{\mathbf{p}_i - \mathbf{p}'_i}{\Delta t}, \tag{4.18}$$

$$\mathscr{T} = \sum_i \mathscr{T}_i = \sum_i (\mathbf{y}_i - \mathbf{X}) \times \mathscr{F}_i. \tag{4.19}$$

Each DSMC simulated molecule represents the large number of real physical gas molecules. Here we need to find the mass of each DSMC simulated molecule to find the momentum of the each gas molecule colliding the rigid body. The momentum of the simulated molecule is the product of its mass and velocity. Now we explain to find the mass of a single DSMC simulated molecule by using the ideal gas equation. From the ideal gas law

$$pV = \eta \mathfrak{R} T, \quad \text{and} \tag{4.20}$$

$$p = \rho R T, \tag{4.21}$$

where η is the number of moles, V is the system volume. $\mathfrak{R}$ and R are respectively the universal and specific gas constants. From (4.20) and (4.21), we can write

$$\eta = \frac{\rho V}{m_{\mathrm{g}} N_{\mathrm{A}}}, \tag{4.22}$$

where N_{A} is the Avogadro number. Total number of physical gas molecules in the system is

$$N = \frac{\rho V}{m_{\mathrm{g}}}, \tag{4.23}$$

where m_{g} is the mass of a real physical gas molecule.
Define

$$\nu := \frac{N}{N_{\mathrm{s}}}, \tag{4.24}$$

where N_{s} is the total number of DSMC simulated molecules in the flow domain, and hence $\nu \geq 1$ represents the number of physical gas molecules representing a single DSMC simulated molecule. The number ν is also known as statistical weight of the

simulated DSMC molecule. Thus the mass of a DSMC simulated molecule is given by

$$m_\mathrm{s} = m_\mathrm{g} \nu. \tag{4.25}$$

Equations (4.23), (4.24) and (4.25) finally gives

$$m_\mathrm{s} = \frac{\rho V}{N_\mathrm{s}}. \tag{4.26}$$

Thus the force (4.18) and the torque (4.19) are written as

$$\mathscr{F} = \sum_i \frac{m_\mathrm{s}(\mathbf{v}_i - \mathbf{v}'_i)}{\Delta t}, \tag{4.27}$$

$$\mathscr{T} = \sum_i (\mathbf{y}_i - \mathbf{X}) \times \frac{m_\mathrm{s}(\mathbf{v}_i - \mathbf{v}'_i)}{\Delta t}, \tag{4.28}$$

where $\mathbf{v}_i$ and $\mathbf{v}'_i$ are the pre- and post- collisional velocities of the simulated molecules in the surface element ∂S_i of the rigid body. With these force and torque exerted on the rigid body due to the collision of gas molecules, we can find the velocity and the position of the rigid body. The translation and the rotational motion of the rigid body are obtained by solving the equations (4.12), (4.13) and (4.14) by performing the time integration using the explicit Euler scheme with given initial velocities $\mathbf{V}(t = 0) = \mathbf{V}_0$, $\omega(t = 0) = \omega_0$, and initial configuration $\mathbf{y}(t = 0) = \mathbf{y}_0 \in S(t = 0)$ of the rigid body.

Chapter 5
Numerical Results

In this chapter we present various test examples to validate the proposed numerical scheme for computing the force and the torque exerted by the surrounding gas on a micro-size rigid particle in 1-, 2- and 3-dimensional domains.

The first numerical experiment is performed to simulate the 1-dimensional actuator problem, and the numerical results are presented to validate with the theoretical values.

The second numerical experiment is performed to transport a rigid circular particle suspended in a closed 2-dimensional cavity that contains the argon gas. The motion of the particle is caused by the flow developed in the gas due to a moving boundary wall of the domain. In this experiment we compute numerical results based on two different physical models (Boltzmann and Navier-Stokes equations) by applying the relevant numerical schemes, and finally we compare the results obtained from these two different models for large and small values of Knudsen numbers.

The third numerical experiment is performed to validate the Brownian diffusion of a spherical particle both in translational and rotational motions in a 3-dimensional domain containing rarefied gas at thermally equilibrium state. Theories for the diffusion of the spherical particle in the translational and the rotational motions are already well-established results which can be found in the literatures [14, 29, 39, 49, 58, 59]. Numerically computed translational and rotational diffusion coefficients using the DSMC simulation are compared with the theoretical values for the spherical particle suspended in rarefied argon gas. The Brownian motion and the diffusion of a circular particle is also performed in a 2-dimensional geometry by using the DSMC method considering only the translation motion. To the best of the author knowledge, there are no well-known theory for the diffusion of the circular particle, so we only present the numerical results on the Brownian motion and the diffusion of the circular particle.

In the last numerical experiment we consider the transport of a rigid particle caused by the thermophoresis. Thermophoresis is one of the well-known phenomenon for the transport of the colloidal particle from the hotter to the colder region if the temperature gradient is provided. In this experiment we take various test cases by simulating the rigid particles in 2- and 3-dimensional geometries by using the DSMC method for solving the Boltzmann equation. In the 3-dimensional geometry we take a stationary spherical particle suspended in the argon gas, and compute the themophoretic force. The numerical results are validated with the theory for different values of Knudsen numbers. We also propose a theory for computing the themophoretic velocity of the spherical particle in the transition regime which is obtained by using the Sherman interpolation of the drag coefficients in two extreme regimes (continuum and free molecular). Furthermore, we simulate the spherical particle in the thermal gradient, and compute the thermophoreic velocity at different values of Knudsen numbers to compare with the proposed theory. We also present the thermophoretic effect for orientation of a spherical and a circular Janus particles, particle having two boundaries differ by physical or chemical properties. We compare the numerical distribution of the polar angle of the spherical Janus particle with the theory, and we numerically explain the orientation and the distribution of the polar angles of the circular Janus particles due to the thermophoretic force and the torque.

5.1 Actuator

In this numerical experiment we present a 1-dimensional actuator containing a monoatomic gas. This problem has already been studied by Dechriste et al [26] using the deterministic numerical scheme based on the immersed boundary method to solve Bhatnagar-Gross-Krook (BGK) model of the Boltzmann equation. In our experiment we solve the flow of gas modeled by Boltzmann equation and solve numerically by using DSMC method where the motion of piston in the actuator is computed by using the equations (4.27) and (4.12). This problem is the first Benchmark to validate the numerical scheme that is proposed in the chapter 4.

Consider a flat piston of width $2l$ whose center is initially at $x = 0$ contained in a slab $[-(L+1),(L+l)]$ containing a monoatomic gas. At initial time, temperature, pressure and density are the same in the whole domain and are denoted by T_0, P_0 and ρ_0. The right wall of the piston is heated to T_1 where as the left wall is maintained at the initial temperature T_0. In the similar way, the right wall of the slab is heated and the left wall is fixed at initial temperature. The experimental set up is illustrated in the figure 5.1.
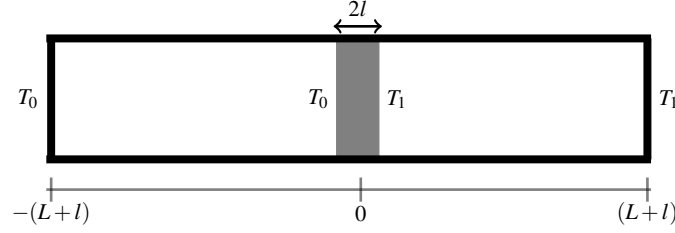
Fig. 5.1: Schematic view of a actuator.

The pressure increases on the right side of the plate because of the rise in the temperature, and the motion of the plate occurs due to the pressure difference between the two sides. The motion of the plate is observed until the equilibrium state is reached. The equilibrium state of the gas and the equilibrium position of the plate can be easily calculated. The state of the gas can be completely described by the equation of state and the mass conservation. Once the system reaches at the equilibrium state, let us denote the P_{equi} and ρ_{left} (ρ_{right}) be the equilibrium pressure and left (right) density, respectively, and x_{equi} be the coordinate of the center of the plate [26].

Now applying the equation of state and the mass conservation on the left side of the place, we have

$$\left.\begin{aligned} \rho_0 RT_0 &= P_0, \\ \rho_{left} RT_0 &= P_{equi}, \\ \rho_0 L &= \rho_{left}(L + x_{equi}). \end{aligned}\right\} \tag{5.1}$$

From (5.1), we get

$$P_{equi} = \frac{L}{(L + x_{equi})} P_0 \tag{5.2}$$

Similarly applying the equation of state and the mass conservation on the right side of the place, we have

$$\left.\begin{aligned} \rho_0 RT_0 &= P_0, \\ \rho_{right} RT_1 &= P_{equi}, \\ \rho_0 L &= \rho_{right}(L - x_{equi}). \end{aligned}\right\} \tag{5.3}$$

From (5.3), we get

$$P_{equi} = \frac{T_1}{T_0} \frac{L}{(L - x_{equi})} P_0. \tag{5.4}$$

Finally from the equations (5.2) and (5.4), the equilibrium position of the piston is given by

$$x_{equi} = L \frac{(T_0 - T_1)}{(T_0 + T_1)}. \tag{5.5}$$

5.1.1 Numerical results

Let us consider one dimension slab with $L = 10^{-1}$ m containing the gas and the width of the piston is $2l = 2 \times 10^{-2}$ m. Initially both sides of the piston are kept at equilibrium with the temperature $T_0 = 270$ K and the pressure $P_0 = 10$ Pascal, and the velocity of the plate is $V = 0$ m/s. We have used the following parameters for the gas. The gas is argon which is monoatomic gas with mass $m_g = 6.63 \times 10^{-26}$ kg. For the Boltzmann constant we have $k_B = 1.38 \times 10^{-23}$ J/K, and we obtained the specific gas constant $R = k_B/m_g = 208$ J/(kgK) [89]. The gas model for the binary collision is taken to be the hard sphere of diameter $d = 3.68 \times 10^{-10}$ m. With these physical parameters, the Knudsen number with respect to the width of the piston is 0.031. The domain is discretized by 400 DSMC cells, and in each active cell, 2000 simulated gas molecules are uniformly distributed with initial velocity sampled from the Maxwellian distribution (2.29) with the mean velocity $\mathbf{u} = \mathbf{0}$ m/s and the temperature $T_0 = 270$ K. The diffuse boundary condition is applied on the walls of the slab and the walls of the piston. When the temperature on the right side increased to $T_1 = 330$ K, the gas molecules on the right side gain the thermal energy, and pushes the piston to the left side with positive acceleration. The motion of the piston is obtained by using the equations (4.27) and (4.12). There is a time at which the system approaches to equilibrium on both the sides, and hence $\frac{dV}{dt} = 0$. But since $V \neq 0$, the piston keeps moving and eventually oscillates around the equilibrium position. The oscillations are observed in the figure 5.2 in which (a) is the plot of the center of the piston and (b) is the plot of the velocity of the piston until the time 0.05 seconds. The oscillatory behavior in the velocity is naturally from the stochasticity in the DSMC method. It is observed that the numerically computed center of the piston oscillates about the theoretical value with maximum 3% of relative error.

(a) Position   (b) Velocity
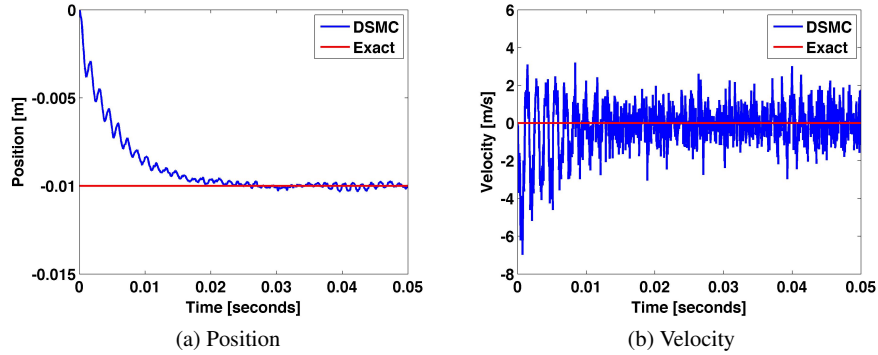
Fig. 5.2: Comparison of the solutions obtained from the DSMC method and the theory. The red curves are the exact values and the blue curves are the numerical values.

5.2 Driven Cavity Flow

Micro-sized mechanical devices such as microelectromechanical system (MEMS) are widely studied, both in commercial applications and scientific inquiry. MEMS devices in micro dimension usually work in gaseous environment under standard atmospheric conditions. In such condition the molecular mean free path is of the order of the characteristic size of the micro device, and hence the flow dynamics associated with MEMS can exhibit rarefied gas phenomenon, and the continuum hypothesis which is the fundamental for the Navier-Stokes equations breakdown [9]. Fluid flows in micro devices differ from those in macroscopic machines. The performance of MEMS-based ducts, nozzles, valves, bearing, turbo-machines, etc, cannot always be correctly predicted or described by using conventional flow models such as the Navier-Stokes equations with no-slip boundary conditions at the fluid-solid interface, which has been successfully applied to the traditional fluid devices. Many questions have been raised when the measurements carried out in the micro devices could not be explained via traditional flow modeling [44]. When the flow is close to the continuum regime ($Kn \ll 1$), the well known hydrodynamic equations coupled with suitable boundary conditions may be applied to yield accurate results for engineering purposes. For $Kn \gg 1$, the kinetic approach based on the Boltzmann equation or simplified kinetic model equations is required [9, 62, 64].

In many instances fluid flows involved in MEMS devices, vacuum systems, and high altitude aerodynamics do not have a local equilibrium. In these applications gas flows in channels, tubes, and ducts due to pressure and temperature gradients in the flow directions are very common and have been extensively investigated by solving the hydrodynamic equations with slip boundary conditions [44] and by the direct

simulation Monte Carlo methods [37, 66, 89]. In addition, due to the similarity between the non-equilibrium flows and the rarefied gas flows, corresponding results obtained over the years implementing classical kinetic theory approaches (Boltzmann equation and simplified kinetic models) are also applicable [64]. Another type of flow which is also encountered in systems not in equilibrium are boundary driven flows. Prototype flows of this kind are the Couette flow problmes in one dimension and the cavity flow problem in two or three dimensions. It is clarified that in the hydrodynamic limit, the cavity problem is a well known typical benchmark problem for testing and verifying continuum solvers and has been throughly studied. However, the research work for the same flow pattern in the free molecular, transition, and slip regimes is very limited [64]. Nie et al. [62] have studied the two-dimensional cavity flow problem using the lattice Boltzmann method with slip boundary conditions. Naris et al. [64] have solved the driven cavity flow of rarefied gas in a rectangular enclosure due to the motion of the upper wall over the whole range of the Knudsen numbers. Moreover the moving rigid body in the micro/nano cavity flow might be an interesting topic for studying the industrial and the scientific applications.

In this section we consider a circular rigid body suspended inside a domain containing gas. The rigid body moves due to the flow developed in the gas by moving one of the wall of the domain with constant velocity. One may choose different methods to compute these types of fluid-solid interaction however, meshfree Lagrangian particle methods seem to be one of the preferred choices for such problems [89]. For the rarefied gas phase we solve the Boltzmann equation (2.2) by DSMC type particle method [9, 18, 63]. The flow of the gas exerts the force on the rigid body, and the motion of the body is computed by the Newton's equations. To validate the solutions obtained by solving the Boltzmann equation, we further solve the flow of the gas by using compressible Navier-Stokes equations (2.39) by using the finite pointset method (FPM) [87, 88], and hence the force exerted on the rigid body is computed to find the motion of the rigid body by solving the Newton's equation. It will be shown in the numerical results that for a small Knudsen number the solutions obtained from the Boltzmann equation are quite close to the solutions obtained from the compressible Navier-Stokes equations. However, the same is no longer true for larger Knudsen numbers. We present the test cases with smaller as well as larger Knudsen numbers. In this numerical experiment we consider a 2-dimensional computational domain $\Omega = [a, b] \times [a, b] \subset \mathbb{R}^2$, where size of the domain is micro-scale that contains the argon gas. A circular rigid body S is kept inside the domain Ω. The boundaries at $x = a$, $x = b$, and $y = a$ are stationary, while the upper boundary $y = b$ is in motion with a constant velocity $\mathbf{V}_w = (u_0, 0)$. All the walls are considered isothermal with a fixed temperature T_0. In $\Omega \backslash S$ we solve either the Boltzmann equation or the Navier-Stokes equations. We assume that the gas is initially in the thermal equilibrium with the values $\rho(0, \mathbf{x})$, $\mathbf{u}(0, \mathbf{x})$ and $T(0, \mathbf{x})$, which are the initial conditions for the compressible Navier-Stokes equations. If we solve the Boltzmann equation in the gas domain, we prescribe the initial condition as the local Maxwellian with parameter $\rho(0, \mathbf{x})$, $\mathbf{u}(0, \mathbf{x})$ and $T(0, \mathbf{x})$. Then we compare the results obtained from

both models. In all cases the circular body is surrounded by the compressible gas inside the computational domain and kept initially at rest.

5.2.1 Numerical experiment I: Comparation between the moment and the momentum approaches for the Knudsen number 0.417 in DSMC simulations

In this numerical experiment we consider a square domain with $a = 0.5 \times 10^{-6}$ m and $b = 1.5 \times 10^{-6}$ m. Initially a circular body S of radius $r = 0.12 \times 10^{-6}$ m occupies the computational domain with the center of mass at the point $(10^{-6}$ m, 10^{-6} m$)$, while gas occupies the rest of the domain. The initial temperature of the computational domain is 300 K, and the boundaries of the domain are always kept at fixed temperature 300 K. For the Boltzmann solver, if the gas molecules cross the physical domain or enter inside the circular body, we reflect them back by using the diffuse reflection boundary condition with new velocity sampled from the half-range Maxwellian velocity distribution (3.1). The Knudsen number with respect to the diameter of the rigid body is $Kn = 0.417$. The simulation is performed until the time 8.4919×10^{-8} seconds.

We generate 100×100 regular DSMC cells in the domain, and in each active DSMC cell, initially 50 simulated gas molecules are uniformly distributed with initial velocity chosen from the Maxwellian distribution (2.29) with mean velocity $\mathbf{u} = 0$ m/s and temperature at $T = 300$ K. The upper wall of the domain is moving with velocity $\mathbf{V}_w = (100, 0)$ m/s and other walls of the domain are kept stationary. The schematic diagram for the physical setup is shown in the figure 5.3.
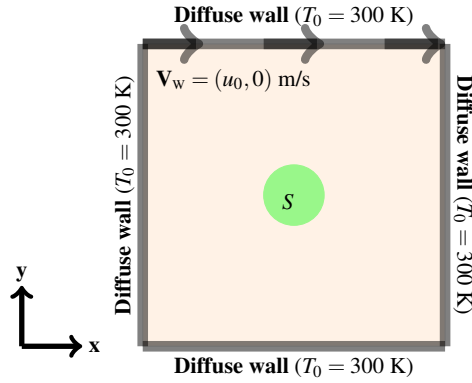
Fig. 5.3: Physical set up for the DSMC simulation.

We compute the force on the circular body by using two different approaches, the moment and the momentum methods, in the DSMC framework as explained in the chapter 4. Applying these forces, computed from two different approaches, in the equations of motion (4.12) and (4.14), we compute the velocity and the trajectory of the rigid body. The comparison of the numerical results obtained from both the approaches are shown in the figure 5.4 where (a) is the trajectory, (b) and (c) are the components of velocity of the rigid body, and (d) and (e) are the components of the force on the rigid body. We observe in the figure 5.4 that the solutions obtained from these two different approaches in DSMC simulation match quite well. In the moment approach the statistical error is reduced by its in-build nature of approximation but in the momentum approach statistical error present which is obvious by the nature of its numerical approximation of the force which can be seen in the plots of two components of the force on the rigid body. These statistical errors in the momentum method can be reduced by taking the average of samples by performing number of independent numerical experiments under similar physical conditions.

(a) Trajectory

(b) x-velocity

(c) y-velocity

(d) x-force

(e) y-force
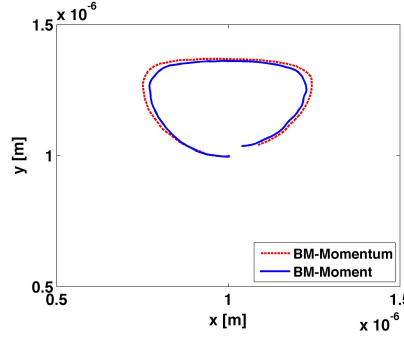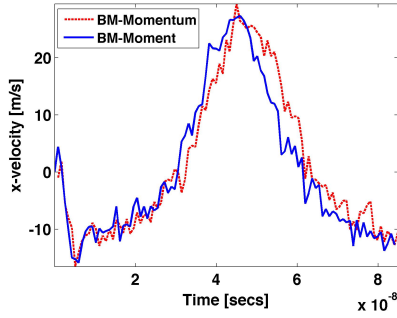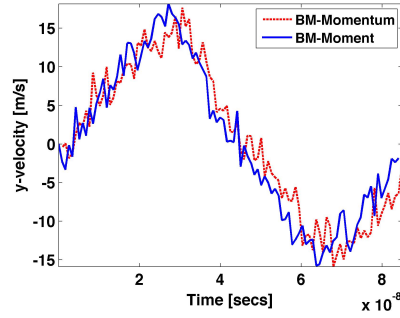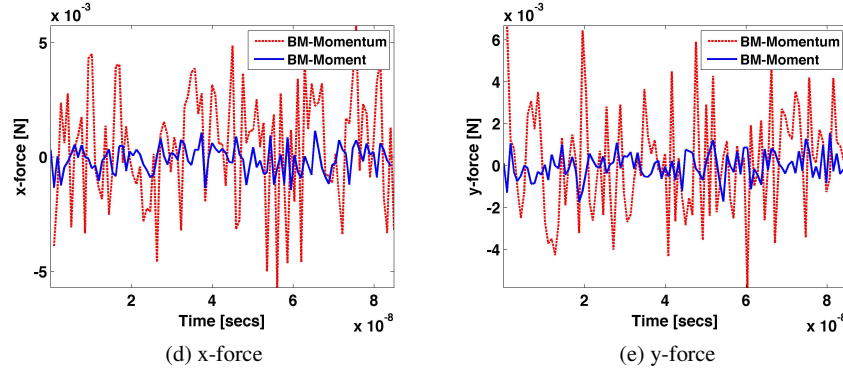
Fig. 5.4: Comparison of the moment and the momentum approaches for the solutions of the Boltzmann equation for the Knudsen number 0.417. The red and the blue curves are, respectively, the solutions obtained from the momentum and the moment methods in the DSMC simulation.

5.2.2 Numerical experiment II: Comparation between the solutions of the Boltzmann and the Navier-Stokes equations for the Knudsen numbers 0.023 and 0.417

In this numerical experiment we consider a square domain with $a = 0.5 \times 10^{-5}$ m and $b = 1.5 \times 10^{-5}$ m. Initially a circular body S of radius $r = 0.12 \times 10^{-5}$ m occupies the computational domain with the center of mass at the point $(10^{-5}$ m$, 10^{-5}$ m$)$, while gas occupies the rest of the domain. The initial temperature of the computational domain is 300 K and the boundaries of the domain are always kept at fixed temperature 300 K. We solve both the Boltzmann and the Navier-Stokes equations separately in the gas domain, and approximate the force on the rigid body by employing these two different models to compute its motion. Finally we compare the numerical results obtained from these two different models for two different values of Knudsen numbers vary from small to large numbers. For the Boltzmann solver, the experimental set up is exactly same as in the numerical experiment in the subsection 5.2.1, see figure 5.3. Taking the characteristics length as a diameter of the circular body we perform the numerical simulations for two different values of Knudsen numbers $Kn = 0.023$ and $Kn = 0.417$. The simulation is performed until the time 8.9390×10^{-7} seconds.

For the Boltzmann solver, we generate 190×190 regular DSMC cells in the domain, and in each active cell, initially 20 simulated gas molecules are uniformly distributed with initial velocity chosen from the Maxwellian distribution (2.29) with mean velocity $\mathbf{u} = 0$ and temperature at $T = 300$ K.

The upper wall of the domain is moving with the velocity $\mathbf{V}_w = (100,0)$ m/s and other three walls are at rest. The schematic diagram for the experimental setup for the DSMC method to solve the Boltzmann equation is shown in the figure 5.3.

We also solve the Navier-Stokes equations by finite pointset method (FPM) in the computational domain. The four boundary walls of the domain and the moving wall of the circular body are modeled to be no-slip boundary walls. The schematic diagram for the experimental setup for the Navier-Stokes equations is shown in the figure 5.5.
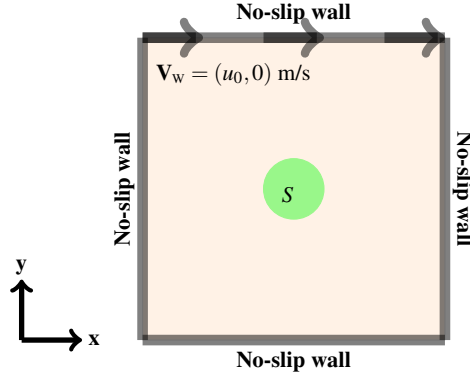
Fig. 5.5: Physical set up for FPM simulation.

In the FPM framework for the Navier-Stokes equations the force on the rigid body is computed by using the equation (4.1), where the stress tensor φ is approximated from the equation (2.35). In the DSMC framework for the Boltzmann equation the force on the rigid body is approximated by using the direct interaction of the gas molecules and the rigid body which is given by the equation (4.27). Using these forces in the equations of motion (4.12) and (4.14), we compute the velocity and the trajectory of the rigid body. The comparisons of the numerical results obtained from two different models are shown in the figure 5.6, where (a) is the trajectory, (b) and (c) are the components of velocity of the rigid body, and (d) and (e) are the components of the force on the rigid body. We observe that the solutions obtained from the Navier-Stokes equations and the Boltzmann equation agree well enough for small value of Knudsen number $Kn = 0.023$.

(a) Trajectory

(b) x-velocity

(c) y-velocity

(d) x-force

(e) y-force

Fig. 5.6: Comparison of the solutions obtained from the Boltzmann and the Navier-Stokes equations for the Knudsen number 0.023. The red curves are the solutions obtained by applying the momentum method in DSMC simulation and the blue curves are the solutions obtained from the stress tensors in FPM.

Next we consider a 10 times larger domain with $a = 0.5 \times 10^{-6}$ m and $b = 1.5 \times 10^{-6}$ m to increase the value of the Knudsen number up to $Kn = 0.417$ by keeping all the physical conditions similar to the last experimental setup. Initially the circular body S of radius $r = 0.12 \times 10^{-6}$ m occupies the computational domain with its center of mass at $(10^{-6}$ m, 10^{-6} m$)$, while gas occupies rest of the domain. The simulation is performed until the time 8.4072×10^{-8} seconds.

For the Boltzmann solver we generate 100×100 regular DSMC cells in the domain and in each active cell, initially 100 simulated gas molecules are uniformly distributed with initial velocity chosen from the Maxwellian distribution (2.29) with mean velocity $\mathbf{u} = \mathbf{0}$ and temperature at $T = 300$ K. The force on the rigid body is computed by FPM for the Navier-Stokes equations and DSMC for the Boltzmann equation as explained in the last example to find the velocity and the trajectory of the rigid body by solving the Newton's equations of motion. The numerical results are presented in the figure 5.7, where (a) is the trajectory, (b) and (c) are the components of velocity of the rigid body, and (d) and (e) are the components of the force on the rigid body. For this larger Knudsen number it can be seen that the solutions obtained from the Navier-Stokes equations significantly deviate from the Boltzmann equation. This is, as expected, due to the failure of the compressible Navier-Stokes equations for the larger values of Knudsen number.

(a) Trajectory

(b) x-velocity

(c) y-velocity

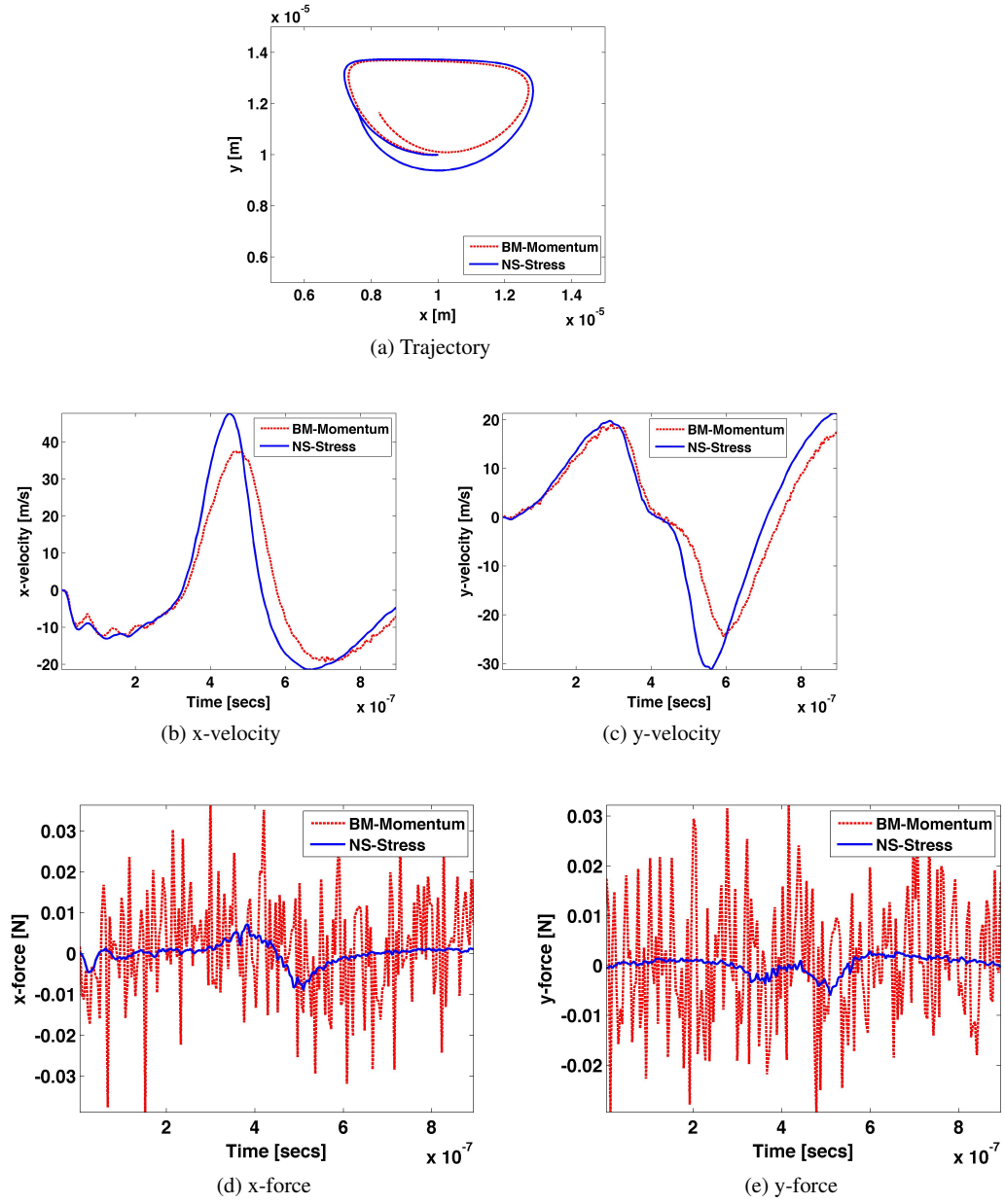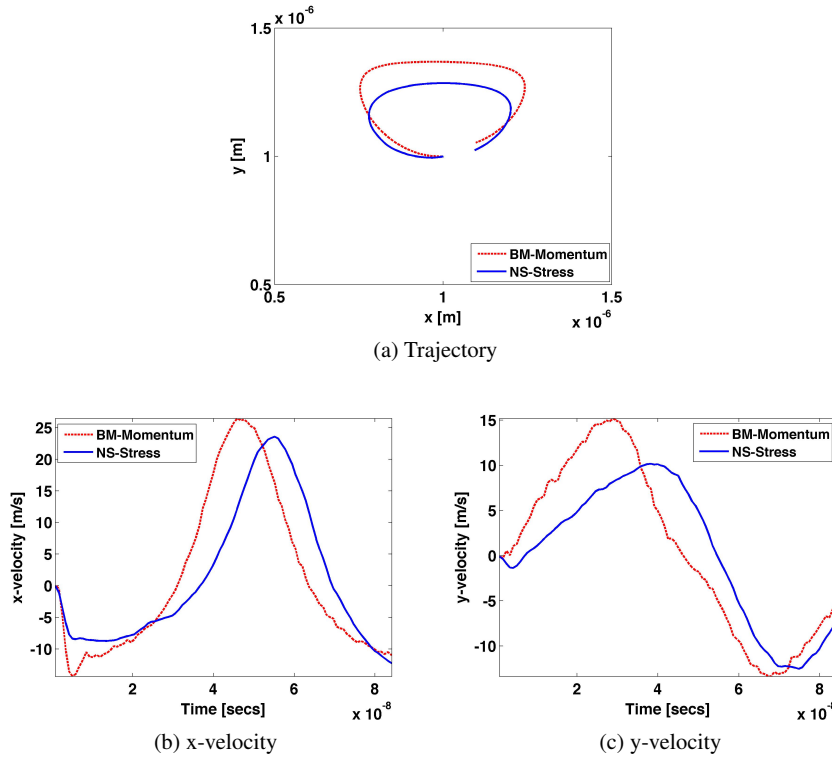(d) x-force   (e) y-force
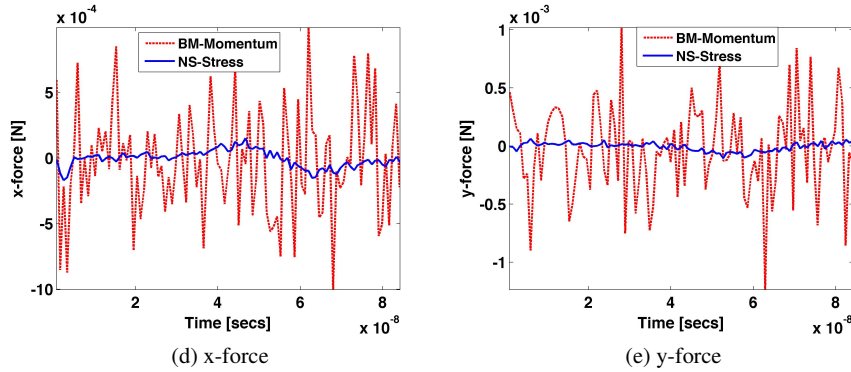
Fig. 5.7: Comparison of the solutions obtained from the Boltzmann and the Navier-Stokes equations for the Knudsen number 0.417. The red curves are the solutions obtained by applying momentum method in the DSMC simulation and the blue curves are the solutions obtained from the stress tensors in the FPM.

5.3 Theory of Brownian Motion and Brownian Diffusion

The continuous random motion of small particles suspended in liquid were first reported by Robert Brown, a biologist, in 1828. Concerning the origin of the motion, for many decades series of experiments were performed by scientists in the nineteenth-century including Perrin and notable theories were developed by Einstein, Smoluchowski, Langevin, and Lorentz. This early work, reviewed by Nelson, eventually confirmed the molecular nature of the matter by relating the particle motion to the thermal fluctuations of the molecules in the fluid [74]. Theory of translational Brownian motion is concerned with the calculation of the probability density for the position of a particle in the fluid. The theory is usually based on the Langevin's equation, which is the Newton's second law with assumption that the force acting on the particle is the sum of a viscous retarding force proportional to the velocity of the particle and rapidly fluctuating force whose statistical properties are such that the probability for the velocity distribution approaches to the Maxwell-Boltzmann distribution [39]. By use of Langevin's equation, a Fokker-Planck equation for the distribution function of the position can be derived, and the equation can be solved to find the distribution function. The derivation is presented in the next section.

Analogously, the rotational motion is concerned with the calculation of the probability density of the orientation of a body in the fluid. The rotational problem is more complicated than the translational problem, primarily because it is not possible to specify the orientation of the rigid body by a vector whose time derivative

is the angular velocity of the body. The specification of the orientation of a body requires three coordinates, such as Euler's angles, whose relation to the components of the angular velocity are not particularly simple [39]. In our work, we consider a simple case where the rigid particle rotates only about a fixed axis through the center of mass of the particle. The theory for the rotational Brownian motion is analog Langevin's equation based on Euler's equation with the assumption that the torque on the particle is the sum of the viscous retarding torque proportional to the angular velocity of the particle and the fluctuating torque whose statistical properties are such that the probability for the angular velocity approaches to the Maxwell-Boltzmann distribution [39]. Hence the corresponding Fokker-Planck equation for the angular distribution of the particle can be derived from Langevin's equation for the rotational motion and the equation can be solved to find the angular distribution of the particle [39].

5.3.1 Translational Brownian motion of a particle

Consider a system composed of N number of monoatomic gas molecules occupying a volume V and having absolute temperature T. Let us consider a particle suspended in a rarefied gas whose size is the order of the mean free path of the gas. Under an ultramicroscope one can observe an irregular motion of the particle. Such a random motion of the particle is well-known as a direct evidence of the thermal molecular motion which is, of course, the very basis of the microscopic theory of the structure of matter, because the random force driving the particle is apparently due to the impacts exerted by the surrounding gas molecules. These are the classical examples of the Brownian motion which always exists, even in thermal equilibrium, as a fluctuation [49]. Let $\mathbf{V} = \frac{d\mathbf{X}(t)}{dt}$ be the velocity of the particle with respect to the gas at a given instant of time. It was realized by A. Einstein and J. Perrin that the Boltzmann distribution not only applied to atoms or molecules. It equally holds for the much larger particles in a colloidal suspension because the principle of 'equipartition of energy' does not distinguish the thermal motion of a solvent molecules from that of a suspended colloid [67]. Thus the particle must follow the Maxwellian velocity distribution at absolute temperature T in thermally equilibrium condition, which is given by [91, 94]

$$f_{\mathbf{V}} = \left(\frac{M}{2\pi k_{\mathrm{B}}T}\right)^{3/2} exp\left(-\frac{M\|\mathbf{V}\|^2}{2k_{\mathrm{B}}T}\right), \qquad (5.6)$$

where M is the mass of the particle, k_{B} is the Boltzmann constant. The Maxwellian distribution $f_{\mathbf{V}}$ of the translational velocity of the particle is a Gaussian with covariance matrix $\Sigma = \sqrt{k_{\mathrm{B}}T/M}\mathbb{I}$ about the mean value $<\mathbf{V}>=\mathbf{0}$. Although the Maxwellian distribution is formally derived in a fixed NVT system, the velocity distribution should be Maxwellian in any equilibrium situation because, in the thermodynamic limit, the properties in different ensembles becomes equivalent. (The thermodynamic limit means that both N and V are made small or large but the ratio

N/V is held fixed.) [38]. The mean square velocity can be calculated by taking the second moment of the velocity distribution (5.6) and given by

$$< ||\mathbf{V}||^2 > = \int_{\mathbb{R}^3} ||\mathbf{V}||^2 f_\mathbf{V} d\mathbf{V} = \frac{3k_\text{B}T}{M}. \tag{5.7}$$

Hence the mean translational kinetic energy of the particle is given by

$$\frac{1}{2}M < ||\mathbf{V}||^2 > = \frac{3}{2}k_\text{B}T. \tag{5.8}$$

The random impact of the surrounding gas molecules generally cause two kinds of effect: firstly they act as a random driving force on the Brownian particle to maintain its endless irregular motion, and secondly they give rise to the frictional force for a forced motion. The first part is the systematic part of the effect and the second is the random part. This in turn means that the frictional force and the random force must be related, because both come from the same origin. This internal relationship between the systematic and the random parts of the microscopic forces is , in fact, a very general matter, which is manifested in so-called the fluctuation-dissipation theorem [49].

In the classical theory of Brownian motion of the center of mass $\mathbf{X}$ of a particle of mass M, we usually start from a phenomenological stochastic differential equation such as [49]

$$M\frac{d^2\mathbf{X}(t)}{dt^2} = -\gamma\frac{d\mathbf{X}(t)}{dt} + \mathbf{F}(t) \tag{5.9}$$

which is the simplest example of the Langevin equation for a free Brownian particle in three dimensional space. The frictional force exerted by the medium is represented by the first term on the right-hand side where γ is the translational friction coefficient assume to be independent of the particle velocity, and it depends only on the particle size and shape, and the second term $\mathbf{F}(t)$ is the random force due to the random collision of the surrounding gas molecules. For the sake of simplicity and idealization, the random force is usually assumed to satisfy two conditions [49]: that (i) the process $\mathbf{F}(t)$ is Gaussian with $< \mathbf{F}(t) > = \mathbf{0}$, and (ii) its correlation time is infinitely short, namely the autocorrelation function of $\mathbf{F}(t)$ has the form [49]

$$< \mathbf{F}(t_1) \otimes \mathbf{F}(t_2) > = \varsigma\delta(t_1 - t_2)\mathbb{I}. \tag{5.10}$$

The Gaussian assumption is quite reasonable for a Brownian particle having mass much larger than the colliding molecules, because then its motion is a result of a great number of successive collisions, which is a condition for the central limit theorem to work. This situation also justifies the second assumption, because correlation between successive impacts remains only for the time of such molecular motion, which is short compared with the time scale of the Brownian motion. The Fourier transform of the autocorrelation function (5.10) is called the power spectral density of the the random force $\mathbf{F}(t)$, and it is just a constant equal to ς. Thus

the random force is said to have a white spectrum. Spectral density measures the strength of the random force $\mathbf{F}(t)$. We will find the value of ς later.

Now taking the dot product on both sides of (5.9) with $\mathbf{X}$, we get

$$M\mathbf{X}(t) \cdot \frac{d^2\mathbf{X}(t)}{dt^2} = -\gamma\mathbf{X}(t) \cdot \frac{d\mathbf{X}(t)}{dt} + \mathbf{X}(t) \cdot \mathbf{F}(t)$$

$$\frac{M}{2}\frac{d^2}{dt^2}||\mathbf{X}(t)||^2 - M||\mathbf{V}||^2 = -\frac{\gamma}{2}\frac{d}{dt}||\mathbf{X}(t)||^2 + \mathbf{X}(t) \cdot \mathbf{F}(t). \qquad (5.11)$$

Taking the expectation $< \cdot >$ on both sides of (5.11), we get

$$\frac{M}{2}\frac{d^2}{dt^2} < ||\mathbf{X}(t)||^2 > -M < ||\mathbf{V}||^2 >= -\frac{\gamma}{2}\frac{d}{dt} < ||\mathbf{X}(t)||^2 > + < \mathbf{X}(t) \cdot \mathbf{F}(t) > . \tag{5.12}$$

Since $\mathbf{X}(t)$ and $\mathbf{F}(t)$ are two independent processes so $< \mathbf{X}(t) \cdot \mathbf{F}(t) >= 0$. Letting $Y := \frac{d}{dt} < ||\mathbf{X}(t)||^2 >$, and using (5.7) in (5.12), we get

$$\frac{dY}{dt} + \frac{\gamma}{M}Y = \frac{6k_{\mathrm{B}}T}{M}. \tag{5.13}$$

Equation (5.13) is the first order linear differential equation. The general solution of (5.13) is given by

$$Y = \frac{6k_{\mathrm{B}}T}{\gamma} + Cexp\left(-\frac{\gamma}{M}t\right). \tag{5.14}$$

Equation (5.14) is also derived in the paper [54] by considering one dimensional Langevin's equation (5.9) for the motion of a spherical particle suspended in the liquid. Equation (5.14) enters a constant regime in which it assumes the constant value of the first term at the end of time of order $\tau_{\mathrm{T}} = M/\gamma$ seconds, i.e. $t >> \tau_{\mathrm{T}}$, for the particle for which Brownian motion is observable [54]. Here τ_{T} is called the gas-particle response time for the translational motion [14]. The response time τ_{T} depends on the fluid properties and the mass of the particle. In our numerical work, we observe motion of the spherical particle at the end of t seconds at which $t >> \tau_{\mathrm{T}}$ so that the second term in the equation (5.14) vanishes.
One therefore has

$$\frac{d}{dt} < ||\mathbf{X}(t)||^2 >= \frac{6k_{\mathrm{B}}T}{\gamma}. \tag{5.15}$$

Integrating on the time interval $[0,t]$, we get

$$< ||\mathbf{X}(t) - \mathbf{X}_0||^2 >= \frac{6k_{\mathrm{B}}T}{\gamma}t, \tag{5.16}$$

where $\mathbf{X}_0 = \mathbf{X}(t = 0)$ is the initial position of the particle.

We present another procedure to derive the relation (5.16) by integrating the Langevin's equation (5.9) to get

$$\mathbf{V}(t) = \mathbf{V}_0 exp(-\frac{\gamma}{M}t) + \frac{1}{M}\int_0^t exp(\frac{\gamma}{M}(\alpha - t))\mathbf{F}(\alpha)d\alpha, \qquad (5.17)$$

where $\mathbf{V}(t=0) = \mathbf{V}_0$ is the initial velocity of the particle. Taking the scalar product of (5.17) with itself and, then taking the expectation, we get

$$< ||\mathbf{V}(t)||^2 >= ||\mathbf{V}_0||^2 exp(-\frac{2\gamma}{M}t) + \frac{1}{M^2}\int_0^t exp(\frac{2\gamma}{M}(\alpha - t))d\alpha \int_0^t < \mathbf{F}(\alpha)\cdot\mathbf{F}(\beta) > d\beta.$$

Applying the relation (5.10) into the interior integral, we get

$$< ||\mathbf{V}(t)||^2 >= ||\mathbf{V}_0||^2 exp(-\frac{2\gamma}{M}t) + \frac{3\varsigma}{2\gamma M}(1 - exp(-\frac{2\gamma}{M})t). \qquad (5.18)$$

The quantity $\tau_\text{T} := \frac{M}{\gamma}$ is called the gas-particle response time for the translation motion [14]. In our numerical experiment, the particle in initially at rest, i.e, $\mathbf{V_0} = \mathbf{0}$, and for the $t >> \tau_\text{T}$ the equation (5.18) becomes

$$< ||\mathbf{V}(t)||^2 >= \frac{3\varsigma}{2\gamma M}. \qquad (5.19)$$

Combining the equations (5.7) and (5.19), we get the power spectral density of the random force $\mathbf{F}(t)$, and given by

$$\varsigma = 2k_\text{B}T\gamma. \qquad (5.20)$$

This relation is known as the fluctuation-dissipation theorem which states that the systematic part of the microscopic force appearing as a friction is actually determined by the correlation of the random force. Conversely the random force has to satisfy this condition, that means, the random force must have the power spectrum determined by the friction. The friction or more generally the resistance of the given system, represents the method by which the external work is dissipated into microscopic thermal energy. The reverse process is the generation of the random force as the result of the thermal fluctuation [49]. The fluctuation-dissipation theorem expresses the balance between the friction and the noise which is required to have a system in thermally equilibrium state for long time.

If the observation time is comparatively larger than the response time τ_T for the translational motion of the particle, i.e. $t >> \tau_T$, the inertial term on the left side of the Langevin equation (5.9) will be negligibly small compared to other existing forces, see [14, 16], and in this condition (5.9) becomes

$$\frac{d\mathbf{X}(t)}{dt} = \frac{1}{\gamma}\mathbf{F}(t). \qquad (5.21)$$

Integrating equation (5.21) from 0 to t, and then taking scalar product with itself, and finally taking the expectation, we get

$$< ||\mathbf{X}(t) - \mathbf{X}_0||^2 >= \frac{1}{\gamma^2} \int_0^t d\alpha \int_0^t < \mathbf{F}(\alpha) \cdot \mathbf{F}(\beta) > d\beta, \qquad (5.22)$$

where $\mathbf{X}(t=0) = \mathbf{X}_0$ is the initial position of the Particle. Now using the relation (5.20) in (5.22), we get

$$< ||\mathbf{X}(t) - \mathbf{X}_0||^2 >= \frac{3\varsigma}{\gamma^2} t. \qquad (5.23)$$

Finally using (5.20) in (5.23) yields the relation (5.16).

5.3.1.1 Translational Brownian diffusion of a particle

Brownian particle diffusion is one of the most important mechanism leading to significant transport rate. Diffusion is well-known in mass transfer of gases and liquids. However, diffusion of the nanoparticles differs because of the wide spectrum of nanoparticle sizes and their morphology (aggregate structure)- a concept understood in particle science and technology but needed in many diverse fields of nanoparticle applications [59].

In this section we derive the diffusion equation which describes the probability density of finding a single Brownian particle in the fluid at any position $\mathbf{x}$ at any time t. Since the autocorrelation function of the random force $\mathbf{F}(t)$ has the form (5.10), the random force $\mathbf{F}(t)$ can be written in the form of

$$\mathbf{F}(t) = \sqrt{\varsigma}\boldsymbol{\xi}(t), \qquad (5.24)$$

where $\boldsymbol{\xi}(t)$ is a standard 3D Gaussian noise with $< \boldsymbol{\xi}(t) >= \mathbf{0}$ and $< \boldsymbol{\xi}(t_1)\boldsymbol{\xi}(t_2) >= \delta(t_1 - t_2)\mathbb{I}$.
Using (5.24) in (5.21), we get

$$\frac{d\mathbf{X}(t)}{dt} = \sqrt{\frac{\varsigma}{\gamma^2}}\boldsymbol{\xi}(t). \qquad (5.25)$$

The stochastic process in the equation (5.25) is equivalent of the Fokker-Planck equation, see [16], for the probability density $p(t,\mathbf{X})$ of a particle to be found at the position $\mathbf{X}$ at time t, and given by

$$\frac{\partial p(t,\mathbf{X})}{\partial t} = D_{\mathrm{T}}\nabla^2 p(t,\mathbf{X}) \qquad (5.26)$$

which is the standard diffusion equation with translational diffusion coefficient

$$D_{\mathrm{T}} = \frac{\varsigma}{2\gamma^2}. \qquad (5.27)$$

If initially at time $t = 0$, the particle is at the position $\mathbf{X} = \mathbf{X}_0$, then the diffusion equation (5.26) with initial condition $p(t = 0, \mathbf{X}) = \delta(\mathbf{X} - \mathbf{X}_0)$ has the solution

$$p(t, \mathbf{X}) = \frac{1}{(4\pi D_\mathrm{T} t)^{3/2}} exp\left(-\frac{||\mathbf{X} - \mathbf{X}_0||^2}{4D_\mathrm{T} t}\right). \tag{5.28}$$

From (5.28), it can be readily shown that the average particle displacement is zero because the particle diffusion is isotropic. However, the mean square displacement of the particles is non-zero. The mean square displacement represents the spreading of the particle concentration (width of the distribution). The mean square displacement can be calculated as the second moment of the spatial distribution given by

$$< ||\mathbf{X}(t) - \mathbf{X}_0||^2 > = \int_{\mathbb{R}^3} ||\mathbf{X}(t) - \mathbf{X}_0||^2 \, p(t, \mathbf{X}) d\mathbf{X} = 6D_\mathrm{T} t. \tag{5.29}$$

This is usually referred as the Einstein equation [29], and shows that the mean square displacement of a diffusion particle is proportional to the diffusion time. Equation (5.29) is a very important expression which is used to derive the particle diffusivity D_T. It also enables the first approximation about the distance that particles are transported by diffusion during any time interval.

By equating the equations (5.16) and (5.29), we get

$$D_\mathrm{T} = \frac{k_\mathrm{B} T}{\gamma}. \tag{5.30}$$

This is known as the Einstein relation [29, 59], and combines the property of the fluid and the particle through the coefficients.

Combining the equations (5.27) and (5.30), we get also the spectral density (5.20) of the fluctuating force $\mathbf{F}(t)$.

The particle friction coefficient γ is the proportionality constant between the drag force, and the relative velocity between the particle and the fluid, that means,

$$\mathbf{F}_\mathrm{D} = -\gamma \mathbf{V}. \tag{5.31}$$

The friction coefficient combines the properties of the fluid such as viscosity, density and the size of the particle. In Stokes flow regime ($Re << 1$), the friction coefficient for the spherical particle has the following form [80]

$$\gamma_\mathrm{c} = 6\pi\mu R_\mathrm{P}, \tag{5.32}$$

where μ is the viscosity of the fluid and R_P is the radius of the spherical particle. This equation is valid under the assumption that the fluid satisfies no-slip boundary condition, that means, the relative velocity of the fluid at the surface of the particle is zero. This assumption holds for the fluid in the continuum regime where the Knudsen number $Kn << 1$. Substituting the value of frictional coefficient γ_c from (5.32) into (5.30), we get

$$D_\mathrm{C} = \frac{k_\mathrm{B} T}{6 \pi \mu R_\mathrm{P}}. \tag{5.33}$$

This is known as the Stokes-Einstein equation [59] for diffusion of the spherical particles in the fluid with low Reynolds number.

In the case of very large Knudsen number $Kn >> 1$, that means, in the free molecular regime an expression for the friction coefficient is derived by Epstein [27] using the kinetic theory, and it is given by

$$\gamma_\mathrm{FM} = \frac{8}{3} R_\mathrm{P}^2 \rho \sqrt{\frac{2 \pi k_\mathrm{B} T}{m_\mathrm{g}}} \left(1 + \frac{\pi \alpha}{8}\right), \tag{5.34}$$

where ρ is the density of the gas and m_g is the mass of the gas molecule. The coefficient α represents the fraction of gas molecules that are reflected diffusively and $(1 - \alpha)$ is the fraction of molecules with specular reflection. In our numerical experiment we consider the complete thermal accommodation, that mean, $\alpha = 1$.
In our work, we are mainly concerned with the Brownian motion of the spherical particle in the rarefied gas. Thus the translational diffusion coefficient of the spherical particle in the bath of rarefied gas is obtained by combining the equations (5.30) and (5.34), and it is given by

$$D_\mathrm{T} = \frac{3}{8} \sqrt{\frac{m_\mathrm{g} k_\mathrm{B} T}{2 \pi}} \frac{1}{(1 + \frac{\alpha \pi}{8}) R_\mathrm{P}^2 \rho}. \tag{5.35}$$

5.3.2 Rotational Brownian motion and Brownian diffusion of a particle

So far we have been discussing only about the translational diffusion, the motion of the center of mass of the spherical particle through the Brownian motion. There also exists rotational diffusion, the change of the orientation of particle due to random torque exerted on it by the surrounding gas molecules. Rotational diffusion is important for the study of dielectric relaxation, fluorescence depolarization, NMR line width, and in short almost any phenomenon that has to do with the relaxation of some polarized quantity [58]. The theory of the rotational diffusion of the spherical particle rotating about a fixed axis can be derived from the rotational analog of the Langevin's equation based on the Euler's equation [39], and it is given by

$$I \frac{d^2 \Theta}{dt} = -\Upsilon \omega_3 + \Gamma, \tag{5.36}$$

where Θ is the angular displacement about a fixed line parallel to z-axis through the center of mass of the spherical particle, $\omega_3 = \frac{d\Theta}{dt}$ is the third component of the angular velocity $\boldsymbol{\omega} = (\omega_1, \omega_2, \omega_3)$, and $I = \frac{2}{5} M R^2$ is the moment of inertia of the

spherical particle. When body rotates only about a line parallel to z-axis, the first two components ω_1, ω_2 of the angular velocity $\boldsymbol{\omega}$ are zero. The first term on the right hand side of (5.36) refers to the friction torque with the rotational friction coefficient Υ. The second term is the stochastic torque on the spherical particle, and this random torque has following two statistical properties [39]:

i. $< \Gamma(t) = 0 >$, for all $t \geq 0$.
ii. $< \Gamma(t_1)\Gamma(t_2) > = 2k_{\mathrm{B}}T\Upsilon\delta(t_1 - t_2)$, for any $t_1, t_2 \geq 0$.

By the theory of equipartition of energy, the distribution of the angular velocity of the spherical particle has to be the Maxwell-Boltzmann expression given by [39, 94]

$$f_{\boldsymbol{\omega}} = \left(\frac{I}{2\pi k_{\mathrm{B}}T}\right)^{3/2} exp\left(\frac{-I||\boldsymbol{\omega}||^2}{2k_{\mathrm{B}}T}\right). \tag{5.37}$$

So the mean square angular velocity of the spherical particle is given to be

$$< ||\boldsymbol{\omega}||^2 > = \int_{\mathbb{R}} ||\boldsymbol{\omega}||^2 f_{\boldsymbol{\omega}} d\boldsymbol{\omega} = \frac{k_{\mathrm{B}}T}{I}, \tag{5.38}$$

and hence the rotational kinetic energy of the particle is given by

$$\frac{1}{2}I < ||\boldsymbol{\omega}||^2 > = \frac{3}{2}k_{\mathrm{B}}T. \tag{5.39}$$

Since the components $\omega_1, \omega_2, \omega_3$ of the rotational velocity of the Brownian particle are mutually independent. The rotational kinetic energy in each component is

$$\frac{1}{2}I < \omega_i^2 > = \frac{1}{2}k_{\mathrm{B}}T, \ i = 1, 2, 3.$$

In analogy to the theory of the translational Brownian motion as explained in the last section, the theory for the rotational Brownian diffusion coefficient can be derived in similar manner. If the observation time is comparatively larger than the response time $\tau_{\mathrm{R}} = \frac{I}{\Upsilon}$ for the rotational motion, i.e, $t >> \tau_{\mathrm{R}}$, the term on the left hand side of (5.36) is negligibly small compared to other existing forces, see [14]. Hence the diffusion equation

$$\frac{\partial P(t, \Theta)}{\partial t} = D_{\mathrm{R}}\nabla^2 p(t, \Theta) \tag{5.40}$$

for the probability density $P(t, \Theta)$ of the orientation Θ of the particle at time t is the Fokker-Plank equation of (5.36) once the rotational inertial term $I\frac{d^2\Theta}{dt} \approx 0$. If initially at time $t = 0$, the orientation of the particle is $\Theta = \Theta_0$, the solution $P(t, \Theta)$ of the diffusion equation is given by

$$P(t, \Theta) = \frac{1}{(4\pi D_{\mathrm{R}}t)^{1/2}} exp\left(-\frac{|\Theta - \Theta_0|^2}{4D_{\mathrm{R}}t}\right), \tag{5.41}$$

where D_R is the rotational diffusion coefficient of the particle. From the density function (5.41), we can find the mean and the mean square angular displacement of the particle, which are given by

$$< \Theta - \Theta_0 > = 0, \tag{5.42}$$

$$< |\Theta - \Theta_0|^2 > = 2D_R t. \tag{5.43}$$

Also the rotational diffusion coefficient is obtained to be

$$D_R = \frac{k_B T}{\Upsilon}. \tag{5.44}$$

In our work, we are only concern with the Brownian diffusion of a spherical particle in the rarefied gas, for $Kn >> 1$. To find the rotational diffusion coefficient of the particle from (5.44), we need to know the rotational frictional coefficient Υ in the rarefied gas. When the particle rotates in the fluid, the rotational motion is slow down by the rotational friction. The rotational friction is the proportionality constant between the drag torque on the particle and the angular velocity of the the particle. The drag torque on the rigid particle rotating about a fixed line parallel to z-axis is given by

$$\Gamma_D = -\Upsilon \omega_3. \tag{5.45}$$

The rotational friction coefficient Υ combines the properties of the fluid and the size of the particle, and it is independent of the angular velocity of the particle. In the continuum regime $(Kn << 1)$, the rotational friction coefficient for the spherical particle is given by [53]

$$\Upsilon_C = 8\pi \mu R_P^3. \tag{5.46}$$

In the continuum fluid regime the rotational friction coefficient Υ_C depends on the viscosity μ of the fluid and the radius of the spherical particle R_P.

In the free molecular regime $(Kn >> 1)$, the expression for the rotational friction coefficient is given by [27, 53]

$$\Upsilon_{FM} = \frac{2\pi}{3} \sqrt{\frac{8k_B T}{\pi m_g}} \rho R_P^4. \tag{5.47}$$

In the free molecular regime the rotational friction coefficient Υ_{FM} depends on the temperature T, density ρ of the gas and the radius R_P of the spherical particle. Our work is mainly on the gas in free molecular regime so the rotational diffusion coefficient is obtained by combining the equations (5.44) and (5.47), and it is given by

$$D_R = \frac{3}{4\pi} \sqrt{\frac{\pi m_g k_B T}{2}} \frac{1}{\rho R_P^4}. \tag{5.48}$$

5.3.3 Numerical results

5.3.3.1 Brownian diffusion: Spherical particle

In this subsection we present the DSMC method to approximate the translational and the rotational diffusion coefficients of a spherical Brownian particle suspended in a rarefied gas contained in a confined cube of size $[0,L] \times [0,L] \times [0,L]$ with $L = 10^{-6}$m which is kept at a uniform temperature of $T = 300$ K. To implement DSMC method, the computational domain is divided into $30 \times 30 \times 30$ regular cells. We have taken the different number n_0 of gas molecules such that $v \geq 1$ to compute the numerical values of the diffusion coefficients and the results are compared with the theoretical values. The radius of the spherical particle is taken to be 10^{-7} m. We have used the following parameters for the gas. The gas is argon which is monoatomic gas with mass $m_g = 6.63 \times 10^{-26}$ kg. For the Boltzmann constant we have $k_B = 1.38 \times 10^{-23}$ J/K, and we obtained the specific gas constant $R = k_B/m_g = 208$ J/(kgK) [89]. The gas model for the binary collision is taken to be the hard sphere of diameter $d = 3.68 \times 10^{-10}$ m. The numerical computation is performed only for the Knudsen number $Kn = 11$ with respect to the particle diameter. The spherical particle in initially kept at rest in the center of the computational domain with center of mass at $(5 \times 10^{-7}, 5 \times 10^{-7}, 5 \times 10^{-7})$. The hard collision is performed between gas molecules and spherical particle. In our simulations diffuse boundary condition is applied on the boundary of the rigid particle as well as on the walls of the domain. The force and the torque are computed using (4.27) and (4.28). The trajectory of the spherical particle is computed using (4.14). The spherical particle shows the continuous irregular motion because of the massive random hit by the surrounding gas molecules. The trajectory of the center of mass of the particle until the time 3.7879×10^{-6} seconds is shown in the figure 5.8.
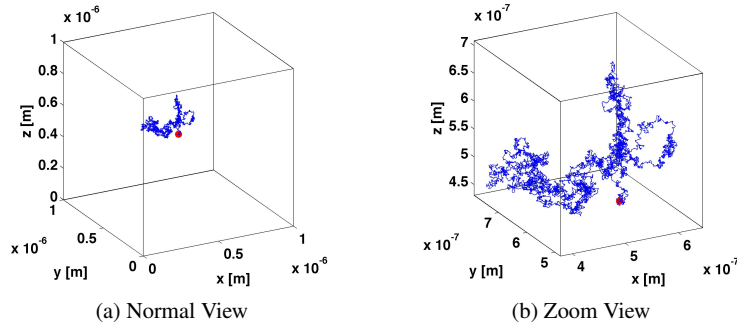

(a) Normal View (b) Zoom View

Fig. 5.8: Brownian motion of the spherical particle until the time 3.7879×10^{-6} seconds.

To compute the diffusion of the spherical particle, we perform the number of independent numerical experiments under similar physical conditions. The displacement of the center of mass of the particle is sampled at end of time $t = 2.617 \times 10^{-8}$ seconds in each experiment. The diffusion of the center of mass of the particle is shown in the figure 5.9 (a) and (b). The distribution of the displacement of the center of mass is shown in the figure 5.10 (a), (b) and (c). The displacement of the center of mass of the particle follows the Maxwellian distribution (5.28) with mean displacement zero and the variance in each direction is approximately equal to $2D_\mathrm{T}t$.

(a) Normal View   (b) Zoom View
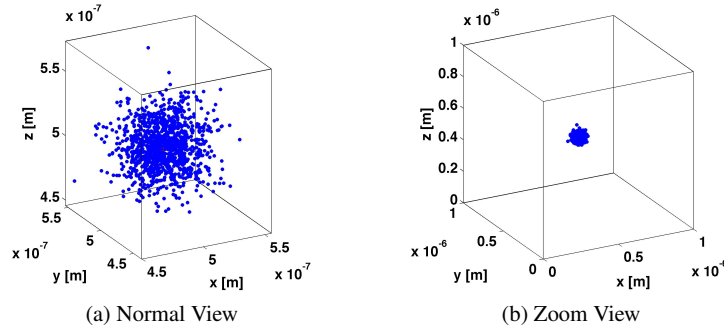
Fig. 5.9: Brownian diffusion of the spherical particle at the end of time 2.2617×10^{-8} seconds.

(a)   (b)   (c)

Fig. 5.10: Distributions of x-, y- and z- displacements at the end of the time 2.2617×10^{-8} seconds. The histograms represent the simulation data and the solid red curves are the Gaussian distribution function.

We have performed the numerical experiments for different number of simulated gas molecules, and the data are sampled for Knudsen number $Kn = 11$ to get the

center of mass of spherical particle at the end of time $t = 2.617 \times 10^{-8}$ seconds, and the translational diffusion coefficient of the particle is numerically computed by using (5.29). The theoretical value of the translational diffusion coefficient is computed from (5.35). Figure 5.11 shows the numerical approximation of the translation diffusion coefficient of the particle that converges to the theoretical value with increasing number of simulated molecules.
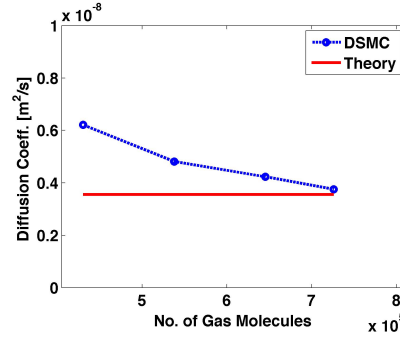
Fig. 5.11: Convergence of transnational diffusion coefficients with increasing number of gas molecules. The solid red line is the theoretical value and blue line with $-o-$ represents DSMC numerical value of the translational diffusion coefficient.

To compute the value of the rotational diffusion coefficient of the spherical Brownian particle using DSMC method, we fix the spherical particle at its center of mass. Then the particle only rotates because of the torque exerted on it by the surrounding gas molecule. The torque on the particle is computed by using (4.28). Applying this torque in the Euler equation (5.36) to get the angular velocity $\omega = (0, 0, \omega_3)$. The first two components of the angular velocity ω are zeros because the rotational motion of the particle is only taken about a fixed line that is parallel to z-axis. Finally the angular displacement Θ is computed by the equation of angular motion given by

$$\frac{d\Theta}{dt} = \omega_3, \quad \text{with initial angle} \quad \Theta_0 = 0. \tag{5.49}$$

Number of independent numerical experiments are performed under similar physical conditions, and the angular displacement of the spherical particle is sampled at the end of time $t = 2.2617 \times 10^{-8}$ seconds in each experiment. The distribution of the angular displacement is shown in figure 5.12. The angular distribution of the particle follows the Maxwellian (5.41) with mean angular displacement zero and the variance is approximately equal to $2D_R t$.
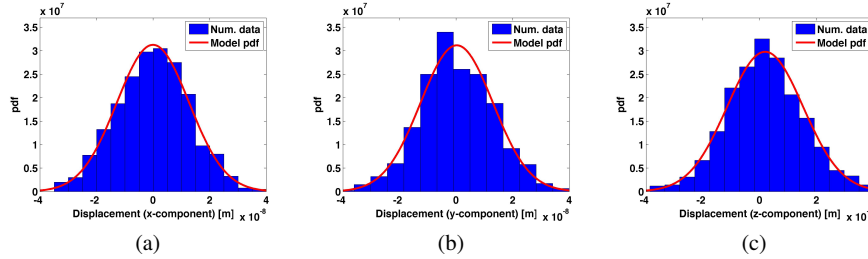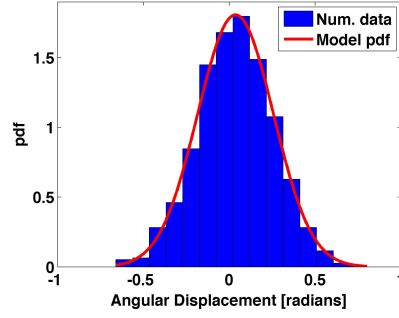
Fig. 5.12: Distribution of angular position about z-axis at the end of time 2.2617×10^{-8} seconds. The histogram represents the simulation data and the solid red curve is the Gaussian distribution function.

We have also computed the rotational diffusion coefficient of the spherical particle by using (5.43) for different number of simulated molecules, and the approximated values are compared with the theoretical value (5.48). The convergence of the numerically computed rotational diffusion coefficient to the theoretical value with increasing number of simulated molecules is shown in the figure 5.13.
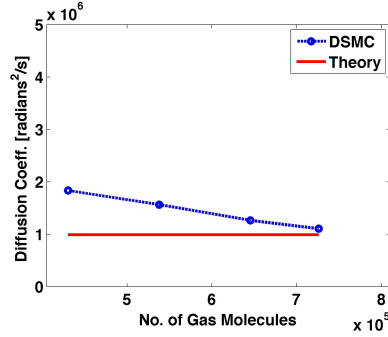
Fig. 5.13: Convergence of rotational diffusion coefficients with increasing number of gas molecules. The solid red line is the theoretical value and blue line with $-o-$ represents DSMC numerical value of the rotational diffusion coefficient.

The translational and the rotational velocities of a Brownian particle must follow the Maxwellian distributions as explained in (5.6) and (5.37). The numerical experiment is run for long time at the given temperature $T = 300$ K of the gas, and the translational and the rotational velocities are sampled at each time step. Figure (5.14) (a), (b) and (c) are the plots of the distribution of the translational velocity in x-, y- and z- directions, and figure (5.15) (a), (b) and (c) are the plots of the distribution of the each component of the rotational velocity. The bar plots represent

the histogram of the simulated data and the red solid curve is the model Gaussian curve. The plots in the figure (5.14) and (5.15) qualitatively agree with the velocity distributions (5.6) and (5.37). To verify that the simulated translational and the rotational velocity distributions agree quantitatively with the theories given by (5.8) and (5.39), we compute the translational and the rotational kinetic energies of the particle by computing the average mean square of the translational and the rotational velocities of the particle. The translational and the rotational kinetic energies of the spherical particle is equal to $\frac{3}{2}k_\mathrm{B}T$. The numerical experiment is performed at temperature $T = 300$ K for the Knudsen number $Kn = 11$ to sample the translational and the rotational velocity of the Brownian spherical particle. Figure 5.16 (a) shows the plots of the numerically approximated translational and rotational kinetic energies of the spherical particle that convergence to the theoretical value of the energy of the particle at the temperature $T = 300$ K of the gas for the increasing number of simulated molecules. Figure 5.16 (b) shows the linear profile of numerically calculated translational and rotational kinetic energies of the particle versus temperature. It can be observed from the figure that both the energies are proportional to the temperature as expected from the theory.

(a)   (b)   (c)
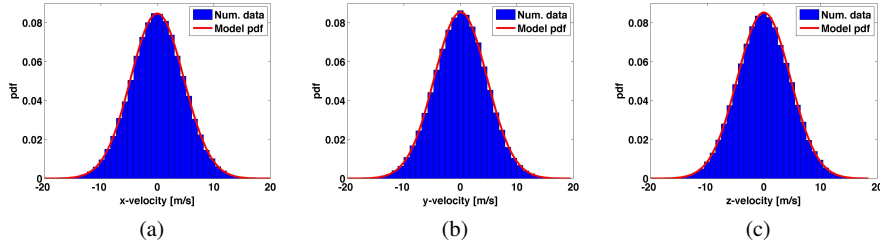
Fig. 5.14: Distributions of x-, y- and z- components of the translational velocity of the spherical particle at $T = 300$ K. The histograms represent the simulation data and the red solid curves are the Gaussian distribution function.

Fig. 5.15: Distributions of three components of the rotational velocity of the spherical particle at $T = 300$ K. The histograms represent the simulation data and the red solid curves are the Gaussian distribution function.
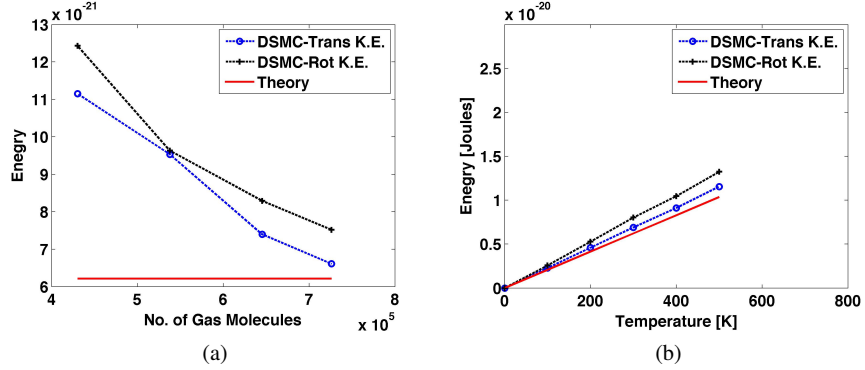
Fig. 5.16: Translational and rotational kinetic energies of the spherical Particle. The red solid line represents the theoretical value, the blue line with $-o-$ and black line with $*-*$ are the simulated translational and rotational kinetic energies.

5.3.3.2 Brownian diffusion: Circular particle

In this subsection we present only the translational motion of the circular Brownian particle in a 2-dimensional square geometry. The particle is suspended in a rarefied gas contained in the computation domain of size $[0 \; L] \times [0 \; L]$, where $L = 10^{-6}$ m. To implement DSMC method, the domain is discretized into $N \times N$, where $N = 50$, regular cells of width $\Delta x = L/N$. The number of cells is chosen in such a way that $\Delta x < \lambda$ for the stability of DSMC method [9]. A circular Brownian particle is introduced inside the domain with center of mass at $(5 \times 10^{-7}, 5 \times 10^{-7})$ with its

initial velocity zero. Then n_0 number of simulated molecules are distributed uniformly in each active DSMC cell with initial velocity $\mathbf{v}$ sampled from the Maxwell distribution (2.29) with mean flow velocity $\mathbf{u} = 0$ and the temperature at $T = 300K$. The numerical computation is performed for the Knudsen number $Kn = 10$ with respect to the particle diameter. The time integration is performed in each time step $\Delta t = 0.3\Delta x/\sqrt{2RT}$. During each time step Δt, the simulated molecules are moved with its velocity $\mathbf{v}$, and the reflection through the boundaries are processed. The diffuse reflection model (3.2) is used on the wall of the domain as well as on the boundary of the particle to sample the velocity of the reflected molecule. To compute the motion of the Brownian particle, we compute the force by using (4.27) and employed in the equations (4.12) and (4.14). A trajectory of the Brownian particle until the time $t = 1.860 \times 10^{-5}$ seconds is shown in the figure 5.17. We have also performed the number of independent numerical experiment under similar physical condition until the time $t = 1.6984 \times 10^{-8}$ seconds to observed the translational Brownian diffusion of the particle. In each numerical experiment, the particle is kept inside the domain with center of mass at the position $(5 \times 10^{-7}, 5 \times 10^{-7})$. Figure 5.18 shows center of mass of the particle after time $t = 1.6984 \times 10^{-8}$ seconds, and figure 5.19 shows the normalized histogram and model probability density function of x- and y- displacement of center of mass of the particle. It can be observed qualitatively that the distribution functions follow the Maxwellian. Though there is no theory to validate the simulated diffusion coefficient for the spherical particle in 2D geometry, we compute the diffusion coefficient of the Brownian particle for the increasing number of simulated molecules, and the convergence plot is shown in the figure 5.20. The simulated diffusion coefficient is computed by using the relation (5.29) for 2-dimensional motion.

(a) Normal View (b) Zoom View
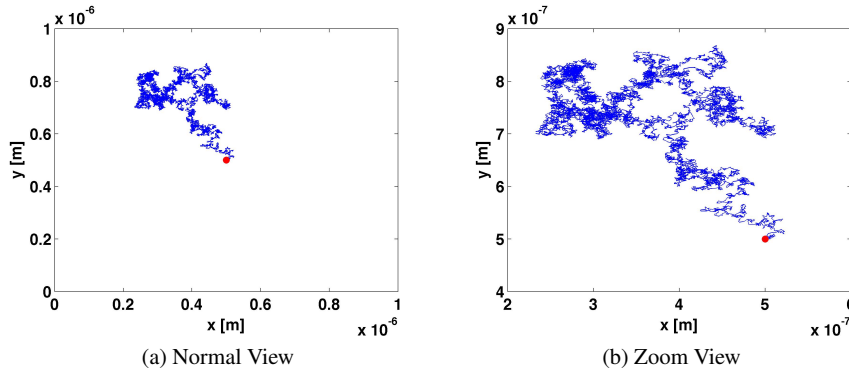
Fig. 5.17: Brownian motion of the circular particle until the time 1.860×10^{-5} seconds

(a) Normal View   (b) Zoom View
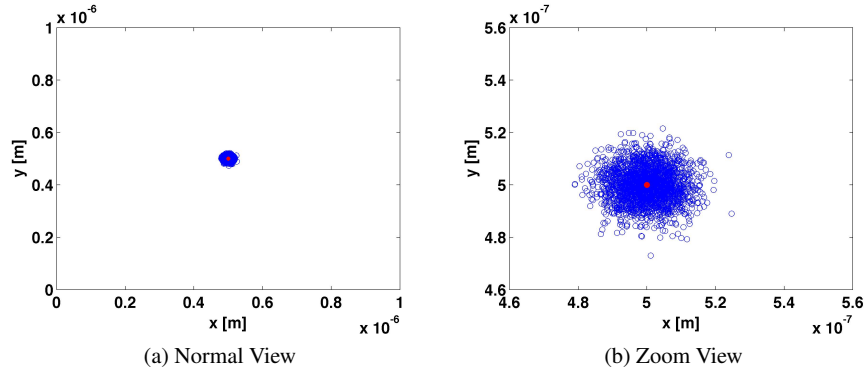
Fig. 5.18: Brownian diffusion of the circular particle at the end of the
time 1.6984×10^{-8} seconds.

(a)   (b)
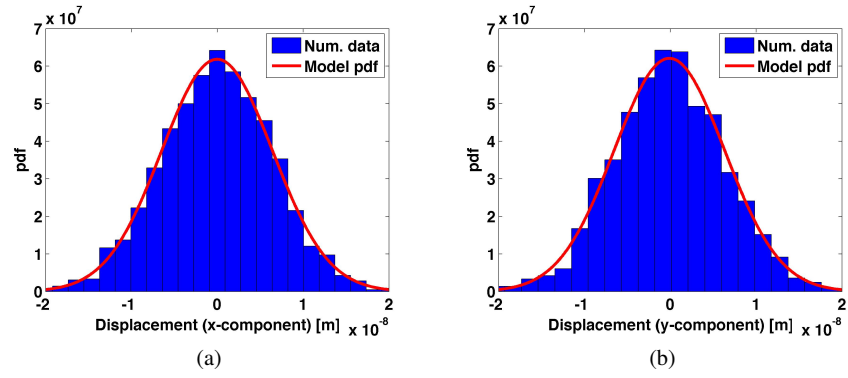
Fig. 5.19: Distributions of *x*- and *y*- displacements at the end of the time
1.6984×10^{-8} seconds. The histograms represent the simulation data
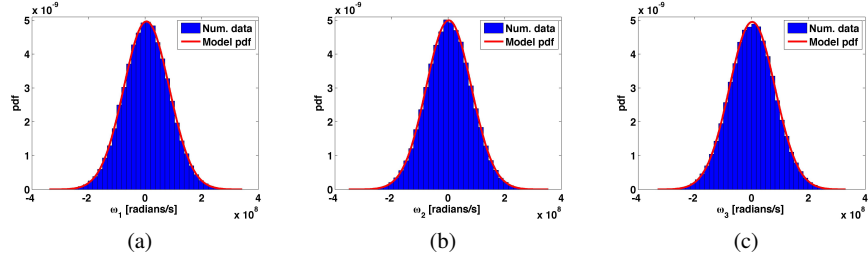and the red solid curves are the Gaussian distribution function.
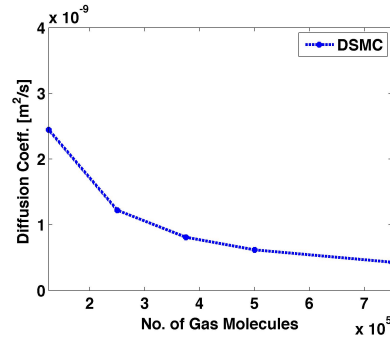
Fig. 5.20: Convergence of transnational diffusion coefficients with increasing number of gas molecules. Blue line with $-o-$ represents DSMC numerical value of the translational diffusion coefficient.

Figure 5.21 (a) and (b) show the *x*- and *y*- components of the velocity distribution of the circular particle in 2-dimensional geometry. Both the components of the velocity follow the Maxwellian distribution.

(a)   (b)
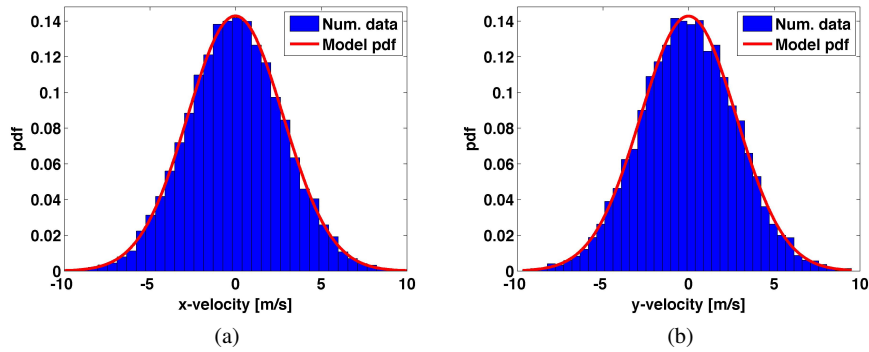
Fig. 5.21: Distributions of *x*- and *y*- components of translational velocity of the spherical particle at $T = 300$ K. The histograms represent the simulation data and the solid red curves are the Gaussian distribution function.

5.4 Thermophoresis

Thermophoresis is a phenomenon by which small particles suspended in a fluid with non-uniform temperature are subjected to move in the direction opposite to

the temperature gradient. The thermophoresis is caused by the energy transferred to the particle by the mean thermal motion of the surrounding gas molecules even in the absence of gas flow, causing the particle to move from the warmer to the cooler regions [85].
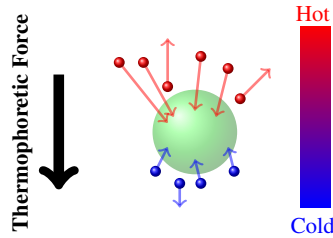
Fig. 5.22: Schematic diagram of a particle suspened in a gas.

Schematic diagram of a particle (large center sphere) immersed in a gas is shown in the figure 5.22. The small dots represent the gas molecules which are randomly fluctuating. Their velocity is the function of gas temperature indicated as vector arrows. In a temperature gradient the mean velocity of the gas molecules also has a gradient. Momentum is transferred upon collision of the gas molecules with the particle. The momentum transfer is a function of the gas molecule velocity. The gradient in the mean molecular velocity produces a force on the particle and, the particle moves against the temperature gradient towards the colder region.

The force arising from a temperature gradient, acting on particles in a rarefied gas has been the subject of the theoretical and the experimental investigation for many years. This kind of force is termed as themophoretic force which describes a phenomenon by which the colloid particles suspended in a fluid with non-uniform temperature are subject to force in the direction opposite to the temperature gradient. This phenomenon was first described by Tyndall [85], who observed that in a chamber filled with dusty air there existed a spatial region around a hot body free of colloid particles. No quantitative explanation of the phenomena was developed until early 1920's when Einstein and Epstein each developed the theories. Both are based on the continuum approach, and only the Epstein theory is of interest today [25].

In the recent years the thermophoretic phenomenon received considerable attention because of its practical importance in a variety of applications, including aerosol science [37, 48], biology [17], combustion [34], and nanocrystals [100]. Many authors have realized the possibility of protecting valuable surfaces from the particles contaminant deposition by keeping the surface warmer than the surrounding gas; examples include thermophoretic protection of painting and other works of art and semiconductor wafers during the manufacturing [37]. The thermophoretic protection has been shown to be powerful wafer-protection strategy at ambient pressure,

but questions have emerged about the potential effectiveness of the thermophoresis at the low pressures likely to encountered in modern semiconductor manufacturing processes [37]. This concern is well founded, as in the limit of a perfect vacuum the thermophoretic force vanishes along with the gas molecules that cause it [37]. Another area of concern is the potential effectiveness of using thermophoresis to protect MicroElectroMechanical Systems(MEMS); although these devices may be operated at ambient pressures, the very small feature size of such devices lead to gas rarefaction effects that could affect the magnitude of the thermophoretic force [37]. Various technological applications require reliable theoretical predictions for the thermophoretic force and velocity over wide range of Knudsen numbers Kn ($Kn = \lambda/R$, where λ is the mean free path of the fluid and R is the radius of the particle), covering the range from the slip flow to the free-molecular flow [15].

Epstein [27] treated the problem for small Knudsen number or near the continuum regime ($Kn << 1$). He considered a spherical, motionless particle in a gas, in which a uniform temperature gradient exists at an appreciable distance from the particle. On application of the linearised Navier-Stokes and energy equations he calculated the stress tensor and the temperature field in the gas which enable the thermal force to be determined. Brock [11] improved on Epstein's solution by considering slip boundary conditions in the continuum derivation. Other attempts were made using the Boltzmann equation as the starting point of the analysis, but the validity of these approaches remains questionable [95]. In the free molecular regime $Kn \to \infty$, the thermophoretic force on the spherical particles in simple monoatomic gases under the assumption of rigid body collision (i.e., gas molecules do not interact with the particles unless they are in physical contact) was developed by Waldmann [95]. He proposed an expression for the thermophoretic force that remains the foundation of the modern engineering analysis for the thermophoresis. The thermophoretic force is often counteracted by the fluid drag on the particle, and in steady state motion of particles has a constant velocity due to the balance between the thermophoretic and the drag forces. This velocity is known as the thermophoretic velocity.

There are at least three length scales needed to quantify the thermophoretic force: a particle size R_P, a characteristic system dimension L, and the molecular mean free path λ. A general description of the thermophoretic would involve at least two dimensionless parameters related to the geometry: a particle Knudsen number, $Kn_R = \lambda/R_p$, and system Knudsen number, $Kn_L = \lambda/L$ [37]. The continuum regime applies for small Knudsen number, $Kn \to 0$, while the free molecular regime is reached in the limit of very large Knudsen number $Kn \to \infty$. The rarefaction effects can be observed either because of small length scales or because of large mean free paths. Extensive literature can be found in the case where the gas is restricted to the continuum regime $Kn_L \to 0$, while the particle Knudsen number may lie in the range $0 < Kn_R < \infty$ [37]. One of the very widely used result is due to Waldmann for the thermophoretic force on a free-molecular particle $(Kn_R \to \infty)$ in a continuum gas described by a first order approximation the Chapman-Enskog molecular velocity

distribution function. Waldmann found that the thermophoretic force for this case is proportional to the particle area and the local gas translational heat flux, is inversely proportional to the mean molecular speed and is independent of pressure. Gallis et al. [36] have provided a new theoretical computation for the thermophoretic force in rarefied gas flow. They have used a force Green's function [36] to compute the force on a spherical particle directly from the molecular velocity distribution calculated by the DSMC method. They have calculated [35] the thermophoretic force, on a motionless spherical particle suspended in a monoatomic, quiescent gas (argon and helium) filling the region between two infinite parallel plates over a range of pressures that spanned the transition regime. Their calculations agreed very well with the theoretical free-molecular results of Brock & Phillips [11, 35, 68] and continuum results of Waldmann [95] respectively. In the transition regime, however their results on the thermophoretic force showed remarkable differences from the model of Phillips.

There is a relation between the thermophoretic force and the gas heat flux on the particle. The thermophoretic force is proportional to the particle cross-sectional area and the local heat flux, and inversely proportional to the mean molecular speed both in the free molecular and the continuum regimes. Gallis et al. [35] has used the DSMC/Green's function to analyze the relation between the gas heat flux and the thermophoretic force though Vestner [92] appears to be the first who noticed the relationship. Gallis et al. [36] have conjectured based on the theoretical arguments that the constant of proportionality depends on the form of the molecular velocity distribution. Even for apparently distinct velocity distributions, such as the Chapman-Enskog (nonequilibrium continuum) or the combination of two half-range Maxwellians (free molecular), the proportionality constant differ by only about 10%. They have calculated the thermophoretic proportionality constant over the entire transition regime and found that the constant varied smoothly from the continuum to the free-molecular for particles in the argon gas in a parallel plate geometry.

In this thesis we present the numerical results on the thermophoretic force, for wide range of Knudsen numbers (Free molecular to Transition regimes), exerted on the micro-scale spherical particle lying between two infinitely extended parallel plates separated by a microscopic distance. We have used the numerical scheme presented in the chapter 4 that is based on the DSMC framework where the force on the particle exerted by the surrounding gas molecules is computed by the direct interaction of particle and gas molecules. We have adopted the theory on the thermophoretic force on the particle from the continuum to the rarefied gas regime presented by Gallis et al. [37] for the validity of the numerical results.

We consider a motionless spherical particle of radius R_P suspended inside a monoatomic gas filling the region between two infinitely extended parallel plates separated by a micrometer size distance L as shown in the schematic diagram (figure 5.23). The particle is assumed to be much smaller than the plate separation,

$R_P << L$. The coordinate system is defined such that $z = 0$ corresponds to the surface of the bottom plate which is kept at the temperature T_c, and $z = L$ corresponds to the surface of the top plate which is kept at the temperature T_h such that $T_h > T_c$ and $T_h - T_c << T_c$. Then the particle experiences a thermophoretic force pushing it away from the warmer surface. The gas is assumed to be quiescent (no mass flow); consequently, heat transfer between the plates is dominated by conduction only. The perfect accommodation is assumed at all gas/solid interfaces, i.e., the thermal tangent and the normal accommodation coefficients are assumed to be unity at each plate and on the particle surface.
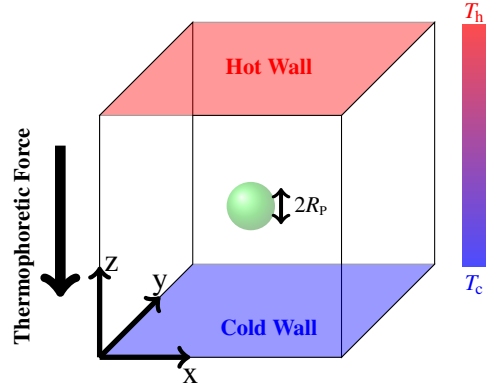
Fig. 5.23: Schematic diagram of a particle suspended between two parallel plates.

5.4.1 Gas heat flux and the thermophoretic force

The gas heat flux and the thermophoretic force acting on a particle are closely related quantities both in the continuum and the rarefied gas limits [36, 37, 92]. In this section we present the closed form expressions for the gas heat flux and thermophoretic force between infinite parallel plates for the case of entire range of the Knudsen numbers. Reliable theories for the gas heat flux and the particle thermophoretic force are well-known results both in the continuum and the free molecular limits, and the approximated expression in the transition regime is given by Gallis et al. [37] by using Sherman interpolation [37, 82]. Applying the similar ideas, the thermophoretic velocity on the particle is also proposed in this section.

5.4.1.1 Continuum gas

Waldmann derived an expression for the thermophoretic force in the free-molecular particle limit ($Kn_R \to \infty$) but where the system is continuum ($Kn_L \to 0$). In his derivation the particle is assumed to be immersed in an infinite bath of gas molecules with a first-order approximation the Chapman-Enskog molecular velocity distribution, and the force on the particle is calculated by integrating the momentum exchange from molecular collision over the particle's surface. Assuming the complete thermal accommodation at the particle surface, the Waldmann thermophoretic force on the spherical particle in a parallel plate geometry is given by [9, 37, 57]

$$F_{th,c} = \frac{32}{15\pi} \frac{\pi R_P^2}{\bar{c}} q_c^{tr},$$ (5.50)

where $\bar{c}$ and q_c^{tr} are, respectively, the gas mean molecular speed and the translational component of the heat flux, which are given by

$$\bar{c} = \sqrt{\frac{8k_B T}{\pi m_g}},$$ (5.51)

$$q_c^{tr} = -\kappa^{tr} \frac{dT}{dz},$$ (5.52)

k_B is the Boltzmann constant, T is the local gas temperature, m_g is the mass of the gas molecule, and κ^{tr} is the translational part of the thermal conductivity. For the monoatomic gas the expression for κ^{tr}, which is accurate to the first approximation according to the kinetic theory [9, 37, 89], is given by

$$\kappa^{tr} = \frac{15k_B}{4m_g} \mu,$$ (5.53)

where μ is the viscosity of the gas which is correct to the first approximation from kinetic theory [9, 89], is given by

$$\mu = \frac{5}{16d^2} \sqrt{\frac{mk_B T}{\pi}},$$ (5.54)

d is the diameter of the gas molecule.
Waldmann equation (5.50) states that the thermophoretic force is proportional to the cross-sectional area of the particle and the translational component of the heat flux, and inversely proportional to the mean thermal speed. It can be seen from the Waldmann equation (5.50) that in the continuum regime the themophoretic force is independent of the gas pressure as long as gas is described by the continuum, the Chapman-Enskog velocity distribution. Clearly the thermophoretic force and the translational heat flux are closely related in the continuum limit.

5.4.1.2 Free-molecular gas

In the free-molecular gas limit ($Kn_{\mathrm{L}} \to \infty$), gas molecules travel back and forth between the plates without colliding with each other; in this case the heat transfer between the plates can be described from the molecular point of view. The walls are assumed to reflect molecules diffusely with thermal accommodation meaning that the molecules reflected from a stationary wall assume a half-range Maxwellian distribution (3.1) in equilibrium with the wall temperature.

An expression for the thermophoretic force between two parallel plates when both the system and the particle are free-molecular ($Kn_{\mathrm{L}} \to \infty$ and $Kn_{\mathrm{R}} \to \infty$) is obtained by Gallis et al. using the idea of force Green's function. For small temperature difference $T_{\mathrm{h}} - T_{\mathrm{c}} << T_{\mathrm{c}}$ along with the approximation $\sqrt{T_{\mathrm{h}}} + \sqrt{T_{\mathrm{c}}} = 2\sqrt{T}$, the thermophoretic force is given by

$$F_{\mathrm{th,FM}} = \frac{3}{4}\left(\frac{\pi R_{\mathrm{P}}^2}{\bar{c}}\right)q_{\mathrm{FM}}^{\mathrm{tr}}, \qquad (5.55)$$

where $q_{\mathrm{FM}}^{\mathrm{tr}}$ is the translational component of the heat flux in the free-molecular limit, and given by

$$q_{\mathrm{FM}}^{\mathrm{tr}} = -\frac{\bar{c}}{2}\rho R(T_{\mathrm{h}} - T_{\mathrm{c}}), \qquad (5.56)$$

ρ is the density of the gas and $R = k_{\mathrm{B}}/m_{\mathrm{g}}$ is the specific gas constant. The heat flux (5.56) between two parallel plates for small temperature difference $T_{\mathrm{h}} - T_{\mathrm{c}} << T_{\mathrm{c}}$ was also derived by Bird [9] in the rarefied gas limit by characterizing the space between the walls by two stream of non-collisional molecules with higher energy molecules streaming downward from the hot plate while lower energy molecules stream upward from the cold plate. Unlike the continuum result, the free-molecular heat flux is directly proportional to the gas density ρ, so in the limit of vanishing density the heat flux approaches to zero, as it must in a vacuum. But as in the continuum limit, the free molecular thermophoretic force (5.55) is proportional to the cross-sectional area of the particle and the local translational heat flux, and inversely proportional to the mean thermal speed.

Observing from the equations (5.50) and (5.55), it can be concluded that the Continuum and the free-molecular limits thermophoretic forces are identical within the numerical factor. This striking result was first realized by Vestner [92] and later exploited by Gallis et al [35, 36, 37]. The resulting numerical factor differs only by 10%, although these two liming cases are derived from substantially different molecular velocity distributions (Chapmann-Enskog for the continuum gas and two half-range Maxwellian at different temperatures for the rarefied gas). In both the limits the thermophoretic force is proportional to the particle cross-sectional area and the local translational component of the heat flux, and inversely proportional to the mean molecular thermal speed.

5.4.1.3 Transition regime gas

The prediction of the heat flux and hence the thermophoretic force on the gas in transition regime is challenging, ultimately requires the complete solution of the Boltzmann equation. Based on the direct relationship between the thermophoretic force and the heat flux in the limits of both continuum and rarefied gas, Gallis et al. [36, 37] explored the relation between the thermophoretic force and the heat flux over entire range of gas in the transition regime using an equation of the form

$$F_{\text{th}} = \xi \left(\frac{\pi R_{\text{P}}^2}{\bar{c}} \right) q^{\text{tr}}, \tag{5.57}$$

where ξ is the constant of proportionality and termed as thermophoresis parameter depends on the local molecular velocity distribution in a weak way. For example, the thermophoretic parameter varies slightly between the free molecular (two half-range Maxwellian) limit $\xi_{\text{FM}} = 0.75$ and the continuum (Chapmann-Enskog) limit $\xi_{\text{CE}} = 0.6791$. Based on these results, Gallis et al. [36, 37] have suggested to approximate the thermophoretic force with equation (5.57) and using the Waldmann thermophoretic result (5.50) to guide the choice for the coefficient:

$$\xi \approx \xi_{\text{CE}} = \frac{32}{15\pi}. \tag{5.58}$$

The use of the value of ξ_{CE} in the equation (5.57) is exact for a first-order approximation the Chapman-Enskog molecular velocity distribution and, except for high anisotropic velocity distribution, is probably accurate to roughly 10% [37].

To compute the thermophoretic force given in the equation (5.57), the expression for the translational heat flux q^{tr} for the transition regime has to be estimated properly so that the limiting cases for the continuum and free-molecular could be obtained. Bird [9, 37] gave an approximate closed-form of the heat flux for a Lee's four-moment solution of the Boltzmann equation for the monoatomic gas. For two parallel plates where the temperature difference is assumed to be small, the heat flux for a monoatomic gas at all pressure P can be approximated by

$$q = -\frac{\frac{\kappa^{\text{tr}}}{L}(T_{\text{h}} - T_{\text{c}})}{1 + \left(\frac{\kappa^{\text{tr}}}{2PL} \right) \left[\sqrt{\frac{\pi m_{\text{g}} T_{\text{h}}}{2k_{\text{B}}}} + \sqrt{\frac{\pi m_{\text{g}} T_{\text{c}}}{2k_{\text{B}}}} \right]}, \quad T_{\text{h}} - T_{\text{c}} << T_{\text{c}}. \tag{5.59}$$

This relation reduces to the continuum heat flux limit for large pressure and to the free-molecular heat flux limit at very small pressure.

A simple interpolation formula for the heat flux has been suggested by Sherman [37, 82] that connects the continuum to the free-molecular heat flux limits, and given by

$$q_{\text{Sh}} = \frac{q_{\text{FM}}}{1 + q_{\text{FM}}/q_{\text{C}}}. \tag{5.60}$$

The heat flux (5.60) given by Sherman, by applying the relations (5.52) and (5.56), reduces to the heat flux (5.59) derived by Bird if the approximation $\sqrt{T_h} + \sqrt{T_c} = 2\sqrt{T}$ is used. Springer [37, 82] has noted that equation (5.60) is identical expression resulting from Lee's four-moment method applied to the linearised (small temperature difference) limit of 3 different one dimensional geometries (concentric spheres, concentric cylinders, and parallel plates) and agree well with the limited experimental data for the monoatomic and the diatomic gases for both large and small temperature differences. Gallis et al. [37] have presented the DSMC calculation for the total gas-phase heat flux for argon, helium and nitrogen gases. For each gas, the DSMC calculations approach the free molecular and the continuum limits in the appropriate regime. In the intervening transition regime, the DSMC data are found to be in acceptable agreement with Sherman/Lees predictions (5.59) and (5.60). They have also presented the thermophoretic force as a function of pressure using DSMC/Green's function for argon, helium and nitrogen. The DSMC/Green's function calculation for the thermophoretic force also approach to the free molecular and the continuum (Waldmann) limits in the appropriate regimes. The closed form expression of the equations (5.57), (5.58), and (5.60) for the thermophoretic force in the transition regime is well approximated by their DSMC/Green's function calculation for the thermophoretic force.

Our present work is to compute the thermophoretic force on the spherical particle suspended inside infinitely extended parallel plates at different temperatures by implementing the numerical scheme to compute the force and the torque in DSMC framework that has been proposed in the chapter 3, and finally validate the results with the theoretical values given by relations (5.57), (5.58) and (5.60) for the wide range of Knudsen numbers.

5.4.2 Thermophoretic velocity

When a small particle is suspended in a non-uniform temperature field in the fluid, the particle experiences a thermophoretic force which pushes it in the direction opposite to the temperature gradient, that means, particle moves from the higher to the lower temperature region. Since the moving particle is also counteracted by the drag force, and the drag force increases with the increasing particle velocity so the velocity gained by the particle due to thermophoretic force can not increase without limit. The balance between the thermophoretic and the drag forces causes the particle to move with constant velocity. This velocity is known as the thermophoretic velocity [21, 57]. Knowledge of thermophoretic velocity is equally important in varieties of applications including aerosol science, biology and combustions. For example, in a study demonstrated that depositing flame-syntesized TiO_2 nanocrystals onto a substrate with the tailored particle sizes and crystal morphology requires a quantitative knowledge of the thermophoretic velocity. For the case of ordinary-temperature gases, the thermophoretic velocity has been employed widely in the

modelling of the thermophoretic deposition onto a cold wall of fine powers suspended in a gas flow [21]. The drag forces on the spherical particle in the continuum and the free molecular limits are well established results which are equated with the thermophoretic forces in the continuum and the free molecular limits respectively to get the thermophoretic velocity in both the limits. In the transition regime, the drag force is not yet established because of the unavailability of the complete solution of the Boltzmann equation. In the next section we propose the drag force on the particle in the transition regime by employing the Sherman interpolation of the drag coefficients in the continuum and the free molecular limits, and it is equated with the thermophoretic force in the transition regime explained in the last section to approximate the thermophoretic velocity of the particle.

Equating the drag force (5.31) using the Stoke's drag coefficient (5.32) with the thermophoretic force (5.50) yields the thermophoretic velocity $V_{\text{th,c}}$ in the continuum limit, and it is given by

$$V_{\text{th,c}} = -\frac{1}{3}\sqrt{\frac{2R}{\pi T}} R_{\text{P}} \frac{dT}{dz}. \tag{5.61}$$

The thermophoretic velocity is proportional to the radius of the particle and the temperature gradient, and inversely proportional to the square root of the temperature of the gas.

Equating the drag force (5.31) using the drag coefficient (5.34) in the free-molecular regime with the thermophoretic force (5.55) yields the thermophoretic velocity $V_{\text{th,FM}}$ in the free molecular limit, and it is given by

$$V_{\text{th,FM}} = -\frac{9}{128}\frac{1}{\left(1+\frac{\pi\alpha}{8}\right)}\sqrt{\frac{2R}{\pi T}}(T_{\text{h}} - T_{\text{c}}). \tag{5.62}$$

Unlike in the continuum regime, the thermophoretic velocity in the free molecular limit does not depend on the particle size but directly proportional to the temperature difference, and inversely proportional to the square root of the gas temperature.

The drag coefficient in the transition regime can be obtained by interpolating the drag coefficients in the continuum and the free molecular limits by applying the Sherman interpolation formula [37, 82], and it is given by

$$\gamma_{\text{Sh}} = \frac{\gamma_{\text{FM}}}{1 + \gamma_{\text{FM}}/\gamma_{\text{c}}}. \tag{5.63}$$

Equating the drag force (5.31) using the drag coefficient (5.63) with the thermophoretic force (5.57) yields the thermophoretic velocity V in the transition regime, and it is given by

$$V = \xi\left(\frac{\pi R_p^2}{\bar{c}}\right)\frac{q_{\text{Sh}}}{\gamma_{\text{Sh}}}, \tag{5.64}$$

where the parameter ξ is given by (5.58). The thermophoretic velocity (5.64) approaches to the velocity (5.61) in the continuum limit for small values of Knudsen numbers ($Kn \ll 1$) and to the velocity (5.62) in the free-molecular limit for large values of Knudsen numbers ($Kn \gg 1$).

5.4.3 Numerical results: Thermophoretic force on a spherical particle

In this section we present the numerical approximation of the thermophoretic force exerted on a motionless spherical particle suspended in a gas between infinitely extended parallel plates by using the DSMC method. The DSMC simulations are performed for the monoatomic argon gas confined between two parallel plates separated by a distance $L = 2 \times 10^{-6}$ m in z-direction. Although the problem is clearly one dimensional, the problem is solved in three dimensional because of the rigid spherical particle introduced in the domain. To acquire the desire physics the walls in x- and y- directions are modeled as the periodic boundary walls thus represent the infinite parallel plates. The upper wall $z = L$ and the lower wall $z = 0$ are kept at the temperatures $T_h = 283$ K and $T_c = 263$ K respectively, and these walls are assumed to be diffuse isothermally reflecting walls. The spherical particle of radius 2×10^{-7} m is kept in the center of the cubic domain of size $[0, L] \times [0, L] \times [0, L]$, where $L = 2 \times 10^{-6}$m, surrounded by the argon gas. The computational domain is divided into $30 \times 30 \times 30$ regular cubic DSMC cells for the binary collision of the simulated gas molecules. The density of the gas is chosen in such a way that the constraint indicated by Bird [9] that cell sizes should be less than the molecular mean free path. We have used the following parameters for the gas. The gas is argon which is a monoatomic gas with mass $m_g = 6.63 \times 10^{-26}$ kg. For the Boltzmann constant we have $k_B = 1.38 \times 10^{-23}$ J/K, and we obtained the specific gas constant $R = k_B/m_g = 208$ J/(kgK) [89]. The gas model for the binary collision is taken to be the hard sphere of diameter $d = 3.68 \times 10^{-10}$ m. The numerical computation is performed for different values of Knudsen numbers ranging from larger to smaller. The Knudsen number is calculated with respect to the particle diameter. The hard collision is performed between the gas molecules and the spherical particle. The diffuse boundary condition is also applied on the boundary of the rigid particle with its temperature equal to the average of T_h and T_c . The force is computed using (4.27). The large sample for the force is computed, and averaged to improve the statistical accuracy. Typically maximum number of simulated gas molecules is used so that the constraint $v \geq 1$ in the equation (4.24) is satisfied. The simulations are initialized using the constant temperature profile at the arithmetic mean of the T_h and T_c. To obtained the steady results, averaging is performed after the transients have been decayed.

Figure 5.24 shows the plot of numerically computed values of the thermophoretic force per unit cross-sectional area of the spherical particle for different values of

Knudsen numbers ranging from free molecular to transition regimes, and compared with the theoretical values computed by using the equations (5.57), (5.58), and (5.60). It can be observed from the results that the numerical results match correctly with the theory in the free molecular limit, that is, for large values of Knudsen numbers, and fit as well correctly with the interpolated thermophoretic result at transition regimes but start to deviate below the Knudsen number 1. The thermophoretic force on the spherical particle at small values of Knudsen number could not be computed with the current set up of the physical domain and the size of particle. It is numerically difficult to get the situation where $Kn_{\mathrm{L}} << 1$ and $Kn_{\mathrm{R}} >> 1$, which are the basic requirements of these two Knudsen numbers to validate the theory in the continuum regime.
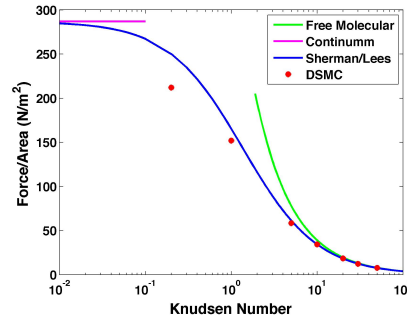

Fig. 5.24: Thermophoretic force on the spherical particle for different values of Knudsen numbers. Red circular dots are the DSMC simulated numerical values and the colored solid curves are the theoretical values.

5.4.4 Numerical results :Thermophoretic velocity of a spherical particle

In this section we present the numerical approximation of the thermophoretic velocity of a spherical particle suspended initially at rest in the monoatomic argon gas. The physical set up and the parameters are similar to the numerical experiment presented in subsection 5.4.3, additionally the particle is allowed to translate and rotate. The equations of motion (4.27) and (4.28) are used to calculate the velocity and the trajectory of the particle in the DSMC simulation. Figure 5.25 shows the trajectory of the spherical particle that moves from the warmer to the colder region because of the thermophoretic force. The DSMC method is stochastically in-built, and hence the force on the particle using this approach is stochastic in nature. To get the statistical accuracy the simulation is run over number of times with similar physical conditions by providing the different initialization seeds to sample the velocity distribution functions and to evaluate the binary collisions of gas molecules to get

the ensemble average of the velocity of the particle. In figure 5.25 the green curves are the different realizations of the trajectory of the particle and the blue curve is the sample average of the trajectories. Figure 5.26 is the plot of the velocity of the particle over time where the green curve is one of the realizations, the red curve is the sample average, and the blue curve is the theoretical value (5.64) of the thermophoretic velocity computed for the Knudsen number $Kn = 30$. It can be observed from the red curve in the figure 5.26 that particle initially gains the velocity from its rest position because of the thermophoretic force acted on it, and later the drag force balances the thermophoretic force to keep the velocity of the particle constant over the time. We have also computed the thermophoretic velocity of the particle for different values of Knudsen numbers. Since the particle acquires the constant velocity due to the balance in the thermophoretic and the drag forces, the time average of the velocity is calculated after the transients have been decayed for each value of Knudsen numbers. The figure 5.27 shows the DSMC simulation for the thermophoretic velocity for different values of Knudsen numbers ranging from larger to smaller, and compared with the proposed theoretical values of the thermophoretic velocity at the free molecular (5.62), and the transition regimes (5.64). The DSMC simulated data fits well enough in the free molecular regime, and started to deviate slightly in the transition regime.
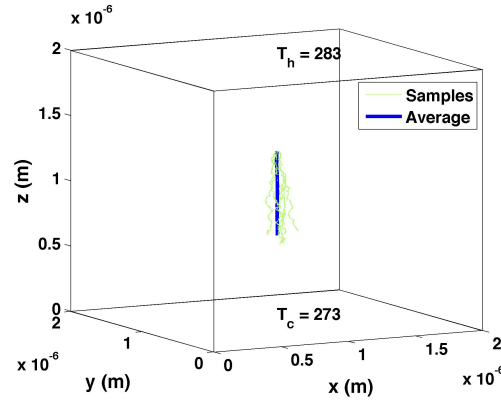

Fig. 5.25: Trajectory of the particle between two parallel plates. The green curves are the independent sample paths and the blue line is the average value.
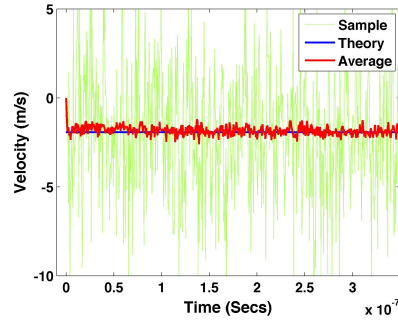
Fig. 5.26: Transnational velocity of the spherical particle. The green curve is a single sample data, the red curve is the sample average and the blue curve is the theoretical value.
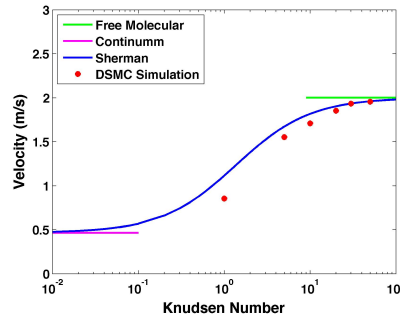
Fig. 5.27: Thermophoretic velocity of the spherical particle for different values of Knudsen numbers. The red circular dots are the DSMC simulated numerical values and the colored solid curves are the theoretical values.

5.4.5 Janus particles

Micro/nanostructures have attracted great attention because of their extremely interesting properties and wide range of applications in electronic, magnetic, sensing, optics, and nanomedicine. Last decades have witnessed rapid development and applications of micro/nanostructure in different disciplines in science and technology. Recent demands for increased functionality, however, have shed light on the limitations of conventional micro/nanostructures. For these complex applications, multifunctional structures are sought to meet the diverse requirements from different disciplines. One of these structures is the Janus particle. The name "Janus" is derived

from the Roman god with two heads placed back to back, and particle has quickly grown as a new member in the colloidal family. A Janus particle should have two faces with different chemical or physical properties with roughly equal areas [98]. In general, Janus particles can be divided into several classes according to their architecture and dimensionality (see Figure 5.28). Most commonly, spherical (3D) Janus particles can be imagined. In addition, two types of cylinders (1D) and two types of disc-like particles (2D) are conceivable [96, 97]. The asymmetry associated with Janus particles is the key to realizing many commercial applications, including electrophoretic displays, nanosviscometers, and self-propelling micromachines. These diverse functionalities were accomplished by using an external electric or magnetic field to control the particle orientation, and in the process, modulate its reflectivity, hydrodynamic mobility, or direction of motion, respectively. The optical trapping techniques that are used to control the translational degrees of freedom of a particle. Optical fields present an effective method for controlling the three translational degrees of freedom for particles ranging from tens of nanometers to micrometers in size. Optical fields have been used in combination with magnetic field to four degrees of freedom of an asymmetric particle or particle aggregate. These optical field and combination with magnetic field has been reported in the paper [28]. Erb et al. [28] have introduced a new type of spherical Janus that can be manipulated by a combination of optical and magnetic fields. They have demonstrated the ability to directly control five degrees of freedom of the particle's motion (three translational and two orientational) while constraining the final sixth degree of freedom.
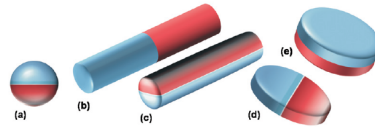

Fig. 5.28: Overview of possible Janus particle architectures. (a) sphere, (b+c) cylinders,and (d+e) discs [96]

Here we introduce a new type of spherical Janus particle that can be manipulated by introducing the thermal field. We demonstrate the ability to control the particle's translational and rotational motions. The particle is suspended in the rarefied gas contained in the micro-scale cuboid/rectangular geometry where two parallel walls are kept at two different temperatures to induce the thermal field. The two faces of the particle are given by two different physical properties such as diffuse and specular reflecting boundary faces. The flow of gas is modeled by the Boltzmann equation (2.2), and solved numerically by applying DSMC procedures to find the force and the torque on the particle. The motion of the particle is computed by using the Newton-Euler equations. We also compute the distribution of the orientation of the Janus particle when only the rotational motion is applied. In this work we take two types of Janus particles. In the 2-dimensional domain we simulate a disc

like particle as shown in the Figure 5.28(d), and in the 3-dimensional geometry a spherical particle as shown in the Figure 5.28(a).

5.4.5.1 Thermophoresis on a spherical Janus particle

Consider the rotation of a Janus spherical particle of radius R_P fixed at its center of mass under the influence of a thermal gradient as shown in the schematic diagram 5.29. Baier [6] has recently proposed a theory to calculate the distribution of the orientation of the rotating Janus microparticles (cylindrical and spherical) in the thermal gradient.
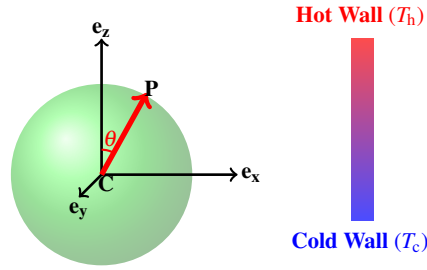
Fig. 5.29: Schematic diagram of a spherical particle suspended in temperature field.

Let θ be the polar angle between the orientation $\mathbf{CP}$ of the particle and the direct of thermal gradient $\mathbf{e}_z$. Then the distribution of the polar angle $\theta, 0 \leq \theta \leq \pi$ is given by [6]

$$p(\theta) = \tilde{N} \sin \theta \exp\left(-\frac{V(\theta)}{k_B T}\right), \tag{5.65}$$

where $V(\theta)$ is damped top spinning in a potential.
The normalization

$$\int_0^\pi p(\theta) d\theta = 1$$

gives the value of the normalized constant $\tilde{N}$. In the free-molecular regime ($Kn \gg 1$), the damped top spinning in a potential $V(\theta)$ is given by

$$V(\theta) = K_T^\infty V_\tau(\theta), \quad V_\tau(\theta) \approx \frac{1}{24}(67 \cos\theta + \cos 3\theta),$$

where

$$K_T^\infty = \frac{v}{2\sqrt{\pi}}(\bar{c}_h - \bar{c}_l)(a^+ - a^-)R_P^3, \quad \bar{c}_{h,c} = \sqrt{\frac{2k_B T_{h,c}}{m}}, \quad v = \rho\sqrt{\frac{k_B T}{2\pi m}},$$

where $a^{\pm}$ denotes the type of boundary conditions (specular or diffuse) on the surface of the Janus particle and ρ is the density of gas.

In our DSMC simulation, we consider a spherical Janus particle of radius 2.5×10^{-8}m with the center of mass at the position $(6.25 \times 10^{-8}, 6.25 \times 10^{-8}, 2.5 \times 10^{-8})$ is suspended in a cuboid domain of size $[0, 1.25 \times 10^{-7}] \times [0, 1.25 \times 10^{-7}] \times [0, 5 \times 10^{-7}]$ containing the argon gas. The walls in the z-direction are separated by a distance $L = 5 \times 10^{-7}$m. The wall $z = 0$ is kept at the temperature $T_{\text{c}} = 295$ K and the wall $z = L$ is kept at the temperature $T_{\text{h}} = 305$ K. These two thermal walls are modeled as the diffuse boundary walls, and the remaining four walls are periodic walls. The domain is discretized by $6 \times 6 \times 24$ cells of equal size. In each cell initially 29 DSMC simulated molecules are uniformly distributed with the velocity sampled from the Maxwellian distribution (2.29) with mean velocity zero and the temperature is taken to be the average of T_{c} and T_{h}. In this numerical experiment the spherical particle only rotates about its fixed center of mass $\mathbf{C}$, see figure 5.29, caused by the themophoresis torque exerted by the massive collision of gas molecules. The northern hemisphere facing towards the warmer region is modeled by the diffuse boundary wall $(a^+ = 1)$ and, the southern hemisphere facing towards the colder region is modeled by the specular boundary wall $(a^- = 0)$ in the DSMC simulation. These boundary conditions on the spherical particle remain same throughout the simulation. The DSMC simulation is performed for the Knudsen number, $Kn = 10$. We compute the distribution of the orientation of the Janus particle in DSMC simulation. The orientation of the particle is given by a reference vector $\mathbf{CP}$ initially aligned with the direction of temperature gradient, that means, $\mathbf{CP}$ is parallel to $\mathbf{e}_z$. The polar angle θ between the $\mathbf{CP}$ and $\mathbf{e}_z$ measures the orientation of the Janus particle. Under the consideration of the Janus particle with two different boundary conditions in two opposite faces make the particle to align slightly with the temperature gradient. The distribution of the orientation of the particle is numerically computed. The comparison of the numerical result with the theory given by (5.65) is shown in the figure in which (a) is the DSMC simulation with binary gas collision, and (b) is the DSMC simulation without binary gas collision. The numerically computed distribution of the polar angle agrees quite well with the theory.

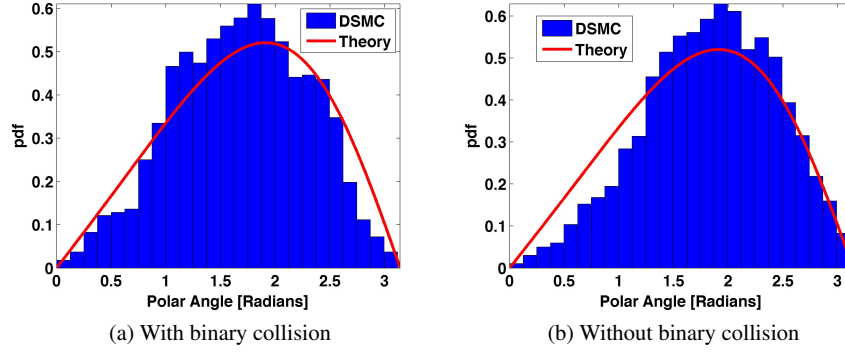(a) With binary collision   (b) Without binary collision

Fig. 5.30: Distribution of polar angle. The histograms represent the
DSMC simulation data and the red solid curves are the theoretical
distribution function.

5.4.5.2 Thermophoresis on a circular Janus particle

A circular particle of radius 0.1×10^{-6}m with the center of mass at the position
$(0.5 \times 10^{-6}, 1.0 \times 10^{-6})$ is suspended in a rectangular domain of size $[0, 1 \times 10^{-6}] \times [0, 2 \times 10^{-6}]$ that is filled by the argon gas. The domain is discretized by 50 cells in
x-direction and 100 cells in y-direction so that the each cell has equal area mea-
sure. In each active DSMC cell of full size initially 50 simulated molecules are
uniformly distributed with the velocity sampled from the Maxwellian distribution
(2.29) with mean velocity zero and temperature is taken to be the average of tem-
peratures at the upper and the lower walls. The upper the wall $y = L$ is kept at 500
K and lower wall $y = 0$ is kept at 300 K. The Knudsen number with respect to the
diameter of the circular particle is 50. The hot and the cold walls are taken to be the
diffuse wall, and other two walls along x-directions are periodic walls. We assign
two different physical properties on the two faces of the particle. We consider the
translational-rotational and, only rotational motion about its center of mass caused
by the thermophoresis.

Orientation of a circular Janus particle

As shown in the Figure 5.31 the circular particle only rotates about its center of mass
C caused by the themophoretic torque exerted by the collision of gas molecules. The
radial vector **CP** is a reference vector to measure the orientation of the particle with
respect to the fixed vector $\mathbf{e}_z$. Initially the reference vector **CP** is aligned to the
temperature gradient in the domain, that mean, **CP** is parallel to $\mathbf{e}_y$. The polar angle
θ between the **CP** and $\mathbf{e}_y$ measures the orientation of the circular Janus particle.
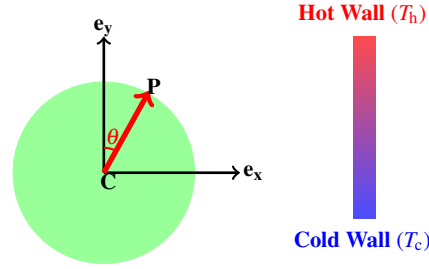
Fig. 5.31: Schematic diagram of a circular particle suspended between parallel plates.

In DSMC simulation, initially the half part of the circular particle that faces towards the hot region is model by the diffuse boundary wall, and the remaining half part is modeled by the specular reflection wall which faces towards the cold region. The particle is kept fixed so that it rotates only about its center of mass cause by the thermophoretic torque. The figure 5.32 shows the orientation of the particle at different instants of time. The particle rotates from its initial orientation, and comes to the specific alignment where the diffuse part faces to the colder region and specular part faces to the hotter region. This typical phenomenon is due to the larger tangential force in the diffuse wall while it is facing towards the hotter region that causes the particle to rotate until it faces towards the colder region. Once the specular wall faces towards the hot region, the normal force on the specular wall becomes dominant and the particle aligns in the specific direction forever. The distribution of the polar angle made by a reference vector **CP** is shown in the figure 5.33.

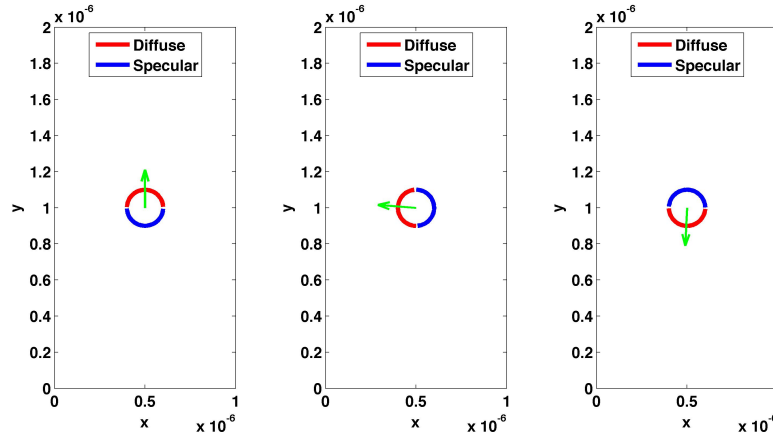Fig. 5.32: Orientation of the circular Janus particle at time (i) 0 sec (ii) 2.6311×10^{-8} secs (iii) 5.7892×10^{-8} secs. from left to right.

Fig. 5.33: Probability density function of the polar angle: Histograms show the simulation data and red solid curve is the model normal distribution.

In the second numerical experiment the half part of the circular particle facing towards the hot region is modeled by the specular boundary and the remaining half part facing towards the colder region is modeled by the diffuse boundary in the DSMC simulation. The circular Janus particle is allowed only rotate about its center of mass because of the torque exerted by the thermophoresis. In this set up particle does not change its orientation, and it remains in the same orientation forever, that means, the specular wall keep facing towards the hotter region and diffuse wall keep facing towards the colder region. The orientation of the particle at different instants of time are shown in the figure 5.34. The distribution of the polar angle is shown in the figure 5.35. The polar angle only fluctuate about the initial orientation.

Fig. 5.34: Orientation of the circular Janus particle at time (i) 0 sec (ii) 2.6311×10^{-8} secs (iii) 5.7892×10^{-8} secs. from left to right.
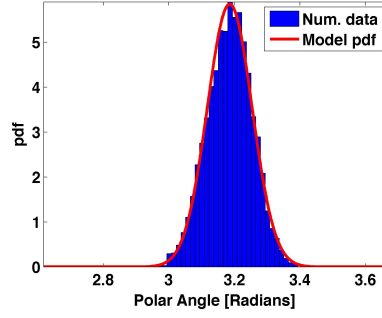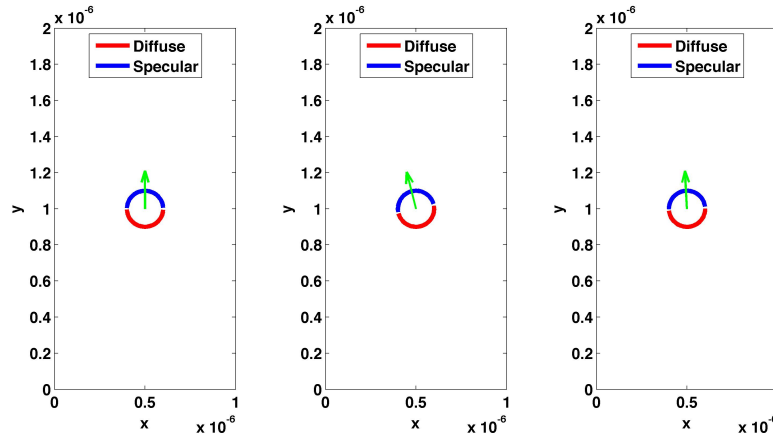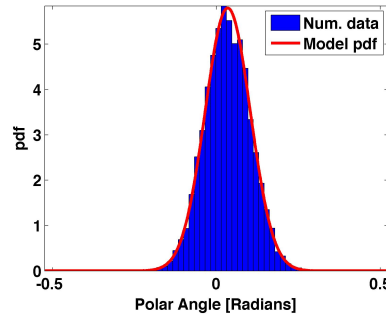
Fig. 5.35: Probability density function of the polar angle: Histograms show the simulation data and red solid curve is the model normal distribution.

Translation motion and the orientation of a circular Janus particle

For the translation motion together with the rotation of the circular Janus particle, we take a long channel with size $[0, 1 \times 10^{-6}] \times [0, 4 \times 10^{-6}]$ filled with the argon gas, and the circular particle is suspended near to the upper wall with the center of mass at $(0.5 \times 10^{-6}, 3.5 \times 10^{-6})$. The domain is divided into 50×200 regular DMSC cells of equal area. The upper wall $y = L$ is kept at the temperature of $T_h = 500$ K and the lower wall $y = 0$ is kept at the temperature $T_c = 300$ K. Initially 50 simulated gas molecules are uniformly distribution in each active DMSC cell with velocity sampled from the Maxwellian distribution (2.29) with mean velocity zero and the temperature equal to the average of T_h and T_c. The temperature of the particle is also taken to be the average of T_h and T_c throughout the motion of the particle. The Knudsen number with respect to the diameter of the circular particle is 50. The upper and the lower walls of the domain are modeled by the diffuse boundary walls, and other side walls are modeled by the periodic boundary walls. Initially the half part of the particle facing towards the hotter region is modeled by the diffuse boundary wall, and the other half part of the particle facing towards the colder region is modeled as the specular boundary walls. The particle exhibits its translational and rotational motion due the thermophoresis force and the torque exerted by collision of gas molecules on it. The particle translates towards the colder region together with the rotational motion, and the diffuse wall rotates towards the colder region . Once the diffuse part aligns towards the colder region it does not change its orientation further and keep facing towards the colder region forever during the motion. The translation motion and the orientation of the circular particle is shown in the figure 5.36 at different instants of time. When initially the half part of the circular particle facing towards the hotter region is modeled by the specular boundary wall and the other half part facing towards the colder region is modeled by the diffuse boundary wall, the particle does not change it orientation. The particle only translate towards the colder region keeping its initial orientation. Figure 5.37 show the motion of the circular Janus particle at different instants of time.

Fig. 5.36: Motion of the circular Janus particle at time (i) 0 secs (ii) 4.3417×10^{-8} secs (iii) 7.7631×10^{-8} secs (iv) 1.9672×10^{-7} secs from left to right.
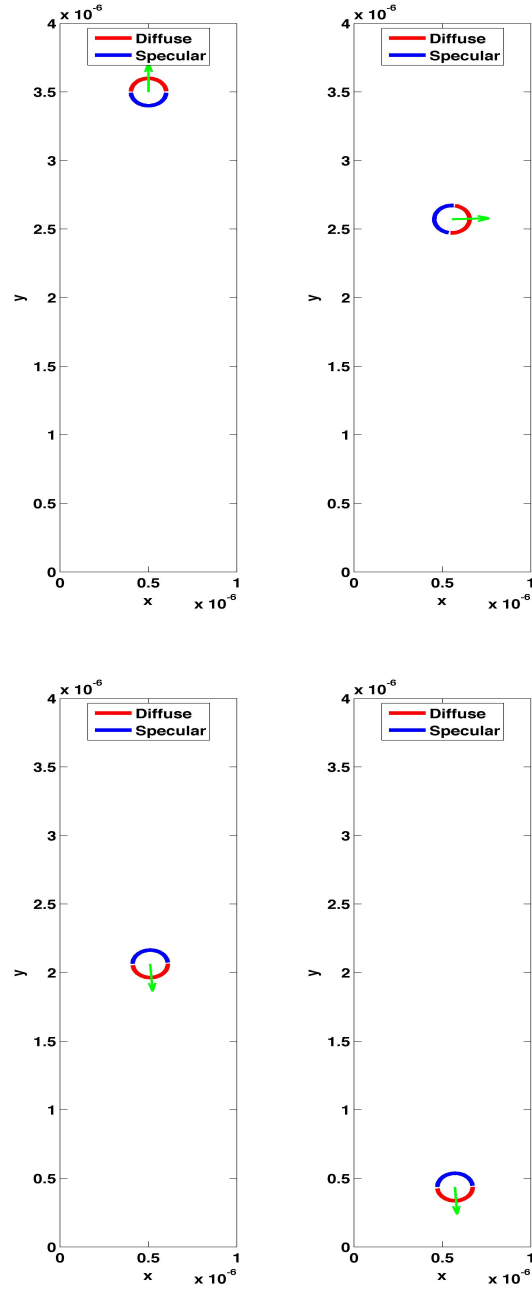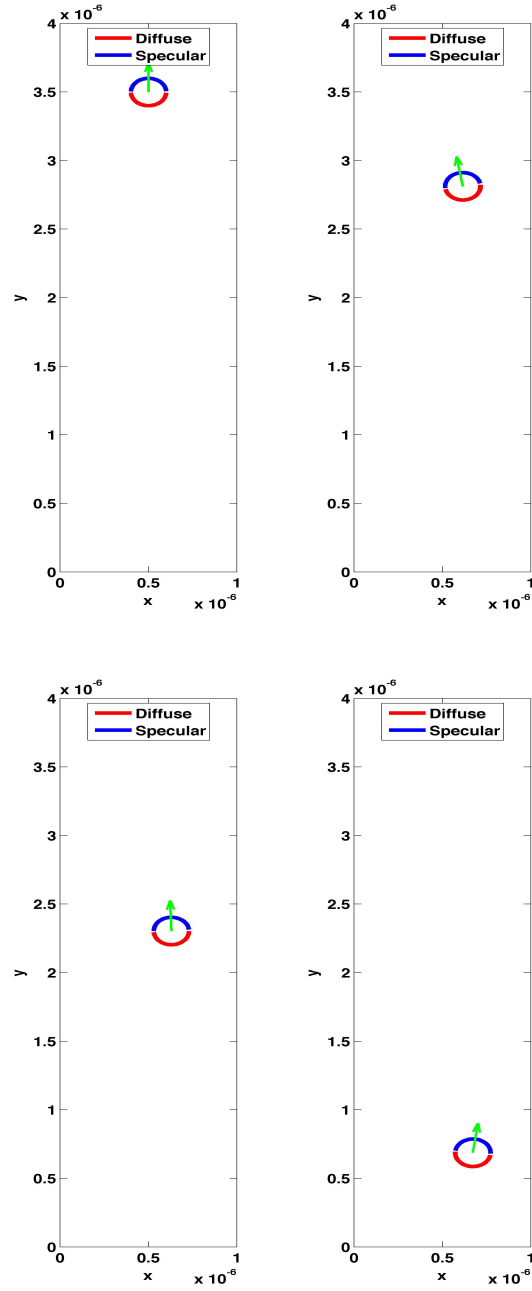
Fig. 5.37: Motion of the circular Janus particle at time (i) 0 secs (ii) 4.3417×10^{-8} secs (iii) 7.7631×10^{-8} secs (iv) 1.9672×10^{-7} secs from left to right.

Chapter 6
Conclusion

We have presented a numerical scheme for a moving rigid body with arbitrary shape in a rarefied gas. The gas is modeled by the Boltzmann equation, and the motion of the rigid body is described by the Newton-Euler equations. The Boltzmann equation is solved by a DSMC type of particle method with hard-sphere collision model. In the DSCM framework, we have developed a naive scheme to compute the force and the torque on the rigid body by applying the momentum transfer during the collision of gas molecules and the rigid body. This scheme in the DSMC framework is named as the momentum approach. We have performed a number of test examples in 1-, 2- and 3-dimensional computational domains to validate the proposed momentum approach in the DSMC framework. In 1-dimensional geometry, we have simulated the gas flow in a actuator to move the piston by providing the temperature difference at two sides of the piston. The numerical result obtained by the momentum approach for computing the equilibrium position of the piston is correctly agreed with the theory. In 2-dimensional geometry, we have performed the numerical simulations of a gas flow in a cavity that contains a suspended rigid circular body. In this test example, we have solve the problem by using DSMC method, and the motion of the rigid body is computed by applying both momentum and moment approaches. The results obtained from both the approaches are agreed quite well. We have also solved the cavity flow problem with the Navier-Stokes equations by using the finite pointset method (FPM) to find the motion of the body, and compared the results obtained by using the momentum approach in the DSMC framework for small and large values of Knudsen number. For a small value of Knudsen number, the solutions obtained from both the models match well enough but for a large value of Knudsen number the solutions differ significantly because of the breakdown of the continuum hypothesis in which the Navier-Stokes equations failed to describe the flow of the gas. To validate the Einstein relation for the Brownian motion in the rarefied gas regime, we have presented the diffusion of the spherical particle with the translational and the rotational motion. The numerical values of the diffusion coefficients are found to converge to the theoretical values as the number of simulated molecules increased. We have also presented the diffusion of the circular particle in 2-dimensional domain. In the last experiment we have performed the DSMC

simulations for the thermophoresis on a spherical particle. The numerical values of the thermophoretic force using the DSMC method with the momentum approach agreed quite well with the theoretical values in the transition and the free molecular regimes. We have also proposed the thermophoretic velocity in the transition regime by applying the Sherman interpolation, and the DSMC simulation is also performed in this regard. The theory agreed well for the large values of Knudsen numbers but started deviate for the small values. We have also simulated the motion of the circular and the spherical Janus particle in the thermophoresis by using the DSMC method with the momentum approach. We have studied the translational and the rotational motions of the circular Janus particle in the thermophoresis. We have presented the distribution of the polar angle of the circular Janus particle when it is fixed at its center of mass just to exhibit the rotational motion. We have also computed the distribution of the polar angle of the spherical Janus particle fixed at its center of mass, and found that the numerical distribution agreed quite well with the theoretical one.

Appendix A
Binary Elastic Collision

The collision term $J(f, f)$ in the Boltzmann equation is derived under the consideration of binary collisions involving just two molecules. The collision is considered to be an elastic in which there is no interchange of translation and internal energy [9]. Given the pre-collision velocities $\mathbf{v}$ and $\mathbf{v}_*$, and the given physical properties of the molecules and the the orientation of the trajectories of the two collision partners in a typical binary collision, we can determine the post-collision velocities $\mathbf{v}'$ and $\mathbf{v}'_*$.

The linear momentum and the energy must be conserved in the elastic collision, which are given by

$$\mathbf{v} + \mathbf{v}_* = \mathbf{v}' + \mathbf{v}'_* = 2\mathbf{v}_c, \qquad (A.1)$$

$$||\mathbf{v}||^2 + ||\mathbf{v}_*||^2 = ||\mathbf{v}'||^2 + ||\mathbf{v}'_*||^2. \qquad (A.2)$$

where $\mathbf{v}_c$ is the velocity of center of mass of the pair of molecules. It can be seen from the equation (A.1) that the velocity of center of mass of the pair of molecules is unchanged by the collision. The pre-collision and the post-collision values of the relative velocity between the molecules are defined by

$$\mathbf{v}_r = \mathbf{v} - \mathbf{v}_*, \qquad (A.3)$$

$$\mathbf{v}'_r = \mathbf{v}' - \mathbf{v}'_*. \qquad (A.4)$$

Adding and subtracting the equations (A.1) and (A.3), we get

$$\left.\begin{aligned} \mathbf{v} &= \mathbf{v}_c + \frac{1}{2}\mathbf{v}_r, \\ \mathbf{v}_* &= \mathbf{v}_c - \frac{1}{2}\mathbf{v}_r. \end{aligned}\right\} \qquad (A.5)$$

The pre-collision velocities relative to the center of mass are $\mathbf{v} - \mathbf{v}_c$ and $\mathbf{v}_* - \mathbf{v}_c$. Equation (A.5) shows that these velocities are anti-parallel in this frame of reference, and if the molecules are point centers of force, the force between them remains in the plane containing the two velocities. The collision is therefore planner in the center

of mass of frame [9]. Similarly the post-collision velocities are obtained by adding and subtracting the equations (A.1) and (A.4) as

$$
\left.
\begin{aligned}
\mathbf{v}' &= \mathbf{v}_c + \frac{1}{2}\mathbf{v}'_r, \\
\mathbf{v}'_* &= \mathbf{v}_c - \frac{1}{2}\mathbf{v}'_r.
\end{aligned}
\right\}
\tag{A.6}
$$

This shows that the post-collision velocities are also anti-parallel in the center of mass frame of reference.

Substituting the equations in (A.5) and (A.6) in the energy equation (A.2), we get the magnitude of the relative velocity is unchanged by the collision, i.e.

$$
||\mathbf{v}_r|| = ||\mathbf{v}'_r||.
\tag{A.7}
$$

Since both $\mathbf{v}_c$ and $\mathbf{v}_r$ may be calculated from the pre-collision velocities, the determination of the post-collision velocities reduces to the calculation of the change in direction χ of the relative velocity vector. The calculation of direction χ depends on the choice of the collision model, see [9] for detail.

Appendix B
Random Sampling

If the physical processes are modeled by the probabilistic approach, the process required the generation of representative value of variables that are distributed in a prescribed manner. This is done through random number and is a key step in the direct simulation Monte Carlo methods. Let us assume the availability of a set of successive random number U that are uniformly distributed between 0 and 1. There are many computational algorithms to generate the random numbers uniformly distributed between 0 and 1, for example, the most common is the linear congruential generator and most widely used is Mersenne Twister. The computational method that is used to generate the sequence of random numbers are based on the deterministic algorithm, so it is called the pseudorandom number generators (PRNG). Using these uniformly distributed random number, we can generate the sequence of random numbers which is described by the given distribution function.

B.1 Monovariate Distribution

Let $x \in [a, b] \subseteq \mathbb{R}$ be a random variable with given distribution function $f_x \geq 0$ such that

$$\int_a^b f_x(x)dx = 1.$$

Then the cumulative distribution function is defied as

$$F_x(x) = \int_a^x f_x(y)dy.$$

We now generate a random number U uniformly distributed between 0 and 1 and equate with $F_x(x)$ to get

$$F_x(x) = U. \tag{B.1}$$

If F_x is an invertible function, then the random variable x can be sampled by solving the equation (B.1) to get

$$x = F^{-1}(U).$$

Example B.1. *(Exponential distribution)*
Consider the probability density function of an exponential distribution for $\lambda > 0$

$$f_x(x) = \begin{cases} \lambda e^{-\lambda x} & \text{for} \quad x \geq 0 \\ 0 & \text{else.} \end{cases}$$

Then

$$F_x(x) = \int_0^x \lambda e^{-\lambda y} dy = 1 - e^{-\lambda x}$$

and therefore $F_x(x) = U$ gives

$$x = -\frac{1}{\lambda} \ln(1 - U),$$

where U is uniformly distributed random number between 0 and 1 so is $1 - U$, and we can also write $x = -\frac{1}{\lambda} \ln U$.

Remark B.1. Sometimes it may be expensive to compute the inverse of the commutative distribution function F_x, since in general a non-linear equation has to be solved. In this case another widely used method to construct the f_x-distributed sequence of random variable is the acceptance-rejection method. For the detail of the method we refer to [61, 70].

B.2 Multivariate Distribution

Suppose we want to sample a n-dimensional random variable $\mathbf{x} = (x_1, \cdots x_n)$, whose probability density function $f_{\mathbf{x}}$ is given.
If the density function can be written as a product of densities of the scalar random variables x_i , i.e. if

$$f_{\mathbf{x}}(x_1, \cdots x_n) = f_{x_1}(x_1) f_{x_2}(x_2) \cdots f_{x_n}(x_n),$$

then the n scalar random variables $x_1 \cdots x_n$ are independent, and they can be sampled separately, i.e. the problem is equivalent to sampling n monovariate random variables.
If this is not the case, then one may look for a transformation $T : \mathbf{x} \to \boldsymbol{\xi}$ such that in the new variables the probability density is factorized, i.e.

$$f_{\mathbf{x}}(x_1, \cdots x_n) dx_1 dx_2 \cdots dx_n = f_{\xi_1}(\xi_1) f_{\xi_2}(\xi_2) \cdots f_{\xi_n}(\xi_n) d\xi_1 d\xi_2 \cdots d\xi_n,$$

sample the variables $\xi_1, \cdots, \xi_n$, and then compute $\mathbf{x}$ by inverting the map T, i.e. $\mathbf{x} = T^{-1}(\boldsymbol{\xi})$.

Example B.2. *(Maxwellian distribution)*
Consider the normalized Maxwellian distribution for velocity vector $\mathbf{v}$

$$f_{\mathbf{v}} = \frac{1}{(2\pi RT)^{3/2}} e^{-\frac{||\mathbf{v}-\mathbf{u}||^2}{2RT}}. \tag{B.2}$$

Substitute $\mathbf{w} = \frac{\mathbf{v}-\mathbf{u}}{\sqrt{2RT}}$, that is, $\mathbf{v} = \sqrt{2RT}\mathbf{w} + \mathbf{u}$. Then $d\mathbf{v} = (2RT)^{3/2}d\mathbf{w}$ and the distribution function for the velocity vector $\mathbf{w}$ is given by

$$f_{\mathbf{w}} = \frac{1}{(\pi)^{3/2}} e^{-||\mathbf{w}||^2}.$$

Transforming $\mathbf{w} = (w_x, w_y, w_z)$ into the spherical coordinates

$$w_x = w\sin\theta\cos\phi; \quad w_y = w\sin\theta\sin\phi; \quad w_z = w\cos\theta,$$

where $w = ||\mathbf{w}||^2 > 0$, $0 \le \theta \le \pi$ and $0 \le \phi \le 2\pi$. Then $d\mathbf{w} = w^2\sin\theta\, dw\, d\theta\, d\phi$ and distribution function for the new transformed variables (w, θ, ϕ) is given by the product of three univariate distributions

$$f_{w,\theta,\phi} = f_w f_\theta f_\phi,$$

where $f_w = \frac{4}{\sqrt{\pi}}w^2 e^{-w^2}$, $f_\theta = \frac{1}{2}\sin\theta$ and $f_\phi = \frac{1}{2\pi}$.
The cumulative distribution function for f_θ is given by

$$F_\theta(\theta) = \int_0^\theta \frac{1}{2}\sin t\, dt = \frac{1}{2}(1 - \cos\theta),$$

and therefore $F_\theta(\theta) = U_1$ gives

$$\cos\theta = 1 - 2U_1, \quad \sin\theta = \sqrt{4U_1(1 - U_1)}.$$

The cumulative distribution function for f_ϕ is given by

$$F_\phi(\phi) = \int_0^\phi \frac{1}{2\pi}dt = \frac{1}{2\pi}\phi,$$

and therefore $F_\phi(\phi) = U_2$ gives

$$\phi = 2\pi U_2.$$

Finally the cumulative distribution function for f_w is given by

$$F_w(w) = \int\limits_0^w \frac{4}{\sqrt{\pi}} t^2 e^{-t^2} dt,$$

and therefore $F_w(w) = U_3$ gives

$$\int\limits_0^w t^2 e^{-t^2} dt = \frac{\sqrt{\pi}}{4} U_3,$$

which has to be solved numerically to compute tha value of w.

Hence the velocity vector $\mathbf{v} = (v_x, v_y, v_z)$ following the Maxwellian distribution (B.2) is give by

$$v_x = \sqrt{2RT}\, w \sqrt{4U_1(1-U_1)} \cos(2\pi U_2) + u_x,$$
$$v_y = \sqrt{2RT}\, w \sqrt{4U_1(1-U_1)} \sin(2\pi U_2) + u_y,$$
$$v_z = \sqrt{2RT}\, w (2U_1 - 1) + u_z,$$

where $\mathbf{u} = (u_x, u_y, u_z)$, and U_1, U_2, U_3 are the uniformly distributed random numbers between 0 and 1.

Example B.3. *(Diffuse reflection)*
In this model the distribution function of the gas molecules which are re-emitted with the velocity $\mathbf{v}$ from the boundary wall at temperature T_w and moving with the velocity $\mathbf{V}_w$ is given by [83]

$$f_{\mathbf{v}} = |\, (\mathbf{v} - \mathbf{V}_w) \cdot \mathbf{n}\,| \, \frac{1}{2\pi (RT_w)^2} exp\Big(-\frac{||\mathbf{v} - \mathbf{V}_w||^2}{2RT_w}\Big), \ (\mathbf{v} - \mathbf{V}_w) \cdot \mathbf{n} > 0, \qquad (B.3)$$

where $\mathbf{n}$ is unit is inward normal vector to the wall . Substitute $\mathbf{w} = \frac{\mathbf{v} - \mathbf{V}_w}{\sqrt{2RT}}$, that is, $\mathbf{v} = \sqrt{2RT}\,\mathbf{w} + \mathbf{V}_w$. Then $d\mathbf{v} = (2RT)^{3/2} d\mathbf{w}$, and the distribution function for the velocity vector $\mathbf{w}$ is given by

$$f_{\mathbf{w}} = |\, \mathbf{w} \cdot \mathbf{n}\,| \, \frac{2}{\pi} e^{-||\mathbf{w}||^2}, \quad \mathbf{w} \cdot \mathbf{n} > 0.$$

Let $\{\mathbf{t}, \boldsymbol{\tau}, \mathbf{n}\}$ be a local orthonormal basis. Then expressing of $\mathbf{w}$ in the frame of reference of $\{\mathbf{t}, \boldsymbol{\tau}, \mathbf{n}\}$ is given by

$$\mathbf{w} = w_t \mathbf{t} + w_\tau \boldsymbol{\tau} + w_n \mathbf{n},$$

where (w_t, w_τ, w_n) are the coordinates of $\mathbf{w}$ w.r.t. $\{\mathbf{t}, \boldsymbol{\tau}, \mathbf{n}\}$. Then $f_{\mathbf{w}}$ can be expressed as the product of two distributions which is given by

$$f_{\mathbf{w}} = f_{w_n} f_{w_t} f_{w_\tau},$$

where $f_{w_n} = 2 w_n e^{-w_n^2}$, $w_n > 0$ and $f_{w_t, w_\tau} = \frac{1}{\pi} e^{-(w_t^2 + w_\tau^2)}$, $-\infty < w_t, w_\tau < \infty$.
Transforming (w_t, w_τ) into polar coordinates

$$w_t = r \cos \theta; \quad w_\tau = r \sin \theta,$$

where $r = \sqrt{w_t^2 + w_\tau^2} > 0$ and $0 \le \theta \le 2\pi$. Then $dw_t dw_\tau = r dr d\theta$ and distribution
function corresponding to f_{w_t, w_τ} with new transformation is give by

$$f_{r, \theta} = f_r f_\theta,$$

where $f_r = 2 r e^{-r^2}$ and $f_\theta = \frac{1}{2\pi}$.
The cumulative distribution function for f_{w_n} is given by

$$F_{w_n}(w_n) = \int\limits_0^{w_n} 2 t e^{-t^2} dt = 1 - e^{-w_n^2},$$

and therefore $F_{w_n}(w_n) = U_1$ gives

$$w_n = \sqrt{-\ln(1 - U_1)} = \sqrt{-\ln U_1}.$$

The cumulative distribution function for f_r is given by

$$F_r(r) = \int\limits_0^r 2 t e^{-t^2} dt = 1 - e^{-r^2},$$

and therefore $F_r(r) = U_2$ gives

$$r = \sqrt{-\ln(1 - U_2)} = \sqrt{-\ln U_2}$$

Finally the cumulative distribution function for f_θ is given by

$$F_\theta(\theta) = \int\limits_0^{2\pi} \frac{1}{2\pi} dt = \frac{1}{2\pi},$$

and therefore $F_\theta(\theta) = U_3$ gives

$$\theta = 2\pi U_3.$$

Hence the velocity vector $\mathbf{v}$ following the distribution (B.3) is give by

$$\mathbf{v} = \sqrt{-2 R T_w \ln U_2} \cos(2\pi U_3) \mathbf{t} + \sqrt{-2 R T_w \ln U_2} \sin(2\pi U_3) \boldsymbol{\tau} + \sqrt{-2 R T_w \ln U_1} \mathbf{n} + \mathbf{V}_w,$$

where U_1, U_2, U_3 are uniformly distributed random numbers between 0 and 1.

Remark B.2. If the density function $f_{\mathbf{x}}$ does not factorized we can also transform a uniformly distributed sequences into f-distributed ones. References [61, 70] give the method of construction and also relevant literatures.

References

[1] F. J. Alexander and A. L. Garcia, The Direct Simulation Monte Carlo Method, *Comp. in Phys.*, **Vol. II**, No. 6, Nov/Dec 1997.

[2] C. K. Aidun, Y. Lu, Lattice Boltzmann Simulation of Solid Suspensions with Impermeable Boundary, *J. Stat. Phys.*, **81**, 49, 1995.

[3] C. K. Aidun, Y. Lu, E. Ding, Direct Analysis of Particulate Suspensions with Inertia Using the Discrete Boltzmann Equation, *J. Fluid Mech.*, **373**, 287, 1998.

[4] M. P. Allen, D. J. Tildesley, *Computer Simulation of Liquids*, Clarendon Press, Oxford, 1987.

[5] H. Babovsky, A Convergence Proof for Nanbu's Boltzmann Simulation Scheme, *Eur. J. Mech. B/Fluids*, **8(1)**, 41, 1989.

[6] T. Baier, Thermophoresis of Janus Microparticles at Large Knudsen Numbers, *Private Communication*, Center of Smart Interfaces, TU Darmstadt, Germany, 2014.

[7] G. K. Batchelor, *An Introduction to Fluid Dynamics*, Cambridge University Press, 1967.

[8] O. Behrend, Solid–Fluid Boundaries in Particle Suspension Simulations via the Lattice Boltzmann Method, *Phys. Rev. E*, **52**, 1164, 1995.

[9] G. A. Bird, *Molecular Gas Dynamics and Direct Simulation of Gas Flows*, Clarendon, Oxford, 1994.

[10] J. F. Brady, G. Bossis, Stokesian Dynamics, *Ann. Rev. Fluid Mech.*, **20**: 111-157, 1988.

[11] J. R. Brock, *J. Colloid Sci.*, **17**, 768, 1962.

[12] H. Bruus, *Theoretical Microfluidics*, Oxford University Press Inc., New York, 2008.

[13] K. Balakrishnan, J. B. Bell, A. Donev and A. L. Garcia Fluctuating Hydrodynamics and Direct Simulation Monte Carlo, 28th International Symposium on Rarefied Gas Dynamics, *AIP Conf. Proc.*, **1501**, 695-704, 2012.

[14] J. Blum, S. Bruns, D. Rademacher, A. Voss, B. Willenberg, M. Krause, Measurement of the Translational and Rotational Brownian Motion of Individual Particles in a Rarefied Gas, *Physical Review Letters*, PRL 97, 230601, 2006.

[15] S. Beresnev, V. Chernyak, Thermophoresis of a Spherical Particle in a Rarefied Gas: Numerical Analysis Based on the Model Kinetic Equations, *Phys. Fluids*, **7**, 1743, 1995.

[16] P. S. Burada, P. Hänggi, F. Marchesoni, G. Schmid, P. Talkner, Diffusion in Confined Geometries, *Wiley-VCH Verlag GmbH & Co. KGaA, Weinheim, ChemPhysChem.*, **10**, 45-54, 2009.

[17] D. Braun, A. Libchaber, *Phys. Rev. Lett.*, **89**, 188103, 2002.

[18] H. Babovsky, R. Illner, A Convergence Proof of Nanbu's Simulation Method for the Full Boltzmann Equation, *SIAM J. Numer.* Anal., **16**, 45-64, 1989.

[19] C. Cercignani, *The Boltzmann Equation and its Applications*, Springer, Berlin, 1988.

[20] C. Cercignani, M. Lampis, Kinetic Model of Gas-surface Interactions, *Transp. Th. and Stat. Phys.*, **1 (2)**, pp. 101-114, 1971.

[21] Xi, Chen, The Thermophoretic Velocity of a Small Particle Suspended in a Plasma, *J. Phys. D: Appl. Phys.*, **32**, 283-290, 1999.

[22] S. Chen, G. D. Doolen, Lattice Boltzmann method for Fluid Flows, *Annu. Rev. Fluid. Mech.*, **30**, 329, 1998.

[23] S. Chapman, T.G. Cowling, *The Mathematical Theory of Non-Uniform Gases*, Cambridge University Press, 1970.

[24] C. Cercignani, R. Illner, M. Pulvirenti, *The Mathematical Theory of Dilute Gases*, Springer- Veglag New York, Berlin, Heidelberg, 1994.

[25] H. A. Dwyer, Thirteen-Moment Theory of the Thermal Force on a Spherical Particle, *Phys. Fluids*, **10**, 976, 1976.

[26] G. Dechristé, L. Mieussens Numerical Simulations of Micro flows with Moving Obstacles, *Journal of Physics: Conference Series*, **362**, 2012.

[27] P. S. Epstein, On the Resistance Experienced by Spheres in their Motion Through Gases, *Phys. Rev.*, **23**, 710, 1924.

[28] R. M. Erb, N. J. Jenness, R. L. Clark, B. B. Yellen, Towards Holonomic Control of Janus Particles in Optomagnetic Traps, *Adv. Mater*, **21**, 1-5, 2009.

[29] R. Fuerth, A.D. Cowper, Investigations on the Theory of the Brownian Movement by Albert Einstein, *PhD, Dover Publications, Inc.*, 1956

[30] H. Grad, On the Kinetic Theory of Rarefied Gases, *CPAM*, **2**, 331-404, 1949.

[31] E. A. Guggenheim, *Elements of the Kinetic Theory of Gases*, Pergamon Press Ltd, 1960.

[32] R. Glowinski, T. W. Pan, T. I. Hesla, D. D. Joseph, A Distributed Lagrange Multiplier/Fictitious Domain Method for Particulate Flows, *Int. J. Multiphase Flow*, **25**, 755, 1999.

[33] R. Glowinski, T. W. Pan, T. I. Hesla, D. D. Joseph, J. Périaux, A Fictitious Domain Approach to the Direct Numerical Simulation of Incompressible Viscous Flow Past Moving Rigid Bodies: Application to Particulate Flow, *J. Comp. Phys.*, **169**, 363-426, 2001

[34] A. Gomez, D. E. Rosner, *Combust. Sci. Techno.*, **89**, 335, 1993.

[35] M. A. Gallis, D. J. Rader, J. R. Torczynski, DSMC Simulation of the Thermophoretic Force on a Spherical Macroscopic Particle, *AIAA Paper 2001-2890, 35th AIAA Thermophysics Conference, June 11-14, Anaheim, CA,*

American Institute of Aeronautics and Astronautics, Washington, DC, pp. 1-12.

[36] M. A. Gallis, D. J. Rader, J. R. Torczynski, An Approach for Simulating the Transport of Spherical Particle in a Rarefied Gas Flow via the Direct Simulation Monte Carlo (DSMC) Method, *Phys. Fluids*, **13(11)**: 3482-3492, 2001.

[37] M. A. Gallis, D. J. Rader, J. R. Torczynski, Thermophoresis in Rarefied Gas Flows, *Aerosol Science and Technology*, **36**: 1099–1117, 2002.

[38] J. M. Haile, *Molecular Dynamics Simulation- Elementary Methods*, John Wiley & Sons, Inc., 1992.

[39] P. S. Hubbard, Rotational Brownian Motion, *Physical Review A*, **Vol. 6**, No. 6, Dec 1972.

[40] T. J. R. Hughes, G. M. Hulbert, Space-Time Finite Element Methods for Elasto-Dynamics: Formulations and Error Estimates, *Comput. Meth. Appl. Mech. Eng.*, **66**, 339, 1988.

[41] H. H. Hu, D. D. Joseph, Direct Simulation of Fluid Particle Motion, *Theoret. Comput. Fluid Dynamics*, **3**: 285-306, 1992.

[42] H. H. Hu, N. A. Patankar, M. Y. Zhu, Direct Numerical Simulations of Fluid-Solid Systems Using the Arbitrary Lagrangian-Eulerian Technique, *J. Comp. Phys.*, **169**, 427-462, 2001.

[43] H. H. Hu, Direct Simulation of Flows of Solid–Liquid Mixtures, *Int. J. Multiphase Flow*, **22**, 335, 1996.

[44] D. Jie, X. Diao, K. B. Cheong, L. K. Yong, Navier-Stokes Simulation of Gas Flow in Micro Devices, *J. Micromech. Microeng*, **10**, 372-397, 2000.

[45] A. Johnson, T. E. Tezduyar, Simulation of Multiple Spheres Falling in a Liquid-Filled Tube, *Comput. Meth. Appl. Mech. Eng.*, **134**, 351, 1996.

[46] A. Johnson, T. E. Tezduyar, 3D Simulation of Fluid–Particle Interactions with the Number of Particles Reaching 100, *Comput. Meth. Appl. Mech. Eng.*, **145**, 301, 1997.

[47] A. Johnson, T. E. Tezduyar, Advanced Mesh Generation and Update Methods for 3D Flow Simulations, *Comput. Mech.*, **23**, 130, 1999.

[48] B. H. Kaye, *Direct Characterization of Fine Particles*, Wiley New York, 1981.

[49] R. Kubo, The Fluctuation-dissipation Theorem, *Rep. Prog. Phys.*, **29**, 255, 1966.

[50] A. J. C. Ladd, Short-Time Motion of Colloidal Particles: Numerical Simulation via a Fluctuating Lattice-Boltzmann Equation, *Physical Review Letters*, **Vol. 70**, No. 9, 1993.

[51] A. J. C. Ladd, Numerical Simulations of Particulate Suspensions via a Discretized Boltzmann equation. I. Theoretical Foundation, *J. Fluid Mech.*, **271**, 285, 1994a.

[52] A. J. C. Ladd, Numerical Simulations of Particulate Suspensions via a Discretized Boltzmann equation. II. Numerical Results, *J. Fluid Mech.*, **271**, 311, 1994b.

[53] S. K. Loyalka, Motion of a Sphere in a Gas: Numerical Solution of the Linearized Boltzmann Equation, *Phy. of Fluid A*, **4(5)**, May 1992.

[54] D.S. Lemons, A. Gythiel, Paul Lagenvin's 1908 paper "On the Theory of Brownian Motion"[**Sur la theorie du mouvement brownien,"C.R. Acad. Sci. (Paris), 146, 503-533, 1908**], *Am J Phys.*, **65 (11)**, 1079-1081, November 1997.

[55] J. R. Lebenhaft, R. Kapral, Translational and Rotational Friction in Rough Sphere in Fluid, *J. Chem. Phy.*, **74**, 6888, 1981.

[56] Z. Li, H. Wang, Drag Force, Diffusion Coefficient, and Electric Mobility of Small Particles. **I. Theory Applicable to the Free-molecular Regime**, *Phy. Rev. E*, **68**, 061206, 2003.

[57] Z. Li, H. Wang, Thermophoretic Force and Velocity of Nanoparticles in the Free Molecular Regime, *Phys. Rev. E* , **70**, 021205, 2004.

[58] R. M. Mazo, *Brownian Motion: Fluctuations, Dynamics, and Applications*, Oxford University Press, 2002.

[59] L. Mädler, S.K. Friedlander, Transport of Nanoparticles in Gases: Overview and Recent Advances, *Aerosol and Air Quality Research*, **Vol. 7**, No. 3, pp. 304-342, 2007.

[60] K. Nanbu, Direct Simulation Scheme Derived from the Boltzmann Equation. I. Monocomponent Gases, *J. Phys. Soc. Japan*, **Vol. 49**, No. 5, 1980.

[61] H. Neunzert, Particle Methods, *AGTM*, Bericht Nr. 115, University of Kaiser-slautern.

[62] X. Nie, G. D. Dollen, S. Chen, Lattice-Boltzmann Simulations of Fluid Flows in MEMS, *J. Stat. Phys*, **107**, Nos. 112, 2002.

[63] H. Neunzert, J. Struckmeier, Particle Methods for the Boltzmann Equation, *Acta Number* **4**, 417-457, 1995.

[64] S. Naris, D. Valougeoris, The Driven Cavity Flow Over the Whole Range of the Knudsen Number, *Phys. of Fluid*, **17**, 097106, 2005.

[65] T. Ohwada, M. Kunihisa, Direct Simulation of a Flow Produced by a Plane Wall Oscillating in its Normal Direction, in: A.D. Ketsdever, E.P. Muntz (Eds.), Rarefied Gas Dynamics, AIP, Melville, pp. 202–209, 2003.

[66] E. S. Oran, C. K. Oh, B. Z. Cybyk, Direct Simulation Monte Carlo: Recent Advances and Applications, *Annu. Rev. Fluid Mech.*, **30**:403-41, 1998.

[67] A.P. Philipse, *Notes on Brownian Motion*, Utrecht University, Debye Institute, Van 't Hoff Laboratory, August 2011.

[68] W. F. Fhillips, Thermal Force on Spherical Particles in a Rarefied Gas, *Phys. Fluid*, **15**, 6, 999-1003, 1972.

[69] N. A. Patankar, D. D. Joseph, Lagrangian Numerical Simulation of Particulate Flows, *International Journal of Multiphase Flow*, **27**, 1685-1706, 2001.

[70] L. Pareschi, G. Russo, An Introduction to Monte Carlo Methods for the Boltzmann Equation, ESAIM: Proceedings, **Vol. 10**, pp. 35-75, 2001.

[71] L. Pareschi, S. Trazzi, Numerical Solution of the Boltzmann Equation by Time Relaxed Monte Carlo (TRMC) Methods, *International Journal of Numerical Methods in Fluids*, **48**, pp. 947-983, 2005.

[72] D. Qi, Lattice-Boltzmann Simulations of Particles in Non-zero Reynolds Number Flows, *J. Fluid Mech.*, **385**, 41, 1999.

[73] S. Roy, R. Raju, H. F. Chuang, B. A. Cruden, M. Meyyappan, Modeling Gas Flow Through Microchannels and Nanopores, Journal of Applied Physics, **93**, 8: 4870-4879, 2003

[74] W.B. Russel, Small Particles Suspended in Liquid, *Ann. rev. Fluid Mech.*, **13**: 425-55, 1981.

[75] G. Russo, Moving Boundary Problems for the BGK Model of Rarefied Gas Dynamics, *PHYSCON*, 2009.

[76] G. Russo, F. Filbet, Semi-Lagrangian Schemes Applied to Moving Boundary Problems for the BGK Model of Rarefied Gas Dynamics, *Kin. and Related Models*, **Vol. 2**, No. 1, pp. 231–250, 2009.

[77] D. J. Radar, M. A. Gallis, J. R. Torczynski, DSMC Moving-Boundary Algorithms for Simulating MEMS Geometries with Opening and Closing gaps, in: D. A. Levin, I. J. Wysong, A. L. Garcia (Eds.), 27th International Symposium on Rarefied Gas Dynamics, 2010, AIP Conf. Proc. 1333, AIP, Melville, pp. 760–765, 2011.

[78] A. A. Rostami, A. S. Mujumdar, N. Saniei, Flow and Heat Transfer for Gas Flowing in Microchannels: A Review, *Heat and Mass Transfer, Springer-Verlag*, **38**, 359-367, 2002

[79] C. G. Ragazzo, E. Tabak, On the Force and Torque on the System of Rigid Bodies: A Remark on an Integral Formula due to Howe, *Physics of Fluid*, **19**, 2007.

[80] G. G. Stokes, On the Effect of Fluids on the Motion of Pendulums, *Trans. Cambridge Philos. Soc.*, **9**, 8, 1851. Reprinted in Mathematical and Physical Papers III (Cambridge University Press, Cambridge, MA).

[81] P. Singh, D. D. Joseph, T. I. Hesla, R. Glowinski, T. W. Pan, A Distributed Lagrange Multiplier/Fictitious Domain Method for Viscoelastic Particulate Flows, *J. Non-Newtonian Fluid Mech.*, **91**, 165, 2000.

[82] G. S. Springer, Thermal Force on Particle in the Transition Regime, *Journal of Colloid and Interface Science*, **Vol. 34**, No. 2, 1970.

[83] S. Tiwari, *Domain Decomposition in Particle Methods for the Boltzmann and Euler Equation*, Shaker Verlag, Aachen, 1998.

[84] S. Tiwari, A LSq-SPH Approach for Solving Compressible Viscous Flows, in: H. Freistueler, G. Warnecke (Eds.), Hyperbolic Problems: Theory, Numerics, Application, *International Series of Numerical Mathematics*, Birkhaeuser, Basel/Switzerland, **Vol. 141**, pp. 901-910, 2001.

[85] J. Tyndall, *Proc. Roy. Inst.*, **6**, 3, 1870.

[86] T. Tsuji, K. Aoki, Moving Boundary Problems for Rarefied Gas: Spatially One-Dimensional Case, *J. Comp. Phys.*, **250**, 574-666, 2013.

[87] S. Tiwari, J. Kuhnert, Modeling Two Phase Flows with Surface Tension by Finite Pointset Method (FPM), *J. Comput. Appl. Math.*, **203**, 376-386, 2007.

[88] S. Tiwari, A. Klar, S. Hardt, A Particle-Particle Hybrid Method for Kinetic and Continuum Equations, *J. Comput. Phys.*, **228**, 2009.

[89] S. Tiwari, A. Klar, S. Hardt, A. Donkov, Simulation of a Moving Liquid Droplet Inside a Rarefied Gas Region, *Computers & Fluids 71*, 283-196, 2013.

[90] T. E. Tezduyar, J. Liou, and M. Behr, A New Strategy for Finite Element Computations Involving Moving Boundaries and Interfaces — The DSD/ST Procedure. I. The Concept and the Preliminary Numerical Tests, *Comput. Meth. Appl. Mech. Eng.*, **94**, 339, 1992a.

[91] G. E. Uhlenbeck, L. S.Ornstein, On the Theory of the Brownian Motion, *Physical Review*, Sep 1930.

[92] H. Vestner, Forces on Small Particles in Nonhomoheneous Polyatomic Gases, *Z. Naturforsch*, **29a**: 1244-1252, 1974.

[93] W. Wagner A convergence proof for Bird's Direct Simulation Monte Carlo Method for the Boltzmann Equation. *J. stat. Phys.*, **Vol. 66**, Nos. 3/4, 1992.

[94] N. Wax, *Selected Papers on Noise and Stochastic Processes*, edited by N. Wax, Dover, New York, 1954.

[95] J. WANG, Z. LI, Thermophoretic Force on Micro- and Nano-particles in Dilute Binary Gas Mixture, *Phys. Rev. E*, **84**, 2011.

[96] A. Walther, A. H. E. Mueller, Janus Particles, *Soft Matter*, **4**, 663-668, 2008.

[97] A. Walther, A. H. E. Mueller, Janus Particle: Synthesis, Self-Assembly, Physical Properties, and Applications, *Chem. Rev.*, **113**, 5194-5261, 2013.

[98] S. Yang, F. Guo, B. Kiraly, X. Mao, M. Lu, K. W. Leong, T. J. Huang, Microfluidic Synthesis of Multifunctional Janus Particles for Biomedical Applications, *Lab Chip*, **12(12)**: 2097-102, 2012.

[99] D. Z. Zhang, A. Prosperetti, Averaged Equations for Inviscid Disperse Two-Phase Flow, *J. Fluid. Mech.*, **Vol. 267**, pp. 185-219, 1994.

[100] B. Zhao, K. Uchikawa, J. C. McCormick, C. Y. Ni, J. G. Chen, and H. Wang, Ultra-fine Anatase TiO_2 Nanoparticles Produced in Premixed Ethylene Stagnation Flame at 1 atm *Proc. Combust. Inst*, **30**, pp. 2569-2576, 2005.

Curriculum Vitae

Samir Shrestha

Date and Place of Birth: 30 November 1976, Doli, Nepal

1994	Bachelor of Science
1999	Master of Science in Mathematics
2008	Master of Science in Industrial Mathematics
10/2011 - till date	Doctorate study in Mathematics at TU Kaiserslautern

Wissenschaftlicher Werdegang

Samir Shrestha

Geboren am 30 November 1976, Doti, Nepal

1994	Bachelor of Science
1999	Master of Science in Mathematik
2008	Master of Science in Industriell Mathematik
10/2011 - till date	Doktorand der Mathematik an der TU Kaiserslautern

Declaration

I, Samir Shrestha, hereby declare that my thesis entitled **Modeling and Simulation of a Moving Rigid Body in a Rarefied Gas** is my own work and effort. All used resources for this purpose are given in the reference. This work has not been submitted for the purpose of academic examination anywhere else.

Kaiserslautern, 16.12.2014   Samir Shrestha